ABSTRACT


| | |
|---|---|
| Title of Document: | INVESTIGATION OF HOUSEHOLD REFRIGERATOR WITH ALTERNATIVE LOW GLOBAL WARMING POTENTIAL REFRIGERANTS |
| | Daniel Thomas Leighton, Master of Science, 2011 |
| Directed By: | Professor Reinhard Radermacher, Mechanical Engineering |

Steady-state and transient thermodynamic models of the refrigeration system were created in order to predict the performance of household refrigerators using different refrigerant types. The models were validated with experimental data taken from a commercially available household refrigerator charged with HFC-134a. The models were then used to simulate the drop-in performance of several alternative low global warming potential (GWP) refrigerants in the household refrigerator. The alternative refrigerant of strongest interest was HFO-1234yf, which was evaluated as a direct drop-in replacement for HFC-134a. HFO-1234yf was found to be a suitable replacement for HFC-134a, with similar performance characteristics and a decrease in overall system efficiency of less than 2%. A parametric study of HFC-134a/HFO-1234yf blends was also conducted in order to evaluate their potential as non-flammable, low GWP replacements for HFC-134a.

INVESTIGATION OF HOUSEHOLD REFRIGERATOR WITH ALTERNATIVE
LOW GLOBAL WARMING POTENTIAL REFRIGERANTS


By


Daniel Thomas Leighton


Thesis submitted to the Faculty of the Graduate School of the
University of Maryland, College Park, in partial fulfillment
of the requirements for the degree of
Master of Science
2011

Advisory Committee:
Professor Reinhard Radermacher, Chair
Professor Jungho Kim
Professor Michael Ohadi
Research Associate Professor Yunho Hwang

# Acknowledgements

I would like to thank my advisor and mentor Dr. Reinhard Radermacher for all of his support. Dr. Radermacher gave me the opportunity to join the CEEE laboratory as an undergraduate researcher, which was the highlight of my undergraduate education and motivated me to pursue an M.S. degree. His encouragement and support have helped me to grow academically, professionally, and personally. I have learned much from him by example, especially his approaches to learning and research, and his exemplary management and mentoring of others.

My thanks go to Dr. Yunho Hwang, who has been another invaluable mentor and teacher. Under Dr. Hwang's direction I have had the enjoyable opportunity to pursue many avenues of research. His insight on how to approach problems has taught me much, and his drive toward producing quality work has greatly improved my analysis, technical writing, and presentation skills.

Additional thanks go to Dr. Jungho Kim and Dr. Michael Ohadi. I appreciate both the generous commitment of time they have given to be a part of my thesis committee, and all that they have taught me during my time as a student.

I would like to thank Jan Muehlbauer, whose hands-on approach to problem solving has helped me over many research hurdles. Working with him has been a great learning experience, as his ability to generate creative solutions to practical engineering problems is inspiring.

To my numerous colleagues at the CEEE who are too long to list, I thank all of you for your friendship and engaging discussions. Our numerous technical and cultural discussions have broadened my understanding of engineering and the world.

# Table of Contents

# List of Tables

# List of Figures

# Nomenclature

| | |
|---|---|
| AC | Alternating current |
| ANSI | American National Standards Institute |
| ASHRAE | American Society of Heating, Refrigerating and Air Conditioning Engineers |
| CEEE | Center for Environmental Energy Engineering |
| COP | Coefficient of Performance |
| DC | Direct current |
| DOE | Department of Energy |
| DP | Differential pressure |
| EES | Engineering Equation Solver |
| EPA | Environmental Protection Agency |
| FPI | Fins per inch [1/in] |
| GAR | Global Alternate Refrigerant |
| GUI | Graphical user interface |
| GWP | Global warming potential |
| HFC | Hydrofluorocarbon |
| HFO | Hydrofluoro-Olefin |
| HTC | Heat transfer coefficient [$W/m^2$-K] |
| MAC | Mobile air conditioning system |
| MFM | Mass flow meter |
| MFR | Mass flow rate [g/s] |

| PID | Proportional-Integral-Derivative |
| --- | --- |
| RH | Relative humidity |
| RMS | Root mean squared |
| RPM | Revolutions per minute |
| SAE | Society of Automotive Engineers |
| SLHX | Suction line heat exchanger |
| TR | TransRef |

## **Abbreviations:**

| C1 | Heat transfer correction factor |
| --- | --- |
| $c_p$ | Specific heat [kJ/kg-K] |
| E | Energy |
| Exp | Experimental |
| *F* | Calculated variable |
| f.s. | Full scale range |
| h | Enthalpy [kJ/kg] |
| $h_F$ | Height of freezer cabinet |
| $h_r$ | Height of refrigerator cabinet |
| *i* | Number of variables |
| Liq | Liquid |
| N | Number of data points |
| P | Pressure [kPa] |
| R1234yf | 2,3,3,3-tetrafluoroprop-1-ene |
| R1234ze | |

| | |
|---|---|
| R134a | 1,1,1,2-tetrafluoroethane |
| R404A | Mixture of R143a/R125/R134a (trifluoroethane/ pentafluoroethane/ tetrafluoroethane) |
| R410A | Mixture of R32/R125 (difluoromethane/pentafluoroethane) |
| Ref | Refrigerator cabinet |
| t | Time [hr] |
| T | Temperature [°C] |
| $\Delta T$ | Temperature difference [K] |
| temp | Temperature |
| u | Uncertainty |
| U | Overall heat transfer coefficient [W/m$^2$-K] |
| UA | Overall heat transfer coefficient times heat transfer area [W/K] |
| $v$ | Measured variable |
| Vap | Vapor |
| $W_f$ | Width of freezer cabinet |
| Wr | Width of refrigerator cabinet |
| $x$ | Variable |
| XV | Expansion device |

**Subscripts:**

| | |
|---|---|
| amb | Ambient |
| avg | Average |
| Fre | Freezer cabinet |
| $j$ | Data point index |

| | |
|---|---|
| Mul | Mulligan |
| R | Refrigerator cabinet |
| SLHX | Suction line heat exchanger |
| STD | Standard deviation |
| sys | Systematic |
| tot | Total |
| vap | Vapor |
| wall | Cabinet wall |

# 1. Introduction

Due to environmental and legislative concerns, the refrigeration and air-conditioning industry is making major efforts to improve the energy efficiency of residential appliances and switch to more environmentally friendly refrigerant types. Unfortunately, many of the viable alternative low global warming potential (GWP) replacement options (GARS) [1] for the current refrigerants tend to have less favorable thermodynamic properties that result in undesirable reductions in system performance, or other drawbacks. Some of the other drawbacks include high flammability, such as in the case of isobutane and propane. Government regulations prohibit the use of these flammable refrigerants in some applications for safety reasons. In order to meet the challenge of minimizing energy consumption while replacing the currently used refrigerants in accordance with regulations, potential working fluid replacement options must be explored through both experimentation and simulation.

One of the major segments of the refrigeration industry is the household refrigerator-freezer market. The widespread use of household refrigerator-freezers provides an opportunity for substantial energy savings, and the 100 million new units sold annually across the globe represent a considerable quantity of refrigerant [2]. Household refrigerators in the North American market typically use HFC-134a as a refrigerant because it has zero ozone depletion potential, favorable thermodynamic properties, and is non-flammable. The issue with R134a is that it has a relatively high 100-year GWP of 1,430 [3], which is a measure of its effect on the environment as a green house gas relative to carbon dioxide.

Two alternative low GWP options that are being considered as replacements for R134a in household refrigerators are HFO-1234yf and HFO-1234ze. The household refrigerator-freezer sector is paying particular attention to using R1234yf as an R134a replacement due to the similar thermodynamic characteristics. Another reason that R1234yf is being considered as a replacement option for R134a is because it has a very low 100-year GWP rating of ~4, which is approximately 350 times lower than R134a [4], [5]. Among the various alternative low GWP refrigerant choices, one of the advantages of using R1234yf as an R134a replacement is that it shows promise as a direct drop-in replacement without system modifications because of the similar thermodynamic properties. The biggest issue for the acceptance and implementation of R1234yf is the fact that it is mildly flammable, which can create potential fire hazards for equipment which utilizes the refrigerant. The burning velocity of R1234yf has been found to be less than 10 cm/s, which qualifies it for the new 2L classification defined in ANSI/ASHRAE Standard 34 [6]. Pending new regulations, this classification has the potential to allow the implementation of R1234yf for household refrigerators, from which Class 2 refrigerants are currently banned [7]. The thermodynamic and transport property libraries of Engineering Equation Solver (EES) [8] were used to develop a chart of the thermophysical properties of R134a, R1234yf, and R1234ze over a temperature range common for household refrigerators. Some of the relevant properties are shown in Table 1.

**Table 1: Thermophysical properties of R134a, R1234yf, and R1234ze [8]**

| Refrigerant | Temperature | Saturation Pressure | Latent Heat | Specific Heat $(c_p)$ | | Density | | Thermal Conductivity | | Viscosity | |
|---|---|---|---|---|---|---|---|---|---|---|---|
| | °C | kPa | kJ/kg | kJ/kg-K | | kg/m$^3$ | | mW/m-K | | μPa-s | |
| | | | | Liq. | Vap. | Liq. | Vap. | Liq. | Vap. | Liq. | Vap. |
| R134a | -25 | 106.5 | 216.3 | 1.280 | 0.796 | 1374.0 | 5.5 | 104.7 | 9.6 | 371.8 | 9.9 |
| | -7.5 | 221.3 | 204.2 | 1.320 | 0.862 | 1319.0 | 11.0 | 97.8 | 11.4 | 292.9 | 10.6 |
| | 10 | 414.9 | 190.8 | 1.369 | 0.941 | 1261.0 | 20.2 | 90.3 | 13.1 | 234.2 | 11.3 |
| | 27.5 | 716.8 | 175.5 | 1.433 | 1.040 | 1197.0 | 34.9 | 82.0 | 14.8 | 188.5 | 12.1 |
| | 45 | 1161 | 157.6 | 1.529 | 1.177 | 1125.0 | 57.7 | 73.1 | 16.6 | 151.2 | 13.0 |
| R1234yf | -25 | 123.0 | 177.9 | 1.217 | 0.847 | 1251.0 | 7.2 | 83.5 | 7.5 | 305.4 | 10.3 |
| | -7.5 | 243.1 | 168.1 | 1.283 | 0.911 | 1199.0 | 13.7 | 77.8 | 8.6 | 242.0 | 11.1 |
| | 10 | 437.7 | 156.8 | 1.350 | 0.983 | 1144.0 | 24.2 | 71.3 | 9.8 | 193.7 | 11.9 |
| | 27.5 | 731.7 | 143.7 | 1.427 | 1.070 | 1083.0 | 40.6 | 64.2 | 11.2 | 156.3 | 12.7 |
| | 45 | 1153 | 127.9 | 1.530 | 1.186 | 1012.0 | 65.9 | 56.4 | 12.8 | 125.9 | 13.8 |
| R1234ze | -25 | 78.5 | 197.1 | 1.179 | 0.742 | 1311.0 | 4.5 | 65.1 | N/A | 187.6 | N/A |
| | -7.5 | 164.5 | 186.5 | 1.225 | 0.811 | 1260.0 | 9.1 | 61.7 | N/A | 162.9 | N/A |
| | 10 | 310.3 | 175.1 | 1.269 | 0.889 | 1208.0 | 16.7 | 58.2 | N/A | 142.4 | N/A |
| | 27.5 | 538.8 | 162.3 | 1.320 | 0.982 | 1154.0 | 28.8 | 54.6 | N/A | 124.3 | N/A |
| | 45 | 876.7 | 147.5 | 1.388 | 1.100 | 1094.0 | 47.6 | 50.6 | N/A | 107.6 | N/A |

To simplify the identification of the differences between the two alternative low GWP refrigerants and R134a, a second chart was created which shows the properties of R1234yf and R1234ze relative to R134a. The chart of the relative properties is shown in Table 2, where the magnitudes of the relative differences have been color-coded. Green is used to identify values within 10%, yellow within 10% to 20%, and red for greater than 20%. One of the important things to note is that the saturation pressures of R1234ze are significantly lower than R134a, which means that the cycle will operate significantly below atmospheric pressure during evaporation. The vapor density of R1234ze is also significantly lower than R134a, which means that the mass flow rate of a compressor would be reduced, possibly requiring a redesign of the compressor.

**Table 2: Thermophysical properties of R1234yf and R1234ze, relative to R134a (green within 10%, yellow between 10% and 20%, and red greater than 20%) [8]**

| Refrigerant | Temperature °C | Saturation Pressure kPa | Latent Heat kJ/kg | Specific Heat (c_p) kJ/kg-K Liq. | Vap. | Density kg/m³ Liq. | Vap. | Conductivity mW/m-K Liq. | Vap. | Viscosity µPa-s Liq. | Vap. |
|---|---|---|---|---|---|---|---|---|---|---|---|
| R1234yf | -25 | 1.15 | 0.82 | 0.95 | 1.06 | 0.91 | 1.30 | 0.80 | 0.78 | 0.82 | 1.04 |
| | -7.5 | 1.10 | 0.82 | 0.97 | 1.06 | 0.91 | 1.24 | 0.79 | 0.76 | 0.83 | 1.04 |
| | 10 | 1.05 | 0.82 | 0.99 | 1.05 | 0.91 | 1.20 | 0.79 | 0.75 | 0.83 | 1.05 |
| | 27.5 | 1.02 | 0.82 | 1.00 | 1.03 | 0.90 | 1.17 | 0.78 | 0.75 | 0.83 | 1.05 |
| | 45 | 0.99 | 0.81 | 1.00 | 1.01 | 0.90 | 1.14 | 0.77 | 0.77 | 0.83 | 1.06 |
| R1234ze | -25 | 0.64 | 1.11 | 0.97 | 0.88 | 1.05 | 0.63 | 0.78 | N/A | 0.61 | N/A |
| | -7.5 | 0.68 | 1.11 | 0.95 | 0.89 | 1.05 | 0.66 | 0.79 | N/A | 0.67 | N/A |
| | 10 | 0.71 | 1.12 | 0.94 | 0.90 | 1.06 | 0.69 | 0.82 | N/A | 0.74 | N/A |
| | 27.5 | 0.74 | 1.13 | 0.93 | 0.92 | 1.07 | 0.71 | 0.85 | N/A | 0.80 | N/A |
| | 45 | 0.76 | 1.15 | 0.91 | 0.93 | 1.08 | 0.72 | 0.90 | N/A | 0.85 | N/A |

It is seen that R1234yf exhibits similar properties to R134a, including very similar saturation pressures, which means that the cycle can operate at similar conditions. The vapor density of R1234yf is moderately higher than that of R134a, which means that the compressor mass flow rate will increase, likely resulting in increased capacity. The major drawback of R1234yf is the lower thermal conductivity of the liquid and vapor phases. This lower conductivity indicates that the heat transfer capabilities of the fluid may be less than R134a, possibly requiring redesign of the heat exchangers or even a reduction in the system efficiency. Overall, it is anticipated that R1234yf will serve as a suitable drop-in replacement for R134a with reduced heat transfer and increased mass flow rate. R1234ze will not match well at drop-in conditions because of lower system pressures and lower mass flow rates, and would likely require the redesign of the compressor and expansion device.

One possible remedy for R1234yf's flammability issue is to create a mixture of R134a and R1234yf. Since the two refrigerants have similar thermodynamic characteristics, a mixture of the two has the potential to work well as a working fluid for a refrigerator-freezer. The addition of R134a to the R1234yf also has the potential to reduce the flammability of the refrigerant, perhaps to levels at which it would fall into non-flammable regulation categories, such as Class 1 in ANSI/ASHRAE Standard 34 [6]. Since R134a is already considered to be non-flammable, certain R134a/R1234yf mixtures have the potential to fall into the same category while having a lower GWP than pure R134a. This compromise between flammability and GWP would allow manufacturers to lower the environmental impact of the refrigerant while still satisfying all of the current flammability standards without major modifications to the current systems. An example of a threshold set by legislation is the European Union's introduction of a mobile air-conditioning regulation that requires the use of refrigerants with 100-year GWP's less than 150 [9].

Simulations and experimental testing have been conducted for R1234yf in the application of automobile air conditioning, and results have been mostly positive. In several cases, R1234yf has been shown to have less than a 5% decrease in energy efficiency when compared with R134a [10],[11]. Since R1234yf is a relatively new refrigerant and is not yet freely available in the market, there has been little analysis of its performance for the household refrigerator application. Additionally, there has been little experimentation performed for stationary applications, and currently there is no published experimental data available for household refrigerators.

Leck (2009) presented modeling results for a basic thermodynamic cycle with a suction line heat exchanger and evaporation temperature of -2°C, which would be considered medium temperature refrigeration [12]. The results indicated that the COP of the R1234yf cycle would be between 1.7% and 7.2% lower than the R134a cycle depending on the condensing temperature, which was studied from 30°C to 56°C.

Leck (2010) also presented modeling results for a basic thermodynamic cycle for medium temperature commercial refrigeration at an evaporation temperature of -10°C and a condensing temperature of 40°C [13]. The results indicated that R1234yf would have a 43% lower evaporation capacity and 7% better COP than the R404A, and an equal evaporation capacity and 1% lower COP than R134a.

Fujitaka et al. (2010) studied the performance of R1234yf as a drop-in replacement for R410A in a 4 kW room air conditioning application [14]. The ideal theoretical model predicted a 5.6% increase in COP when using R1234yf, while the experimental work showed a COP decrease of 58% and cooling capacity decrease of 30%. The differences between the theoretical model and the experimental work were attributed to the increased pressure drop of the pipes and the evaporator when using R1234yf, which would indicate that a system redesign would be required.

Spatz (2009) performed experimental work on a beverage cooler for medium temperature refrigeration [15]. The evaporation temperature was -6.5°C, and the condensing temperature 45°C. For a drop-in replacement of R134a, the data showed that R1234yf would exhibit a 4% decrease in both evaporator capacity and COP, and R1234ze would exhibit a decrease in evaporator capacity of 17% and a decrease in COP of 13%.

In summary, R1234yf looks to be a promising alternative low GWP refrigerant replacement for R134a in household refrigerators from both an environmental impact and thermophysical property view-point. The modeling studies that have been published show promising performance for R1234yf, but it is apparent that a more detailed study specific to household refrigerators is needed. Thus, an analysis must be performed to identify the steady-state and transient performance of R1234yf when used as a drop-in replacement fluid in a household refrigerator. Additionally, steady-state simulations must be conducted to determine the viability of using R134a/R1234yf mixtures for household refrigerators. A quantification of the performance characteristics of the alternative low GWP refrigerants mentioned will aid manufacturers when making decisions about the development direction of new refrigerants as legislative requirements require the phase-out of R134a.

# 2. Experimental Work

To evaluate the potential of alternative low GWP fluids through simulations, the first step was to experimentally validate the models. In order to validate the models, experimentation must be performed at fixed test conditions to produce repeatable, accurate data. A test facility was created to measure all of the relevant thermodynamic properties of a household refrigerator under transient cycling conditions. Beyond system operation performance experimentation, additional reverse heat leak testing was performed. The reverse heat leak testing evaluated the insulation properties of the cabinets to determine the overall heat transfer coefficients. The overall heat transfer coefficients were necessary to create accurate models of the transient heat transfer between the interior air of the cabinets and the ambient air.

## 2.1. *Test Facility Configuration*

A household 27.6 ft$^3$ (782 L) French door refrigerator-freezer was outfitted with measurement equipment for testing and evaluation purposes. The refrigerator-freezer unit had a bottom mounted freezer, French door style fresh food compartment with through-the-door ice and water dispenser, 115 V AC reciprocating hermetically-sealed compressor, automatic electrical defrost heater, and was charged with 140 grams of R134a refrigerant as a working fluid. The compressor was a single fixed-speed type, with thermostat-based on and off control. The condenser was a forced convection type, which utilized an AC motor driven fan. The unit utilized a single evaporator in the freezer compartment which had an AC motor driven fan and an electrically actuated mechanical damper. The damper system was controlled by a refrigerator compartment thermostat which toggled the damper between fully closed or partially opened. When the damper

was fully closed, all of the evaporator outlet air flow was routed to the freezer compartment. When the damper was partially opened, a fixed portion of the volumetric air flow rate was routed to the refrigerator compartment in addition to the remaining air flow to the freezer compartment.

The refrigerator-freezer unit was installed in an environmental test chamber in the Heat Pump Laboratory of the Center for Environmental Energy Engineering at the University of Maryland. The environmental chamber is capable of controlling the ambient temperature conditions over a range from $5^{\circ}$C to $43.3^{\circ}$C using a 3.5 kW capacity refrigeration system. The environmental chamber uses a baffled dropped ceiling in order to maintain air velocities below 1 m/s at all points surrounding the refrigerator-freezer unit.

In the fresh food cabinet three thermocouple masses were installed in order to measure the average air temperature within the compartment. The thermocouple masses were constructed by soldering a T-type special thermocouple into a hole drilled in the middle of a solid cylindrical copper mass with a diameter of 2.54 cm and height of 2.54 cm. These thermocouple masses were spatially distributed as shown in Figure 1 and Figure 2 in order to provide an average air temperature reading for the cabinet. The freezer cabinet also used three copper thermocouple masses of the same type in order to measure the average air temperature within the compartment; the spatial distribution of these masses is shown in Figure 1 and Figure 3.
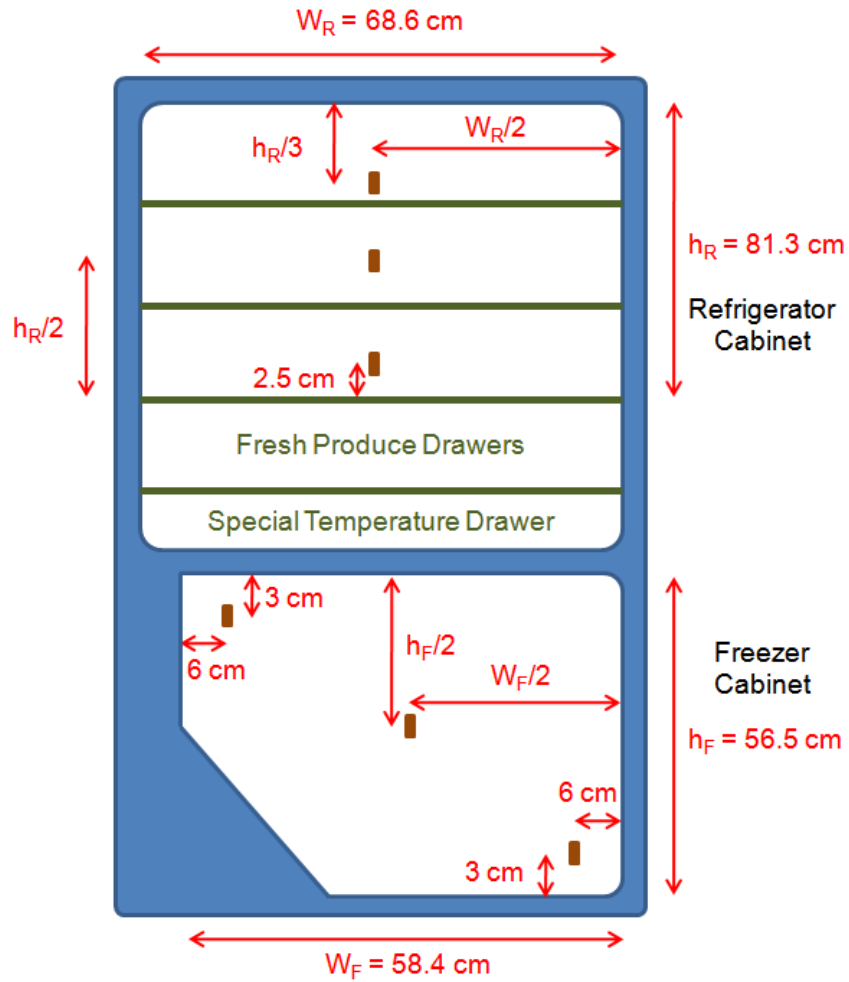
**Figure 1: Side view of thermocouple mass placement in refrigerator-freezer cabinets (thermocouple masses were centered along the width with respect to a front view)**

**Figure 2: Thermocouple mass placement in refrigerator cabinet**

**Figure 3: Thermocouple mass placement in freezer cabinet**

The thermocouple wires which connected the thermocouple masses on the interior of the cabinets to the data acquisition system were routed out of the sides of the front of the cabinet where the doors seal against the cabinet walls. At locations where the door seals were displaced by the wires, moldable duct sealant (clay) was used to block air flow through the gaps, and insulation foam was used to reduce the heat gain introduced by the modifications made. The insulated sections of the fresh food and freezer cabinet seals are shown in Figure 4**.**

**Figure 4: Insulation of the door gaskets where the thermocouple wires enter the fresh food cabinet (left) and freezer cabinet (right)**

The vapor compression cycle consists of four main components: a reciprocating compressor, a steel spiral fin and tube heat exchanger condenser, a capillary tube expansion device which is brazed to the suction line to create a suction-line heat exchanger (SLHX), and an aluminum tube and fin heat exchanger with variably spaced fins as the evaporator. The compressor compresses low-pressure superheated vapor refrigerant to a high-pressure superheated vapor. This superheated high-pressure vapor then enters the condenser where forced air convection transfers heat from the refrigerant to the ambient air in order to condense the refrigerant into the liquid phase. The liquid refrigerant then enters the hot pipe component, which is a steel tube that is routed along the inside of the exterior cabinet shell in order to reject additional heat and maintain the cabinet door seals above the dew point to prevent condensation of water vapor. The hot

pipe provides additional subcooling to the high-pressure liquid refrigerant, bringing it closer to the ambient air temperature. The subcooled liquid then enters the capillary tube SLHX where it is expanded to a low-pressure two-phase fluid and exchanges heat with the superheated vapor from the evaporator suction outlet. The SLHX lowers the vapor quality of the two-phase refrigerant at the inlet of the evaporator in order to increase evaporation capacity, as well as increasing the degree of superheat of the refrigerant from the evaporator outlet to the compressor inlet. The additional heating of the refrigerant after the evaporator outlet ensures that liquid doesn't enter the compressor suction port, which would cause severe damage to the compressor components. The two-phase refrigerant at the outlet of the capillary tube is then evaporated inside of the freezer cabinet through forced convection heat transfer with the cabinet air. This refrigerant is generally a slightly superheated vapor at the evaporator outlet which then exchanges heat in the SLHX before entering the compressor suction and completing the cycle.

The measurement instrumentation that was installed into the refrigeration cycle was designed so that all of the relevant properties of the cycle could be measured or calculated. This included the measurement of the power consumption of the entire unit as well as the compressor individually. Another measured system property was the refrigerant mass flow rate, which was accomplished by installing a Coriolis mass flow meter before the suction port of the compressor. Additionally, the pressures and temperatures of the refrigerant were measured at all of the relevant state points, i.e. the component inlets and outlets. A component level schematic of the refrigeration cycle can be seen in Figure 5.
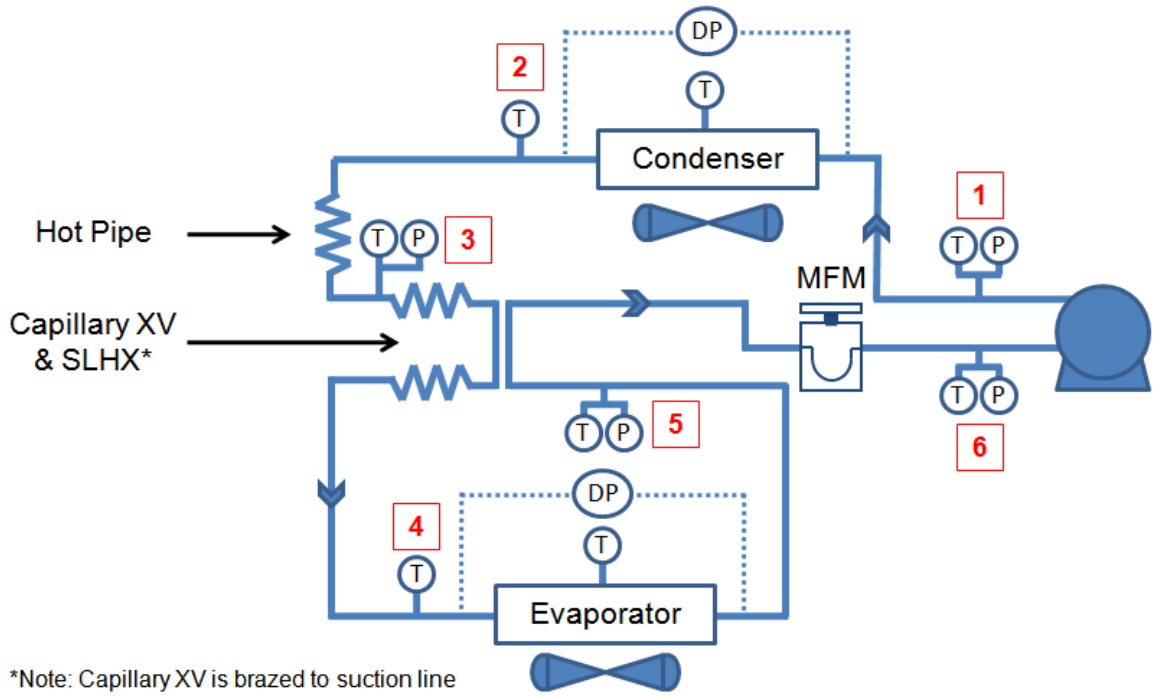
**Figure 5: Component-level schematic of the refrigerator-freezer test facility**

To measure the effect of the additional suction line pressure drop caused by the Coriolis mass flow meter, a system of valves was used to create a bypass. The configuration and installation of the valves is shown in Figure 6.
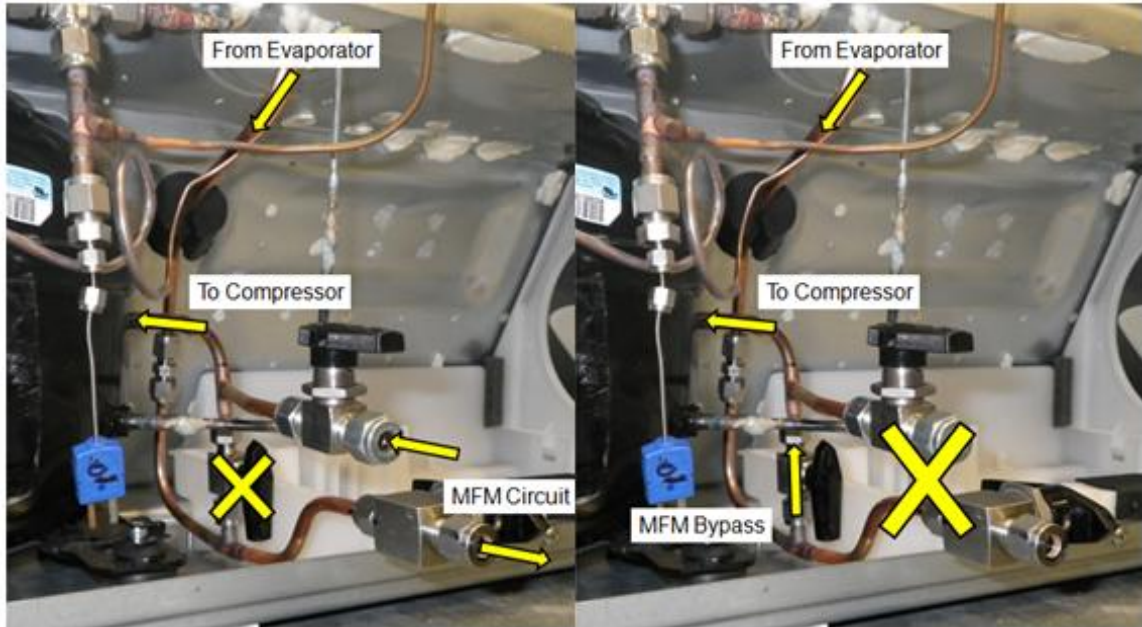
**Figure 6: Physical hardware setup for mass flow meter bypass valves**

In order to measure pressure drop across the evaporator, two pressure taps were created. These pressure taps were made from capillary tubes which connected to the refrigerant circuit directly before and after the evaporator within the interior evaporator compartment of the freezer cabinet. The capillary tubes were then routed through a 1 cm hole drilled through the rear cabinet wall, as demonstrated in Figure 7.
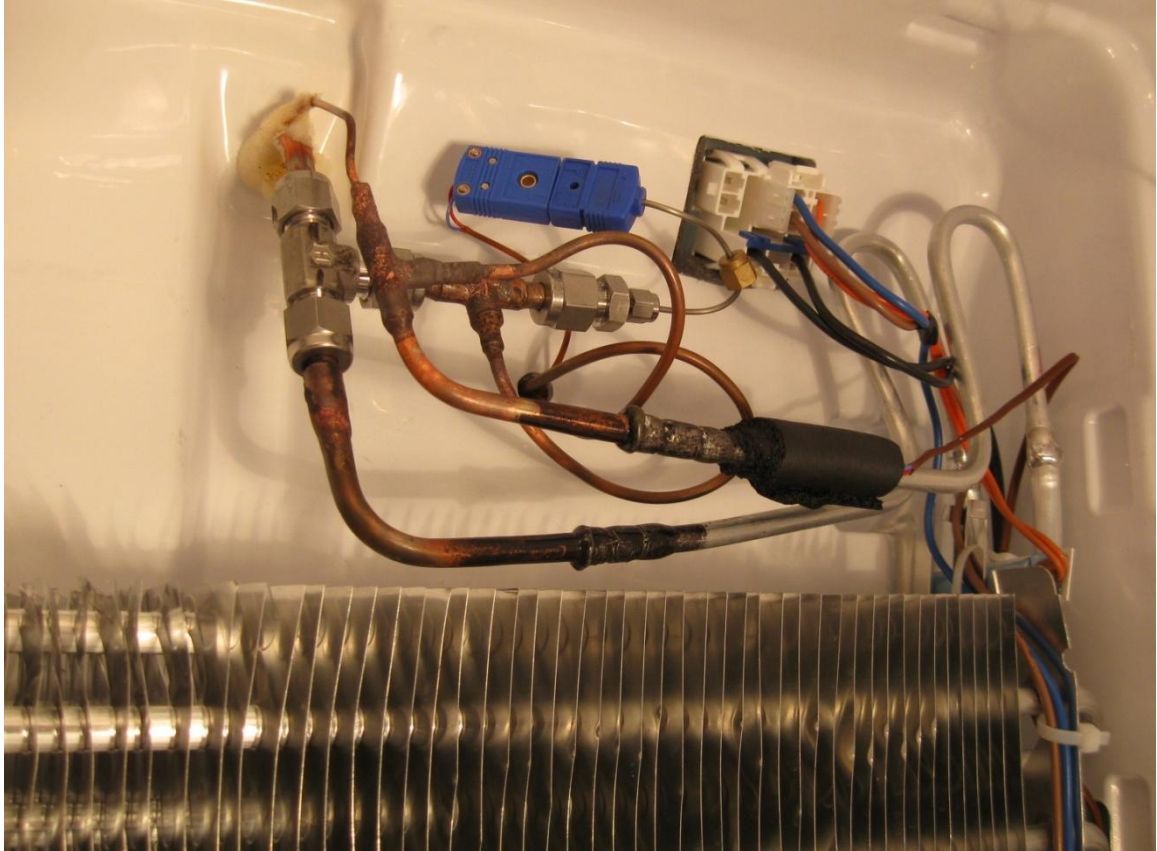
**Figure 7: Evaporator pressure tap capillary tubes**

All of the pressure transducers were attached to the exterior rear of the cabinet using adhesive tape, and the mass flow meter was mounted horizontally, where it was supported by, and insulated from, the floor of the environmental chamber. In order to install the sensor cabling and refrigerant tubing, some modifications were made to the panel enclosing the condenser/compressor compartment. Small amounts of material were removed from sections of the panel which were already perforated for air flow purposes. Although these modifications affect the airflow which exits the condenser and flows over the compressor, the degree of interference is slight considering that the air flow perforations were already greater than 50% of the area. A picture of the exterior rear of the cabinet with all of the sensors installed is shown in Figure 8. After all of the sensor

equipment was installed it was calculated that the increased tubing volume required an

increase in R134a refrigerant charge of 15 grams. The total refrigerant charge was

therefore increased from the original 140 grams to a new charge level of 155 grams.



**Figure 8: Exterior rear of the cabinet with installed sensors shown**

The power supplied to the unit was regulated in order to eliminate transient

fluctuations, and maintain a root mean squared (RMS) voltage of 115 V AC. The

regulation was accomplished by converting the main building electricity of 115 VAC to

24 V DC, and then converting the 24 V DC to 220 V AC. The 220 V AC supply was then

controlled with a Variac (autotransformer), to supply 115 V power to the tested unit, to within ±1 V AC.

A list of the manufacturer, model number, range, and systematic uncertainty specifications for all of the measurement equipment is given in Table 3. All of the instruments were connected to National Instruments field point modules, and LabVIEW software was used to record data and calculate system performance parameters in real-time.

**Table 3: Specifications of instruments**

| Instrument | Type | Manufacturer | Model # | Range | Systematic Uncertainty |
|---|---|---|---|---|---|
| Mass Flow Meter | Coriolis | Micro Motion | CMF025 | 0.8 – 5 g/s | ±0.833% f.s. |
| Pressure | Strain | Setra | 280E | 0 – 17.2 bar | ±0.11 f.s. |
| Differential Pressure | Strain | Setra | 2301010P D2F11B | 0 – 68.9 kPa | ±0.25% f.s. |
| Watt Meter (System) | Watt Transducer | Ohio Semitronics | GW5-001E | 0 – 500 W | ±0.2% reading |
| Watt Meter (Compressor) | Watt Transducer | Ohio Semitronics | PC5-002X5 | 0 – 1000 W | ±0.5% f.s. |
| Thermocouple | T-type (special) | Omega | N/A | -250 to 350°C | ±0.5°C |
| Relative Humidity | Capacitance | Testo | 6651 | 0 – 100 %RH | ±1.7% RH |

### 2.2. *Uncertainty Analysis*

In order to calculate the uncertainty in a measured variable, both the systematic uncertainty of the measuring device and the random error experienced during measurement must be considered. The systematic errors of the measurement equipment used are given in Table 3. The random measurement errors are equal to the standard deviation of the data used to calculate the average value. The total error is the summation

of the systematic and random error, defined as Equation (1).

$$u_{tot} = u_{sys} + u_{STD} \qquad (1)$$

Where:

$u_{tot}$ = total uncertainty of a measured value

$u_{sys}$ = systematic uncertainty of a measured value

$u_{STD}$ = random uncertainty of a measured value (one standard deviation)

In order to calculate the systematic uncertainty of a calculated variable, the systematic uncertainty of each measured variable used in the calculation must be included. In order to propagate these uncertainties, the Pythagorean summation of uncertainties method is used, which is defined as Equation (2).

$$u_F = \sqrt{\left(\frac{\partial F}{\partial v_1} * u_1\right)^2 + \left(\frac{\partial F}{\partial v_2} * u_2\right)^2 + \cdots + \left(\frac{\partial F}{\partial v_i} * u_i\right)^2} \qquad (2)$$

Where:

$F$ = calculated variable

$u_F$ = uncertainty in the calculated variable "F"

$u_i$ = uncertainty of the measured variable

$v_i$ = measured variable

$i$ = number of variables used to calculate "F"

The random error was calculated as one standard deviation of the measured variable from the collected data set, as defined in Equation (3).

$$u_{STD} = \sqrt{\frac{1}{N-1}\sum_{j=1}^{N}(x_j - \bar{x})^2} \qquad (3)$$

Where:

$N$ = number of data points in the collected data set

$j$ = data point index

$x_j$ = measured variable data point at index $j$

$\bar{x}$ = average of the measured variable over the entire data set

For each of the measured and calculated variables typical values for the propagated systematic uncertainties, the random uncertainties, and the total uncertainties are shown in Table 4. The definitions of several of these variables and calculated values will be introduced in subsequent sections.

**Table 4: Typical variable uncertainties**

| Variable | Units | Systematic | Random | Total |
|---|---|---|---|---|
| Pressure | kPa | 1.90 | 2.18 | 4.08 |
| In-stream Temperature | °C | 0.5 | 0.19 | 0.69 |
| Average Cabinet Air Temperature | °C | 0.29 | 0.05 | 0.34 |
| Average Ambient Temperature | °C | 0.17 | 0.09 | 0.26 |
| Differential Pressure | kPa | 0.17 | 0.10 | 0.27 |
| Mass Flow Rate | g/s | 0.025 | 0.019 | 0.044 |
| Total Power Consumption | W | 0.20 | 0.51 | 0.71 |
| Enthalpy | kJ/kg | 0.75 | 0.10 | 0.85 |
| Evaporator Superheat | K | 0.59 | 0.17 | 0.76 |
| System COP | - | 0.71 | 0.024 | 0.095 |
| Evaporator Capacity | W | 0.12 | 2.92 | 3.04 |
| Energy Input (Reverse Heat Leak Testing) | W-hr | 0.2 | - | 0.2 |
| Yearly Energy Consumption | kWh/yr | 1.8 | - | 1.8 |

## 2.3. *Energy Consumption Testing*

### 2.3.1. Test Procedures and Conditions

As stated previously, the tested unit was housed within a temperature-controlled environmental chamber. All of the testing performed was done in accordance with the United States Department of Energy (DOE) testing standard conditions [16]. The testing standard can be found in the United States Federal Registry: 10 CFR Part 430, entitled "Uniform Test Method for Measuring the Energy Consumption of Electric Refrigerators and Electric Refrigerator-Freezers." This testing standard is designed to simulate the

typical energy use of a household refrigerator-freezer while implementing testing procedures which minimize testing complexity, duration, and potential for testing repeatability issues. The unit is tested at an ambient temperature of 32.2°C, which is higher than what would be expected in an average household. This higher ambient temperature allows for an approximation of the cabinet heat losses without needing to simulate cabinet door openings, which tend to be difficult and expensive to implement reliably. There was also additional testing performed using all of the DOE standard procedures except for the ambient temperature, which was decreased to 20°C. The lower ambient temperature testing condition allowed for the analysis of system performance trends based on ambient temperature. For all of the testing conducted, the special temperature drawer was set to the coldest setting "Meat" (1°C), and the automatic ice maker was electrically disabled using the switch, as per the DOE testing standard instructions.

In the DOE testing standard, the ambient temperature around the cabinet is to be maintained at a constant 32.2±0.6°C. The refrigerator-freezer unit that was tested falls into the DOE standard category of "refrigerator-freezer with variable defrost control." The energy test is conducted in two parts: the standard steady-state energy consumption test, and the long time automatic defrost energy consumption test. The practical definition of "steady-state" operation of a transient system is when the unit is transiently cycling with whole cycles which don't change relative to one another. The official DOE criterion for the "Steady State Condition" is that the temperature measurements in the cabinets are not changing by more than 0.023°C per hour during a stabilization period. For purposes

of consistency and repeatability, all of the DOE testing results for yearly energy consumption are extrapolated from six complete on and off cycles.

For the steady state energy test, the first phase of testing occurs with the unit's thermostat set to its middle settings, which are a refrigerator temperature of 4.4°C and a freezer temperature of -17.2°C. The test is then run, and the average cabinet temperatures are compared with the standardized maximum average refrigerator/freezer cabinet temperatures of -15°C/7.2°C. The thermostat conditions for the second phase test are chosen to be either the warmest or coldest possible settings such that the cabinet temperatures from the two test phases bound the standardized cabinet temperatures. For the unit tested, the middle thermostat settings resulted in temperatures lower than the standardized temperatures, and therefore the warmest thermostat settings were used for the second phase of the testing. The warmest thermostat settings corresponded to a refrigerator temperature of 7.8°C and a freezer temperature of -13.3°C. The results of the warmest thermostat setting tests were then used in the yearly energy consumption calculations, which will be discussed in subsequently.

The second part of the DOE standard is the long time automatic defrost energy consumption test, which was performed in order to estimate the yearly energy consumption of the evaporator defrosting system. The testing was repeated for both the middle and warmest thermostat settings for use in the yearly energy consumption calculations. The test involves measuring the energy consumption of the unit during a defrost cycle. The defrost cycle is measured from the start of the off-cycle of the last compressor on-cycle before the "precool" cycle occurs to the end of the recovery cycle after the defrost period. The "precool" cycle is an extended compressor on-cycle which

cools the freezer cabinet to temperatures below the normal thermostat "off" point. This extra cooling ensures that the freezer compartment remains at adequately low temperatures throughout the duration of the defrost cycle in order to protect the food contents from thawing. The defrost period then occurs, in which an electrical resistance heater is used to heat the evaporator coil above the freezing point of water in order to melt and remove accumulated frost. The energy consumption measurement continues until the end of the off-cycle which occurs after the "recovery" cycle. The recovery cycle is the first compressor on-cycle after the defrost period occurs, and it is typically an extended cycle which is used to return the freezer cabinet to the appropriate temperature level after being heated during the defrost period. A basic schematic of the measured defrost period is given in Figure 9.
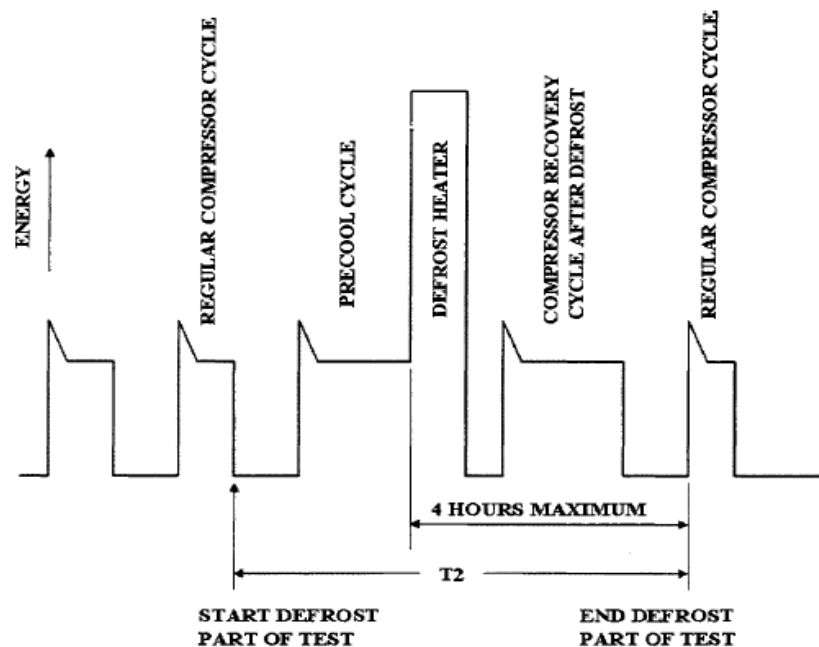


**Figure 9: Measured defrost cycle of DOE testing standard [16]**

After the completion of both parts of the energy consumption test, the overall yearly energy consumption of the unit can be calculated. This calculation is performed

using the DOE standard equation for long time automatic defrost units. The formula takes into account the energy consumption during steady state cycling as well as the defrost cycle, all weighted by the frequency of the defrost cycle. The defrost cycle frequency factor in the equation is "CT," which was known. The explicit yearly energy consumption formula is given in Equation (4).

$$E = \left(\frac{1440*EP1}{T1}\right) + \left(EP2 - \left(\frac{EP1*T2}{T1}\right) * \left(\frac{12}{CT}\right)\right) \tag{4}$$

Where:

$E$ = total energy consumption [kWh/day]

$EP1$ = energy expended in first (steady-state) portion of test [kWh]

$T1$ = duration (time) of first (steady-state) portion of test [min]

$1440$ = conversion factor for minutes to days [min/day]

$EP2$ = energy expended in second (defrost) portion of test [kWh]

$T2$ = duration (time) of second (defrost) portion of test [min]

$12$ = factor to adjust for 50% run time of compressor

$CT$ = time between defrost cycle

### 2.3.2.  Results

The DOE testing standard was implemented for testing the R134a system as outlined previously. After conducting the tests with and without bypassing the mass flow meter, it was found that the additional pressure drop penalty incurred by having the mass flow meter in the circuit was only a 0.7% increase in the yearly energy consumption. Since the effect of the mass flow meter pressure drop on the yearly energy consumption was so small, the mass flow meter was not bypassed in any of the testing results shown in order to reduce testing complexity.

The most relevant test for measuring the refrigerator-freezer energy consumption is the official DOE standard conditions. For the tested unit those conditions are an ambient temperature of 32.2°C, and the warmest refrigerator/freezer thermostat settings of 7.8°C/-13.3°C. The first "steady-state" testing occurred over a time period encompassing six complete on/off cycles of the compressor. Some of the key system measurements including the system powers and average cabinet air temperatures, in-stream temperatures, pressures, mass flow rate, subcooling/superheating, and heat exchanger pressure drops are shown in the graphs of Figure 10 through Figure 15.
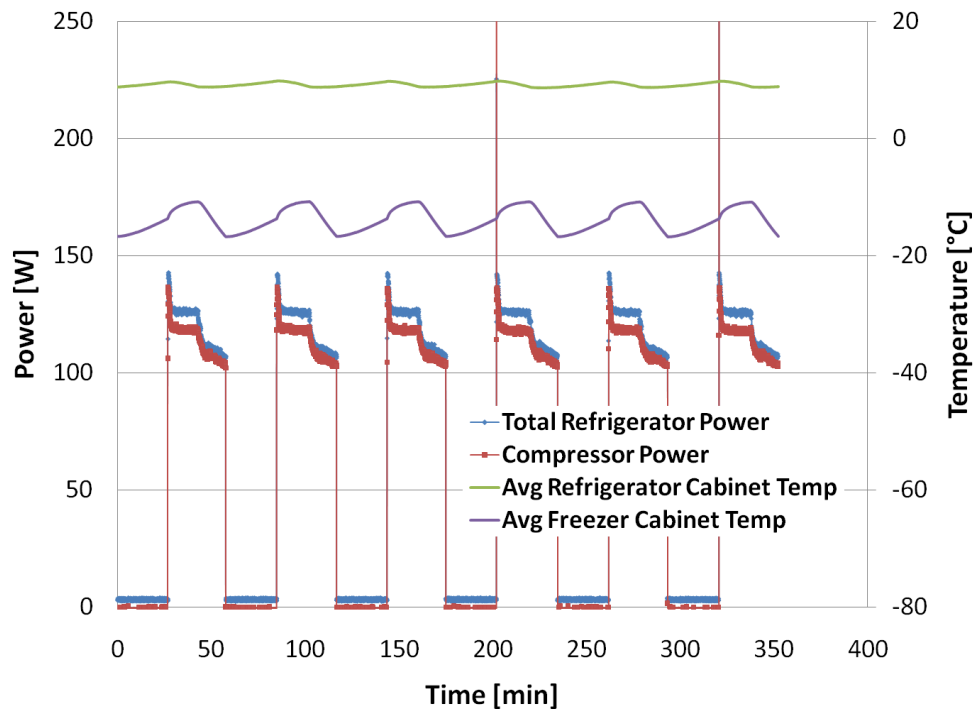


**Figure 10: System powers and average cabinet air temperatures (experimental DOE "steady-state" at T_amb = 32.2°C and "warmest" thermostat)**

26

**Figure 11: Pressures (experimental DOE "steady-state" at T_amb = 32.2°C and "warmest" thermostat)**
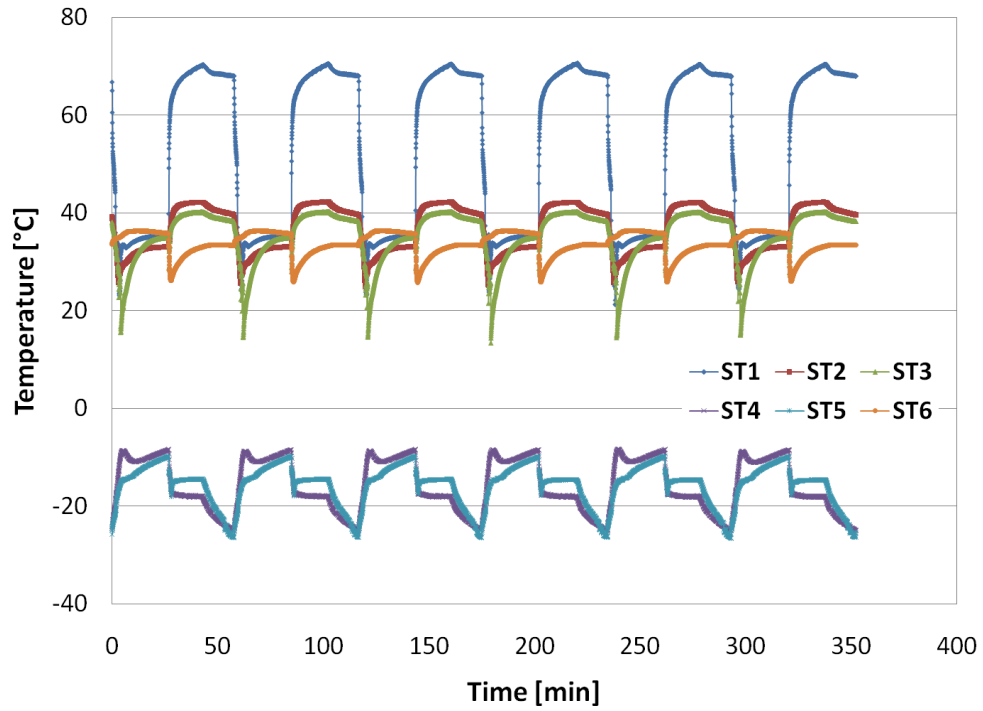
**Figure 11: Pressures (experimental DOE "steady-state" at $T_{amb} = 32.2°C$ and "warmest" thermostat)**
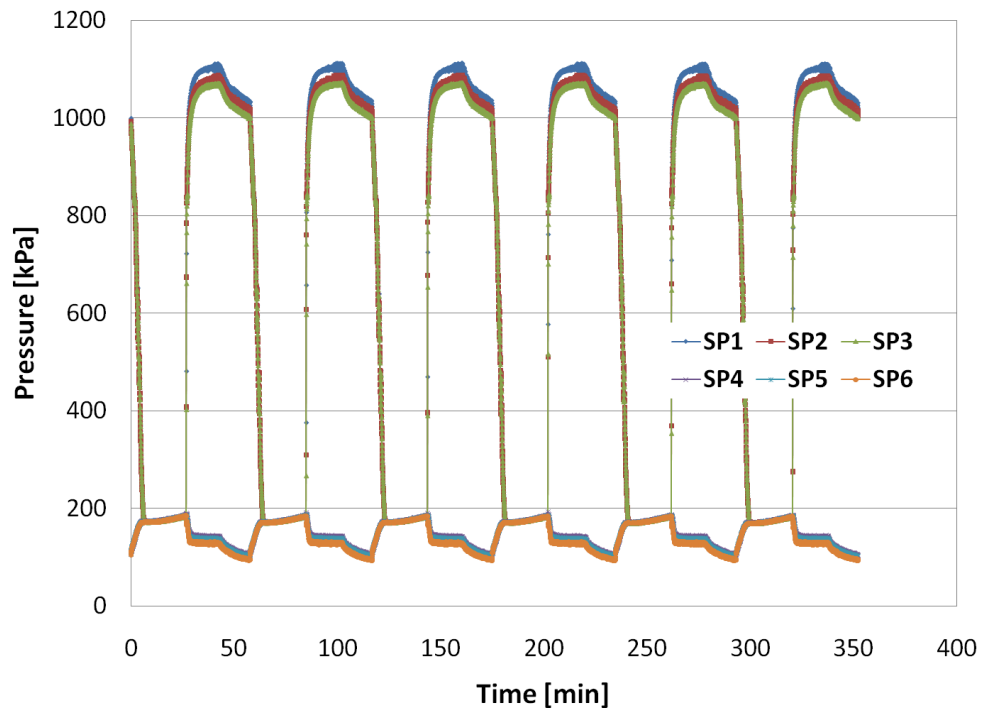


**Figure 12: In-stream temperatures (experimental DOE "steady-state" at $T_{amb} = 32.2°C$ and "warmest" thermostat)**
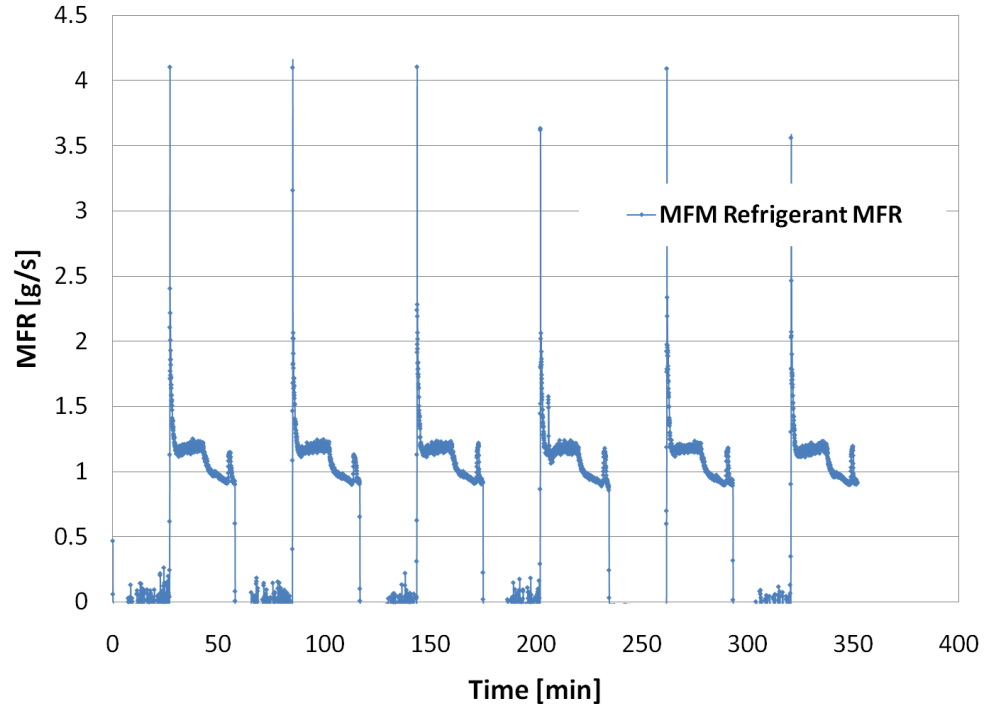
**Figure 13: Refrigerant mass flow rate (experimental DOE "steady-state" at $T_{amb}$ = 32.2°C and "warmest" thermostat)**
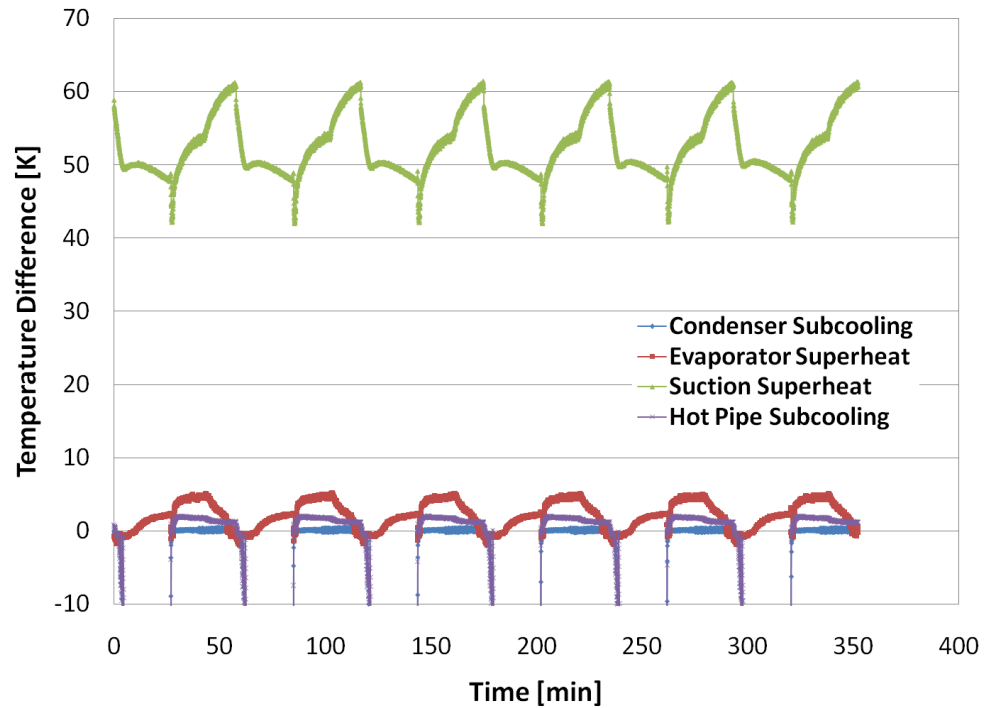


**Figure 14: Subcooling and superheat (experimental DOE "steady-state" at $T_{amb}$ = 32.2°C and "warmest" thermostat)**
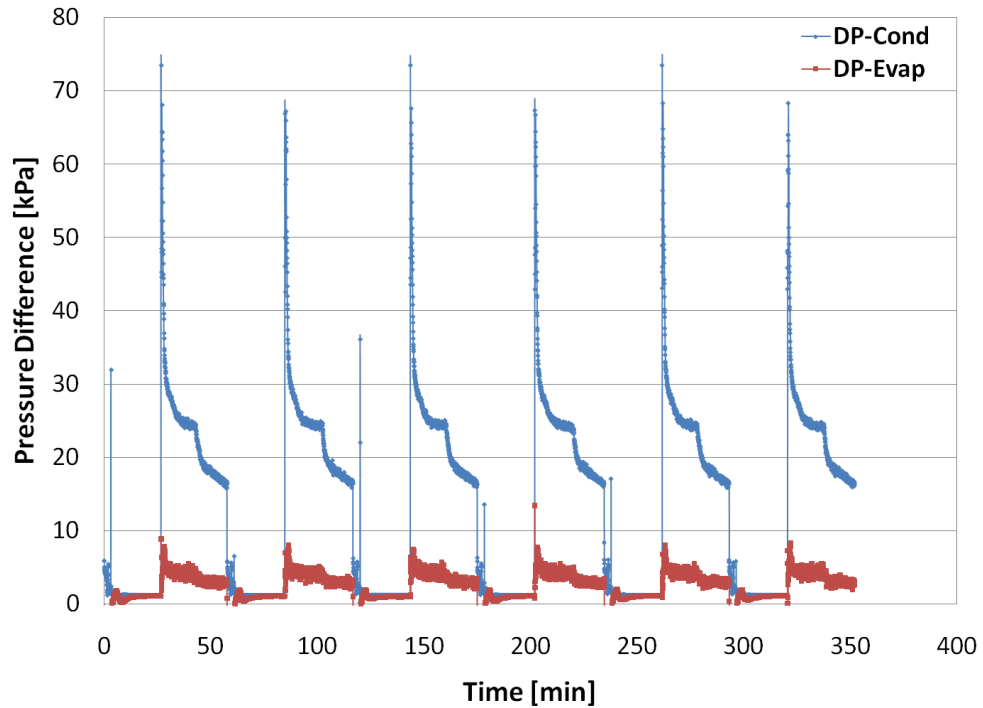
**Figure 15: Heat exchanger pressure drops (experimental DOE "steady-state" at $T_{amb} = 32.2°C$ and "warmest" thermostat)**

The energy consumption was also measured for the second phase of the DOE testing standard, the defrost cycle. The measurement included the pre-cooling cycle, the electrical resistance defrost heater cycle, and the recovery cycle as stated in the testing procedures. The total power consumption and average cabinet air temperatures are shown in Figure 16 for an ambient temperature of 32.2°C and "warmest" thermostat settings.
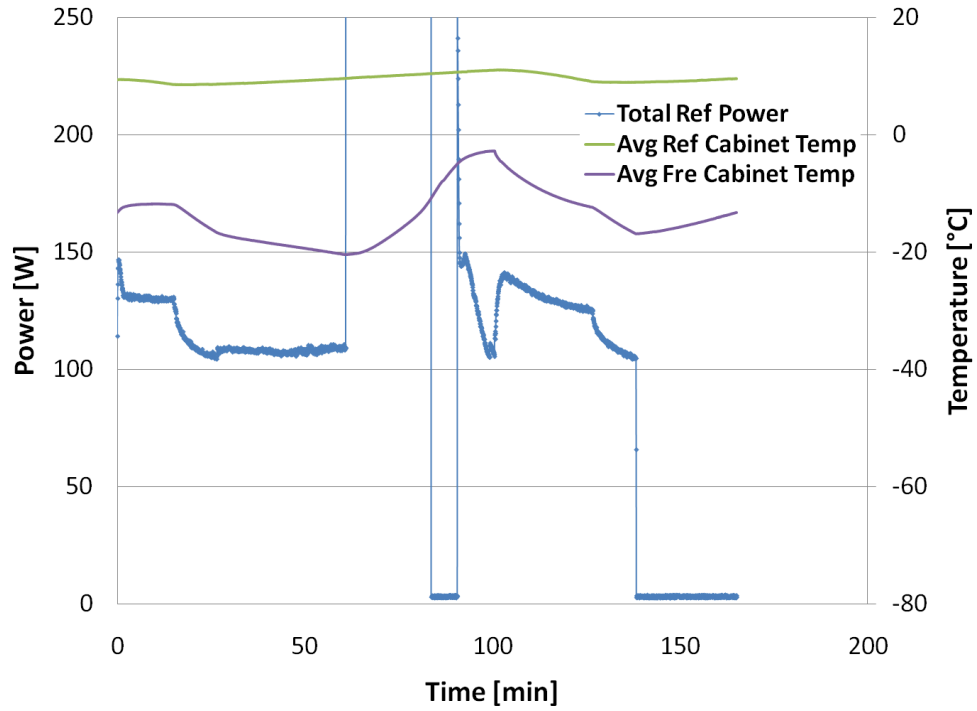
**Figure 16: System power and average cabinet air temperatures (experimental DOE defrost phase at $T_{amb} = 32.2°C$ and "warmest" thermostat)**

In order to better quantify the results from the "steady-state" portion of the testing, the total average was calculated for each of the most relevant measurement values over the on-cycle periods of all six cycles. These average on-cycle values are given in Table 5.

**Table 5: On-cycle measurement value averages (experimental DOE "steady-state" at $T_{amb}$ = 32.2°C and "warmest" thermostat)**

| Measurement | Units | Value |
|---|---|---|
| Total Refrigerator Power | W | 119.6 |
| Compressor Power | W | 114.0 |
| Average Refrigerator Cabinet Temperature | °C | 9.1 |
| Average Freezer Cabinet Temperature | °C | -12.5 |
| Refrigerant Mass Flow Rate | g/s | 1.12 |
| Evaporator Pressure Drop | kPa | 3.8 |
| Condenser Pressure Drop | kPa | 23.5 |
| Evaporator Superheat | K | 3.2 |
| Evaporator Capacity | W | 190.9 |
| Hot Pipe Subcooling | K | 1.4 |
| Discharge Pressure | kPa | 1,066.9 |
| Discharge Temperature | °C | 68.0 |
| Suction Pressure | kPa | 119.4 |
| Suction Temperature | °C | 32.1 |
| Average On-cycle Duration | min | 31.7 |
| Average Off-cycle Duration | min | 27.0 |
| Compressor Yearly Energy Consumption (without defrost) | kWh/year | 536.0 |
| Total Yearly Energy Consumption (without defrost) | kWh/year | 577.6 |

The yearly energy consumption of the compressor without defrost is 536.0±1.8 kWh/year, the total yearly energy consumption of the unit (including fans, electronic circuitry, etc.) without defrost is 577.6±1.8 kWh/year, and the total energy consumption of the unit with defrost, which is the official DOE testing standard value, is 607.6±1.9 kWh/year. The United States government mandates that each manufacturer must implement the DOE test procedures for each refrigerator-freezer unit that they sell in order to determine the yearly energy rating for an "EnergyGuide" label attached to the retail units. For the refrigerator-freezer tested herein, the "EnergyGuide" energy consumption was listed as 563 kWh/year, which is within 8% of the experimental results. The discrepancy between the manufacturer rating and the experimentally measured value can be accounted for by the modifications made to the test facility when compared with

an unmodified unit. The experimentally measured performance was degraded by both the additional refrigerant pressure drop due to the various sensors and the additional cabinet load due to wires and capillary tubing.

In addition to the results mentioned for an ambient temperature of 32.2°C and "warmest" thermostat settings, the "steady-state" DOE testing procedures were followed using the "middle" thermostat settings at an ambient temperature of 32.2°C, as well as the "warmest" and "middle" thermostat settings at an ambient temperature of 20°C. Some of the basic tabulated results for these three test conditions are given in Table 6, where the yearly energy consumption calculations are made per the DOE testing standard, and the measurement values are average values for six compressor on-cycles. The transient data including the system powers and average cabinet air temperatures, in-stream temperatures, pressures, mass flow rates, subcooling/superheating, and heat exchanger pressure drops are plotted in graphs shown in the Appendix.

**Table 6: On-cycle measurement value averages and calculated yearly energy consumptions for DOE testing standard (experimental DOE "steady-state")**

| Variables | Units | Values | | | |
|---|---|---|---|---|---|
| Ambient Temperature | °C | 32.2 | 32.2 | 20 | 20 |
| Thermostat Settings | N/A | Warmest | Middle | Warmest | Middle |
| Total Refrigerator Power | W | 119.6 | 118.4 | 106.2 | 106.1 |
| Compressor Power | W | 114.0 | 108.9 | 98.5 | 94.3 |
| Average Refrigerator Cabinet Air Temperature | °C | 9.1 | 6.1 | 8.7 | 5.4 |
| Average Freezer Cabinet Air Temperature | °C | -12.5 | -15.4 | -14.6 | -17.6 |
| Refrigerant Mass Flow Rate | g/s | 1.12 | 1.03 | 0.99 | 0.93 |
| Evaporator Pressure Drop | kPa | 3.8 | 3.5 | 4.0 | 3.6 |
| Condenser Pressure Drop | kPa | 23.5 | 20.7 | 28.0 | 24.8 |
| Evaporator Superheat | K | 3.2 | N/A | 4.4 | 3.4 |
| Evaporator Capacity | W | 190.9 | 178.2 | 183.5 | 172.0 |
| Hot Pipe Subcooling | K | 1.4 | 1.4 | 3.3 | 3.2 |
| Discharge Pressure | kPa | 1,066.9 | 1,045.6 | 762.9 | 748.3 |
| Discharge Temperature | °C | 68.0 | 68.4 | 46.2 | 47.5 |
| Suction Pressure | kPa | 119.4 | 110.7 | 100.4 | 94.1 |
| Suction Temperature | °C | 32.1 | 32.4 | 18.8 | 19.2 |
| Average On-cycle Duration | min | 31.7 | 45.5 | 18.6 | 23.2 |
| Average Off-cycle Duration | min | 27.0 | 24.7 | 37.4 | 31.5 |
| Compressor Yearly Energy Consumption (without defrost) | kWh/year | 536.0 | 616.4 | 282.7 | 344.9 |
| Total Yearly Energy Consumption (without defrost) | kWh/year | 577.6 | 681.7 | 328.2 | 409.0 |

The most notable differences between the data sets for the different thermostat settings is that as the set points become lower, the average refrigerator and freezer cabinet air temperatures decrease. The decrease in the average cabinet air temperatures causes the suction pressures to decrease due to the colder air inlet temperatures to the evaporator. The lower suction pressure results in a lower mass flow rate because the compressor moves less mass with each stroke due to the lower vapor density at the inlet. The lower mass flow rate in turn decreases the evaporator cooling capacity. The lower cabinet temperatures also increase the temperature differences between the cabinets and the

ambient air for a given ambient temperature condition. The larger temperature differences then cause an increase in cabinet heat loads. All of these factors combine to create longer compressor on-cycle times at colder thermostat settings, and subsequently increased yearly energy consumption. For instance, in the 32.2°C ambient temperature case the total yearly energy consumption rating of the unit (without defrost) at the "middle" thermostat settings is 18% higher than when the thermostat is at the "warmest" settings.

One of the most important differences between the ambient temperature cases of 20°C and 32.2°C for a given thermostat setting is that the discharge pressure is drastically reduced due to the lower condensation temperature. The lower pressure difference across the compressor reduces the compressor work and increases the volumetric efficiency. The reduced compressor work in turn reduces the yearly energy consumption of the refrigerator-freezer. In addition to the lower discharge pressure, the lower ambient temperature case also shows an increase in the off-cycle duration due to the smaller cabinet heat load. The heat load is smaller in the lower ambient temperature case because of the smaller temperature difference across the cabinet walls between the cabinet air zones and the ambient air. Increased off-cycle duration means that the ratio of on-cycle time to total refrigerator-freezer operational time is reduced. A reduction in on-cycle duration fraction leads to a reduction in the yearly energy consumption rating.

## 2.4. *Reverse Heat Leak Testing*

In addition to the experimentation done to evaluate the energy consumption of the vapor compression cycle, there was experimentation done in order to measure the overall heat transfer coefficients (UA's) of the cabinets [17]. In order to measure the overall heat transfer coefficients, a reverse heat leak test was conducted. The reverse heat leak test

utilizes controlled heating loads inside of the cabinets in order to maintain the inside

average air temperatures at fixed values above the fixed ambient temperature. The testing

is conducted while the vapor compression cycle of the refrigerator-freezer is disabled so

that the amount of heat required to maintain a fixed temperature difference between the

cabinet air and ambient air can be measured. The known heat input and temperature

differences can then be used to calculate the overall heat transfer coefficients of the

cabinets, including the walls and the door seals, which can then be used to model the heat

transfer properties of the cabinets.

### 2.4.1. Test Procedures and Conditions

In order to measure the overall heat transfer coefficients of the cabinets using a

reverse heat leak test, uniform temperatures must be maintained on the inside and outside

of the cabinet walls. In a reverse heat leak test the interior cabinet air temperatures are

elevated above the ambient temperature through the use of a variable heat load. In order

to simplify the control and measurement of the heat load, an electrical resistance heater

was used. The electrical resistance heater of choice was a 100-Watt light bulb which was

covered with opaque tape such that the radiation between the light bulb surface and the

interior cabinet walls was minimized. The average air temperature inside of the cabinets

was measured using the six thermocouple masses which were distributed within the

cabinet spaces for the energy consumption testing. In order to maintain uniform

temperature profiles within the cabinets, small air fans were used to mix the air. The fan

outlets were directed toward the heating elements for maximum dispersion of the heated

air. To promote air temperature uniformity, all of the shelves and drawers were removed

from the cabinet. It is important to note that the use of air fans increases the convective

heat transfer coefficient between the cabinet air and the interior of the cabinet walls. The fans used were similar in size to the internal fans of the unit, so this airflow, and therefore convective heat transfer coefficient approximates the air flow during an on-cycle of the refrigerator-freezer.

To be able to maintain a constant average air temperature inside of the two cabinets, the average heat load output of the light bulbs had to be controlled. A control system was created using LabVIEW software which utilized two separate PID controllers. Each of these PID controllers was connected to a relay so that the light bulb heaters could be powered for a variable fraction of each second. In this way the average power output per second of each of the heat sources could be controlled individually, since the rate of heat transfer from each of the cabinets was different. A watt meter was used to measure the aggregate integrated energy consumption over the test period of both the light bulb and the fan motor. The controllers were able to maintain the average cabinet air temperatures to within 0.1°C, which is within the uncertainty of the measurement.

The two cabinets each have insulating walls between the cabinet air and the ambient air, as well as a wall between them called the "Mulligan." Two sets of tests must be run in order to separate the effect of the heat leak between the cabinets from the heat leak between the cabinets and the ambient air. For the first test both average cabinet air temperatures were set to a value of 40°C, so that there would be no heat transfer across the Mulligan. This first test allowed for the calculation of the UA value for each of the cabinets, not including the heat transfer between them. In the second test the average air temperature of the cabinets were set to different values in order to determine the heat

transfer across the Mulligan by isolating the effects of the other walls from the

calculations. In this test the refrigerator average air temperature was set to 40°C and the

freezer average air temperature was set to 50°C. In both tests the system was allowed to

reach steady-state and then data was recorded for a period longer than 5 hours in order to

minimize the uncertainties in the time and energy measurements. A basic schematic of

the placement of the light bulb heaters and mixing fans is shown in Figure 17. In addition

to the schematic an example picture is shown of the heating unit in the refrigerator

compartment in Figure 18.
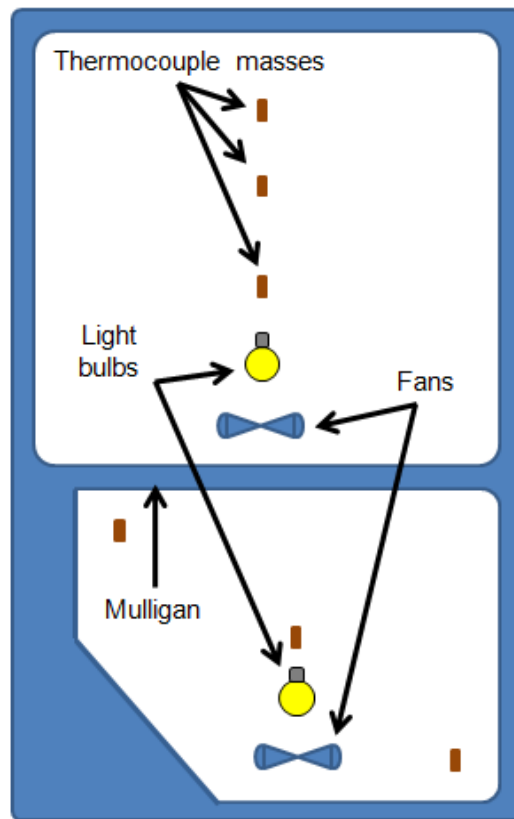


**Figure 17: Refrigerator-freezer cabinet schematic for reverse heat leak testing**

**Figure 18: Refrigerator cabinet reverse heat leak test heating element and fan [17]**

When calculating the overall heat transfer coefficients using the reverse heat leak test, it is important to accurately measure the temperature difference between the air in the cabinets and the ambient air. In order to make an accurate measurement of the ambient air temperature surrounding the refrigerator-freezer cabinet, nine thermocouple masses were installed. The thermocouple masses were identical to the ones used in the interior of the refrigerator and freezer cabinets. Four of the thermocouple masses were installed five to ten centimeters from the exterior cabinet wall at the respective centers of the refrigerator left, right, front, and back sides. Four additional thermocouple masses were installed in the same configuration for the freezer cabinet, and one thermocouple mass was installed five to ten centimeters above the top of the refrigerating cabinet, at the center of the wall. The placement of nine thermocouple masses allowed for both the

detection of non-uniform temperature distribution, and redundant measurements to lower the measurement uncertainty.

### 2.4.2. Results

As mentioned previously there were two phases to the reverse heat leak tests, the first to measure the overall heat transfer coefficients of the cabinet walls and the second to measure the overall heat transfer coefficient of the Mulligan. In both phases the test duration, total energy consumptions of the heating systems, average interior cabinet air temperatures, and average exterior ambient air temperature were recorded and are shown in Table 7.

**Table 7: Reverse heat leak testing measurement results**

| Variable | Units | Wall UA Test | Mulligan UA Test |
|---|---|---|---|
| Test Duration | min | 333.0 | 361.0 |
| Total Energy Input – Refrigerator Cabinet | W-hr | 177.8 | 170.4 |
| Total Energy Input – Freezer Cabinet | W-hr | 109.2 | 206.8 |
| Average Ambient Temperature | °C | 20.91 | 20.92 |
| Average Interior Temperature –Refrigerator | °C | 40.06 | 40.07 |
| Average Interior Temperature – Freezer | °C | 40.04 | 50.07 |

The equation to calculate the overall heat transfer coefficients for the refrigerator and freezer walls uses the "Wall UA Test" data from Table 7 and is given in Equation (5) [18],[19].

$$UA_{wall} = \frac{E}{t*\Delta T} \tag{5}$$

Where:

$UA_{wall}$ = overall heat transfer coefficient of the cabinet walls [W/K]

$E$ = integrated total energy input into the cabinet [W-hr]

$t$ = test duration [hr]

$\Delta T$ = average temperature difference between ambient air and cabinet air [K]

The equation to calculate the overall heat transfer coefficient for the Mulligan uses the "Mulligan UA Test" data from Table 7 and is given in Equation (6).

$$UA_{mul} = \frac{1}{2*\Delta T_{mul}} \left( \left| \frac{E_{ref}}{t} - UA_{ref} * \Delta T_{ref} \right| + \left| \frac{E_{fre}}{t} - UA_{fre} * \Delta T_{fre} \right| \right) \qquad (6)$$

Where:

$UA_{mul}$ = overall heat transfer coefficient of the Mulligan [W/K]

$UA_{ref}$ = overall heat transfer coefficient of the refrigerator cabinet walls [W/K]

$UA_{fre}$ = overall heat transfer coefficient of the freezer cabinet walls [W/K]

$\Delta T_{mul}$ = temperature difference between refrigerator and freezer cabinet air [K]

$\Delta T_{ref}$ = temperature difference between ambient and refrigerator cabinet air [K]

$\Delta T_{fre}$ = temperature difference between ambient and freezer cabinet air [K]

$E_{ref}$ = integrated total energy input into the refrigerator cabinet [W-hr]

$E_{fre}$ = integrated total energy input into the freezer cabinet [W-hr]

$t$ = test duration [hr]

The results of the calculations are shown with their respective uncertainties in Table 8.

**Table 8: Overall heat transfer coefficient calculation results**

| Variable | Units | Value | Uncertainty |
|---|---|---|---|
| Refrigerator Cabinet (UA_ref) | W/K | 1.673 | ±0.029 |
| Freezer Cabinet (UA_fre) | W/K | 1.028 | ±0.018 |
| Mulligan (UA_mul) | W/K | 0.405 | ±0.061 |

# 3. Modeling and Simulation

Computer modeling and simulation of the system and its components was performed using several software packages including CoilDesigner [20], VapCyc [21], and TransRef [22]. CoilDesigner is a steady-state simulation tool for determining individual heat exchanger performance based on inlet conditions and the geometry characteristics of the heat exchanger. VapCyc is a steady-state component-by-component simulation tool for modeling system performance based on directly calling CoilDesigner heat exchanger models as well as basic expansion device and compressor models [23],[24]. TransRef is a transient simulation tool for modeling system performance and charge distribution based on lumped component models for the expansion device, heat exchangers, compressor, and cabinet. TransRef allows the implementation of a variety of control algorithms including thermostat on/off compressor control and thermostat air damper control.

The on-board control logic of the refrigerator-freezer unit cycles the compressor on and off according to the capacity needed to maintain the compartment average air temperatures at the desired thermostat settings. This control logic inherently creates transient operation of the cycle. After an initial pull-down period to the desired cabinet temperatures, the cycling becomes periodic and each cycle is approximately equivalent to the last. For each of these cycles there is a pull-down period immediately after the compressor turns on which occurs because of the additional power needed to overcome the off-cycle pressure equalization. Although the individual cycles are transient in nature, the operation during the middle of the cycle is relatively constant with the changing variable being a gradual decrease in the air temperature of the cabinets. From this

41

relatively stable period of operation a "quasi-steady-state" point is chosen. This quasi-steady-state point represents a small time period over which the rate of change in the system operating characteristics is relatively small, and it is reasonable to compare the results with the VapCyc steady-state simulations. Specifically, the experimental quasi-steady-state point is the average of three data points taken in 2.5 second intervals; this is done in order to account for the small random deviations in the measured values. An example of the power consumption of the unit during an on cycle is shown in Figure 19; the arrow marks the location of a quasi-steady-state point.
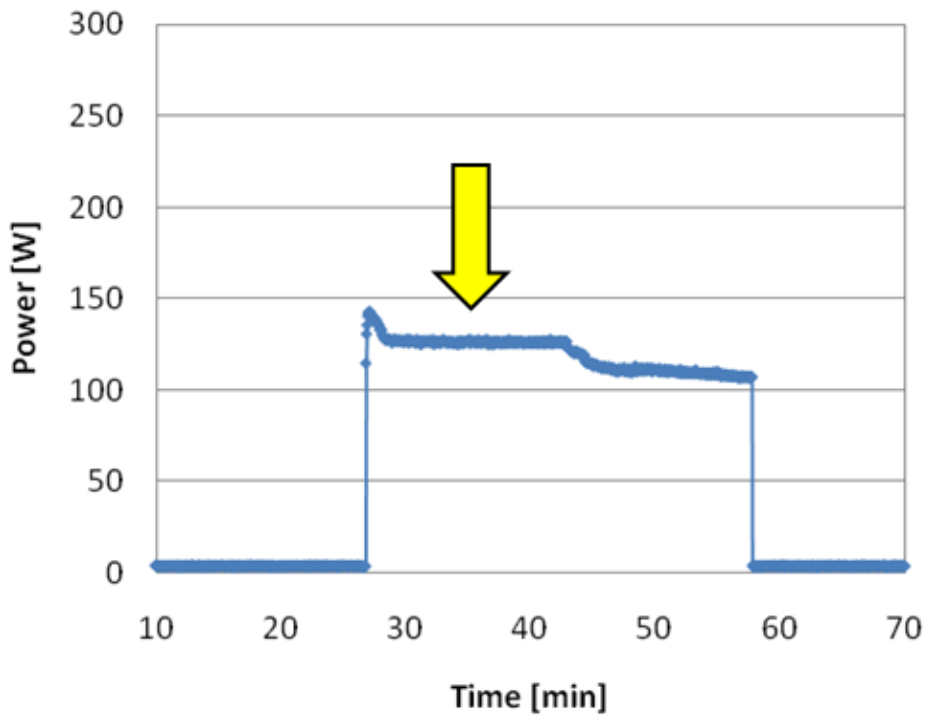


**Figure 19: Compressor on-cycle power consumption; arrow demarks the "quasi-steady-state" point**

*3.1.  CoilDesigner*

The first step to the system modeling process was to model the evaporator and condenser heat exchanger components individually using CEEE's CoilDesigner software. CoilDesigner is a physics and correlation-based modeling software which can be used to create a variety of heat exchanger geometries. In the modeling work performed, fin-and-tube heat exchangers were created which exchanged heat between the refrigerant (R134a) and air. Since the geometry of the evaporator was variable, and the condenser was of unique design, some approximations needed to be made for the modeling. For both of the heat exchangers, quasi-steady-state experimental data was used for model validation.

3.1.1.  Evaporator

The evaporator was modeled using both known values as well as measurements conducted using electronic calipers. All of the relevant specifications are given in Table 9. The spacing between evaporator fins was variable both along the tube length and along the height of the heat exchanger. The fin type was "flat" with non-touching collars. The spacing of the tubes was also variable in both the vertical and horizontal directions. Both the fin and tube material were aluminum.

**Table 9: Evaporator specifications**

| | | |
|---|---|---|
| Total Tube Length | 12.98 | m |
| Outer Tube Diameter | 8.0 | mm |
| Inner Tube Diameter | 6.6 | mm |
| Total Tube Volume | 440.8 | cm$^3$ |
| Heat Transfer Area (Fin and Tube) | 2.37 | m$^2$ |
| U-bend to U-bend Tube Length | 0.705 | m |
| Vertical Tube Spacing (Outer Two) | 23.5 | mm |
| Vertical Tube Spacing (Center) | 31.9 | mm |
| Horizontal Tube Spacing | 18 | mm |
| Fin Thickness | 0.15 | mm |
| Total Fin Height | 0.162 | m |
| Total Fin Width | 0.075 | m |
| Width of Finned Portion of Heat Exchanger | 0.629 | m |
| Freezer Volumetric Air Flow Rate (Damper Closed) | 1.1 | m$^3$/min |
| Freezer Volumetric Air Flow Rate (Damper Open) | 1.0 | m$^3$/min |
| Refrigerator Volumetric Air Flow Rate (Damper Closed) | 0 | m$^3$/min |
| Refrigerator Volumetric Air Flow Rate (Damper Open) | 0.27 | m$^3$/min |

Since CoilDesigner is unable to directly handle variable spacing of the fins in both along the pipe and as a function of the height, or variable spacing of the tubes in both the vertical and horizontal directions, approximations were made for the geometry. One of the most important geometric parameters to match between the actual heat exchanger and the model is the air-side heat transfer area, since this is one of the major limiting factors for the heat transfer. Two other important parameters that must be matched are the volumetric air flow rate and the velocity of the air flow, since these also affect the air-side heat transfer. The air flow velocity was matched by matching both the volumetric air flow rate and the frontal heat exchanger dimensions. Some of the other important parameters which needed to be maintained at their actual values in order to have an accurate model were the number of tubes, tube length, and the number of tube banks. In order to match all of these important parameters, while also matching the total air-side heat transfer area, the fin spacing input to CoilDesigner was modified. It was found that the air-side heat transfer area matched the true value when a fin spacing of

6.42 mm (3.955 FPI) was used. Basic schematics of the actual and model evaporators are
shown in Figure 20.
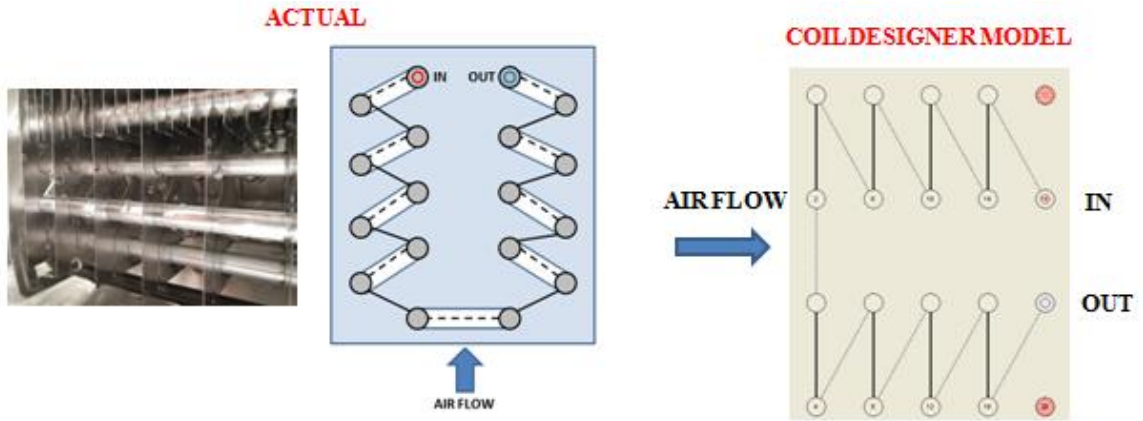


**Figure 20: Picture and schematic showing the actual evaporator geometry (left), and
a schematic showing the approximated CoilDesigner evaporator geometry (right)**

The model was executed for a couple of different operating conditions in order to
ensure that the modeling results matched the experimental results. The experimentally
determined inputs for the model are quasi-steady-state points at two different ambient
temperatures, and the conditions are listed in Table 10. For both of the ambient
temperature conditions, the thermostat was set to the "warmest" settings. The key outputs
of the model are compared with their experimental values for an ambient temperature of
32.2°C in Table 11, and 20°C in Table 12.

**Table 10: Experimental inputs for CoilDesigner evaporator model**

| Ambient Temperature | 32.2°C | 20°C |
|---|---|---|
| Volumetric Air Flow Rate | 1.27 m$^3$/min | 1.27 m$^3$/min |
| Inlet Air Temperature | -9.9°C | -11.5°C |
| Inlet Air Relative Humidity | 74.5 %RH | 72.9 %RH |
| Inlet Refrigerant Pressure | 141.7 kPa | 125.9 kPa |
| Inlet Refrigerant Quality | 0.201 | 0.165 |
| Refrigerant Mass Flow Rate | 0.90 g/s | 0.94 g/s |

**Table 11: Experimental and CoilDesigner outputs for evaporator at an ambient temperature of 32.2°C**

| Variable | Experimental | CoilDesigner | Difference |
|---|---|---|---|
| Evaporator Capacity | 155.6 W | 155.9 W | 0.2% higher |
| Evaporator Superheat | 4.7 K | 4.9 K | 0.2 K higher |
| Refrigerant Pressure Drop | 3.56 kPa | 2.26 kPa | 36.5% lower |
| Air-side Heat Transfer Coefficient | N/A | 27.35 W/(m$^2$-K) | N/A |

**Table 12: Experimental and CoilDesigner outputs for evaporator at an ambient temperature of 20°C**

| Variable | Experimental | CoilDesigner | Difference |
|---|---|---|---|
| Evaporator Capacity | 172.0 W | 172.2 W | 0.1% higher |
| Evaporator Superheat | 5.9 K | 5.8 K | 0.1 K lower |
| Refrigerant Pressure Drop | 3.94 kPa | 2.61 kPa | 33.8% lower |
| Air-side Heat Transfer Coefficient | N/A | 27.35 W/(m$^2$-K) | N/A |

As shown in the previous tables, the evaporator capacity and outlet superheat are predicted extremely well by the CoilDesigner model, but the refrigerant pressure drop is off by more than 30%. This shows that the evaporator model will do a very good job predicting the heat transfer of the evaporator, and is therefore validated for the intended purposes. It also shows that the correlations for two-phase refrigerant pressure drop are highly inaccurate due to the inherent difficulties of predicting the effects of the two-phase flow patterns. The pressure drop results should therefore be used carefully when considering performance trends. Additionally, since approximations were made for the external geometry, the air-side pressure drop correlations are unlikely to be very accurate. Considering that the air-side pressure drop was not measured experimentally, and the model prediction of the air-side pressure drop is likely in accurate, the air-side pressure drop will not be considered in any of the analysis.

### 3.1.2. Condenser

The condenser was modeled using both known specifications as well as
measurements conducted using electronic calipers. All of the relevant specifications are
given in Table 13. The tubing of the condenser was constructed in spiraling banks, and
the fins were wrapped around the tubing in a spiraled helical fashion. Both the fin and
tube material were steel. CoilDesigner currently doesn't have the capability to model the
spiraling tube banks, so an approximation to the tubing geometry was made. The
applicable range of the correlations available in the literature for air-side heat transfer of
spiraled helical fins doesn't include the heat exchanger in question, and therefore an
approximation was made using a constant value of 45 W/m$^2$-K, which was a known value
from previous analysis.

**Table 13: Condenser specifications**

| | | |
|---|---|---|
| Total Tube Length | 13.80 | m |
| Outer Tube Diameter | 4.8 | mm |
| Inner Tube Diameter | 3.4 | mm |
| Total Tube Volume | 125 | cc |
| Heat Transfer Area (Fin & Tube) | 1.39 | m$^2$ |
| Volumetric Air Flow Rate | 1.7 | m$^3$/min |
| Fin Spacing | 5.51 (4.61 FPI) | mm |
| Number of Tube Banks | 10 | # |
| Tube Length Per Bank | 1.194 | m |
| Tube Length Per Bank Divided Into 6 Tubes | 0.199 | m |
| Fin Thickness at Outer Edge | 0.47 | mm |
| Fin Thickness at Root | 1.75 | mm |
| Fin Outer Diameter | 16.5 | mm |
| Fin Neutral Diameter | 15.5-16.5 | mm |
| Horizontal Spacing Between Banks | ~19 | mm |
| Vertical Spacing Between Tubes | 26.3 | mm |
| Total Cross Sectional Area of a Tube Bank | 0.06526 | m$^2$ |

Since CoilDesigner is unable to directly model the spiraling tubes or the helical
spiraling fins, approximations had to be made for the geometry. One of the most
important parameters to match between the actual heat exchanger and the model is the

air-side heat transfer area, since this is one of the major limiting factors for the heat transfer. Two other important parameters that must be matched are the volumetric air flow rate and the velocity of the air flow, since these also affect the air-side heat transfer and temperature profile. The air flow velocity was matched by matching both the volumetric air flow rate and the frontal heat exchanger dimensions. Some of the other important parameters which needed to be maintained at their actual values in order to have an accurate model were the number of tube banks and the total tube length. Each of the tube banks was divided into six equal length tubes in order to approximate each of the spiraled banks. In order to match all of these important parameters, while also matching the total air-side heat transfer area, the fin spacing input to CoilDesigner was modified. It was found that the air-side heat transfer area matched the true value when a fin spacing of 9.07mm (2.80 FPI) was used. The actual and model condensers are shown in Figure 21.
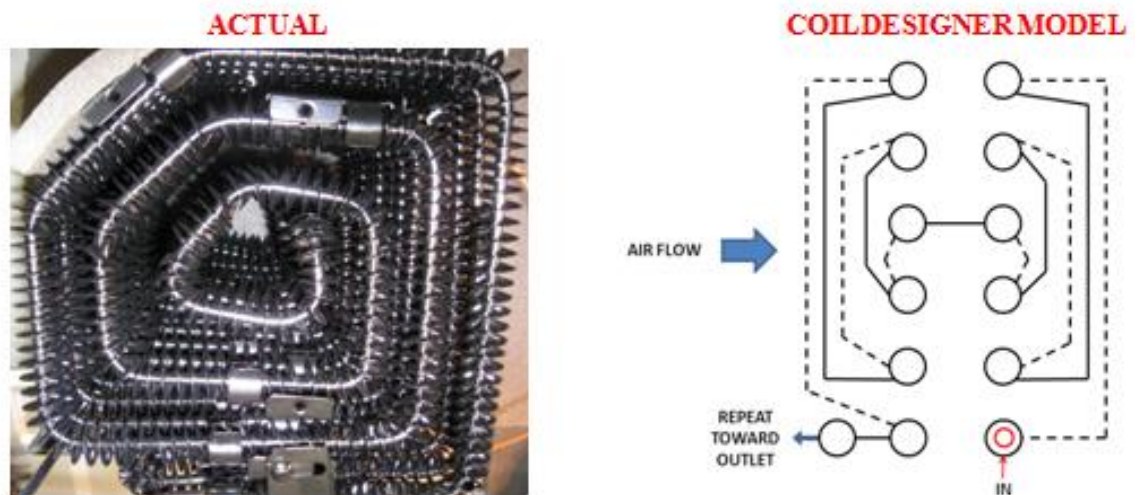


**Figure 21: Picture showing the actual condenser (left), and a schematic showing the CoilDesigner condenser model geometry (right)**

The model was executed for a couple of different operating conditions in order to ensure that the modeling results matched the experimental results. The experimentally

determined inputs for the model are quasi-steady-state at two different ambient

temperatures, and the conditions are listed in Table 14. For both of the ambient

temperature conditions, the thermostat was set to the "warmest" settings. For the

experimental results, the capacity of the condenser couldn't be directly calculated

because the outlet enthalpy couldn't be determined due to the two-phase conditions.

Instead, an estimation of the condenser capacity was made using an energy balance on

the system where the condenser heat rejection capacity was equal to the compressor

cooling subtracted from the sum of the evaporator heat input and the compressor

electrical heat input. The compressor cooling was mostly due to air flow over the

compressor shell and thermal storage of the compressor shell and oil due to transient

cycling. The compressor cooling was estimated by subtracting the energy input to the

refrigerant across the compressor from the electrical power input to the compressor. The

key outputs of the model are compared with their experimental values for an ambient

temperature of 32.2°C in Table 15, and 20°C in Table 16.

**Table 14: Experimental inputs for CoilDesigner condenser model**

| Ambient Temperature | 32.2°C | 20°C |
|---|---|---|
| Volumetric Air Flow Rate | 1.7 m$^3$/min | 1.7 m$^3$/min |
| Inlet Air Temperature | 32.7°C | 20.5°C |
| Inlet Refrigerant Pressure | 1063.4 kPa | 773.3 kPa |
| Inlet Refrigerant Temperature | 67.1°C | 47.8°C |
| Refrigerant Mass Flow Rate | 0.90 g/s | 0.94 g/s |

**Table 15: Experimental and CoilDesigner outputs for condenser ($T_{amb}$ = 32.2°C, "warmest")**

| Variable | Experimental | CoilDesigner | Difference |
|---|---|---|---|
| Condenser Capacity | 172.3 W | 176.6 W | 2.5% higher |
| Condenser Subcooling | ~0 K | 4.4 K | N/A |
| Refrigerant Pressure Drop | 25.44 kPa | 7.71 kPa | 69.7% lower |
| Air-side Heat Transfer Coefficient | 45 W/(m$^2$-K) | 45 W/(m$^2$-K) | N/A |

**Table 16: Experimental and CoilDesigner outputs for condenser ($T_{amb} = 20°C$, "warmest")**

| Variable | Experimental | CoilDesigner | Difference |
|---|---|---|---|
| Condenser Capacity | 184.4 W | 186.3 W | 1.0% higher |
| Condenser Subcooling | ~0 K | 4.3 K | N/A |
| Refrigerant Pressure Drop | 28.96 kPa | 11.67 kPa | 59.7% lower |
| Air-side Heat Transfer Coefficient | 45 W/(m²-K) | 45 W/(m²-K) | N/A |

As is shown in the previous tables, the condenser capacity is predicted very well by the model, but the refrigerant pressure drop is off by more than 50%, and the outlet refrigerant conditions are erroneous. This shows that the condenser model will do a good job of predicting the heat transfer of the condenser, a poor job predicting the exact outlet conditions of the refrigerant, and will be completely inaccurate for predicting the refrigerant pressure drop. Once again, the uncertainty of the two-phase pressure drop correlation is large because of the inherent difficulties in predicting the two-phase flow patterns. Additionally, since approximations were made for the external geometry, the air-side pressure drop correlations are unlikely to be very accurate. Considering that the air-side pressure drop was not measured experimentally, and the model prediction of the air-side pressure drop is likely inaccurate, the air-side pressure drop will not be considered in any of the analysis. The differences in the outlet conditions can be explained in part by the small differences in condenser capacity, since the degree of subcooling is especially sensitive to small changes in capacity because it is in the single phase heat transfer region. Since the condenser capacity is predicted within 5% of the experimental value, the model is considered to be validated for heat transfer calculations.

*3.2.*  *VapCyc*

The VapCyc software package is a GUI-based modeling software which executes a steady-state thermodynamic simulation for a component-by-component model. For the compressor component, calculations are performed using fundamental heat and mass transfer equations. In the case of capillary tube suction line heat exchangers (SLHXs), a segment-by-segment approach is used for calculations based on fundamental heat-transfer and mass-transfer equations. For the heat exchanger components, VapCyc calls another software package, CoilDesigner, which makes heat exchanger calculations based on pressure drop and heat transfer correlations for both the air- and refrigerant-sides, as discussed previously. The VapCyc model uses the component models, a fixed discharge pressure based on experimental results, and initial guesses for the discharge and suction pressures in order to iteratively solve the model until convergence to a stated residual.

### 3.2.1.  Experimental Validation of R134a Baseline Model

The compressor and capillary tube SLHX models require the input of all of the basic specifications in order to execute physics-based models. The input specifications for the capillary tube SLHX are shown in Table 17, and the specifications for the compressor are: a displacement of 6.9 cm$^3$, rotational speed of 3,000 RPM, isentropic efficiency of 69%, and a mechanical efficiency of 85%. The volumetric compressor efficiency was calculated for each test condition by dividing the experimentally measured refrigerant mass flow rate by the ideal mass flow rate assuming 100% efficiency per compression stroke. For the heat exchangers, VapCyc accesses the CoilDesigner software package in order to make calculations for the heat exchanger models previously created.

**Table 17: VapCyc capillary tube SLHX model inputs**

| Parameter | Units | Value |
|---|---|---|
| Capillary Tube Inner Diameter | mm | 0.8 |
| Capillary Tube Outer Diameter | mm | 1.4 |
| Capillary Tube Length | m | 2.545 |
| Adiabatic Entrance Length | m | 0.3 |
| SLHX Length | m | 1.939 |
| Suction Line Inner Diameter | mm | 6.0 |

Since the actual refrigerator-freezer transiently cycles the compressor on and off, an approximation must be made when modeling the steady state performance. The approximation of a quasi-steady-state point is used, as was presented previously and shown in Figure 19. Since a quasi-steady-state point is used, the transient nature of the compressor cooling must be taken into account in order to achieve the correct compressor discharge temperature, and subsequently the correct condenser outlet conditions. In order to account for the compressor cooling, a constant heat rejection load is inserted in the cycle diagram after the compressor. This component removes a constant amount of heat dictated by the compressor cooling for the chosen experimental quasi-steady-state point. As was stated previously, the compressor cooling was estimated using a simple energy balance where the heat input to the refrigerant across the compressor was subtracted from the electrical power input to the compressor, less the power that was lost due to compressor motor efficiency. The VapCyc model assumes that the 15% loss from the motor efficiency doesn't contribute to the work being done on the refrigerant. A schematic of the system model created within VapCyc is shown in Figure 22.
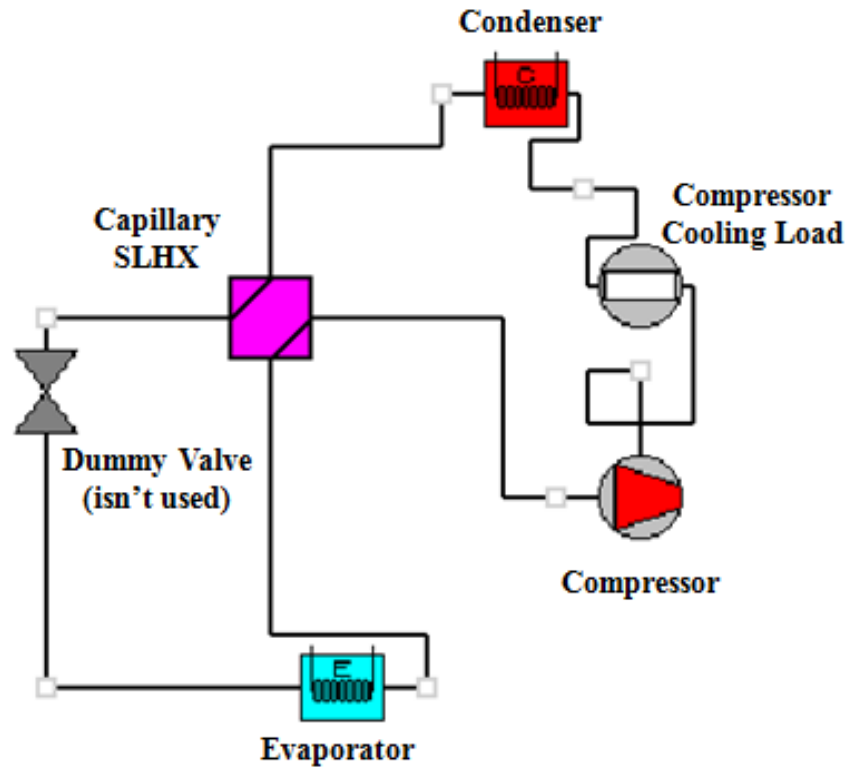
**Figure 22: VapCyc model schematic**

The VapCyc model was executed for the inputs mentioned previously using a quasi-steady-state data point at an ambient temperature of 32.2°C and thermostat settings of "warmest." The convergence criteria for the cycle model was the discharge pressure, which was set to match the experimental discharge pressure of 1,095.4 kPa for the given test conditions. Using the experimental data point, the compressor volumetric efficiency was calculated to be 63.9%, and the compressor cooling was calculated to be 78.4 W. The results of the R134a baseline model are compared with the experimental R134a baseline data for several important criteria including the mass flow rate, suction pressure, compressor power, and evaporator capacity. The tabulated results can be seen in Table 18.

**Table 18: VapCyc R134a baseline modeling results (T$_{amb}$ = 32.2°C, "warmest")**

| Variable | Units | Experimental R134a | VapCyc R134a | Difference |
|----------|-------|--------------------|--------------| -----------|
| Mass Flow Rate | g/s | 1.17 | 1.21 | 3.4% increase |
| Suction Pressure | kPa | 128.3 | 124.2 | 3.2% decrease |
| Compressor Power | W | 118.4 | 109.7 | 7.3% decrease |
| Evaporator Capacity | W | 202.6 | 182.5 | 9.9% decrease |
| COP | - | 1.71 | 1.66 | 2.9% decrease |

The results of the R134a baseline model match the given experimental quasi-steady-state point within 10% for several important criteria including the suction pressure, compressor power, COP, and mass flow rate. It is seen that the evaporator capacity has the largest difference between the model and the experimental data at 9.9%, but this may be attributable to a variety of factors including the fact that the capillary tube inner diameter is a nominal value instead of a measured value. Error in the capillary tube inner diameter can lead to inaccurate prediction of the pressure drop during the expansion process, which is seen to be 3.2% lower in the model. For a given mass flow rate and capillary tube inlet enthalpy, a lower evaporation pressure is going to result in a higher vapor quality at the evaporator inlet. A higher vapor quality at the evaporator inlet will then lead to a lower evaporator capacity. Another potential source of inaccuracy is that the system is being considered to be in steady-state operation, when in reality it is a point chosen from a relatively stable portion of the transient cycle.

In order to better analyze the differences between the experimental data and the VapCyc model, the thermodynamic state points of the system should be considered. To simplify the visualization of the system state points, a P-h diagram was created. The P-h diagram is shown in Figure 23, with the experimental cycle shown in red and the VapCyc model shown in green. All of the numbered state points correspond to the state points

shown in the system schematic in Figure 5. The point labeled "Comp Out" is the

theoretical compressor discharge temperature calculated in VapCyc before applying the

compressor cooling to return to the experimental conditions of state point 1.
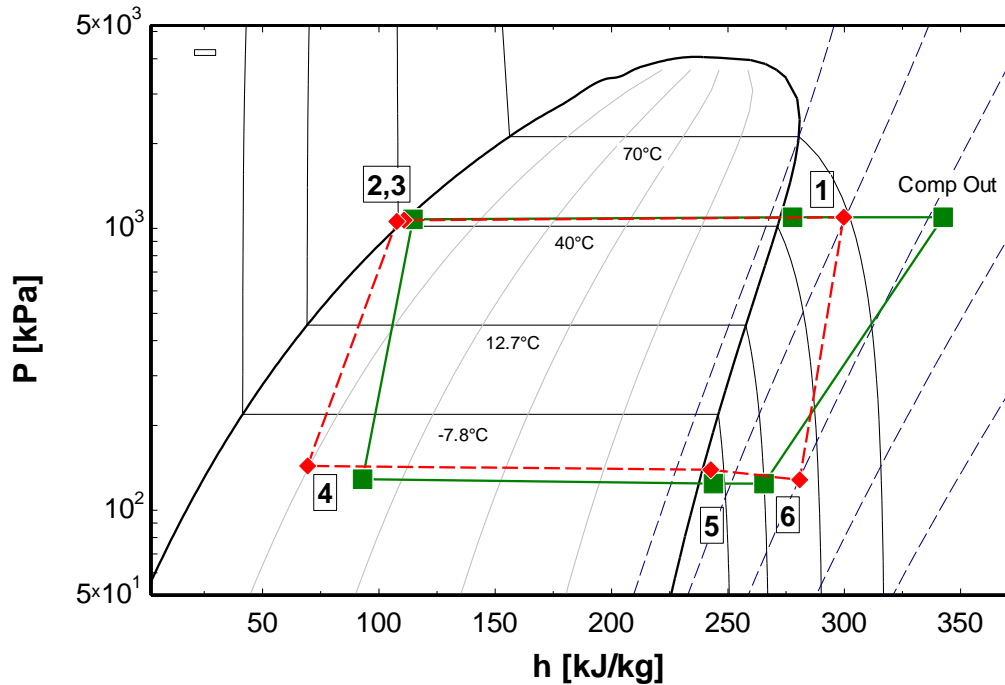


**Figure 23: P-h diagram comparing experimental data and VapCyc model ($T_{amb} = 32.2°C$, "warmest")**

The P-h diagram comparison highlights the fact that the capillary tube SLHX

model doesn't match well with the experimental data. It can be seen that the

expansion/heat exchange process from state point 3 to state point 4 is very different

between the experimental and VapCyc model results. When calculated, it was found that

the experimental SLHX capacity was 44.8 W, while the VapCyc SLHX capacity was

only 26.2 W. This difference in SLHX capacity causes an increase from the experimental

evaporator inlet vapor quality of 0.20, to the VapCyc value of 0.32. This difference in

evaporator inlet vapor quality explains the error in the evaporator capacity prediction. In

order to account for the inaccuracy of the SLHX heat transfer model in VapCyc, a

correction factor for the SLHX heat transfer was implemented such that the SLHX

capacities and suction temperatures would more closely match. The heat transfer of the

SLHX is mostly limited by the thermal resistance of the vapor-side heat transfer. The

contribution to the thermal resistance by the metal conduction, liquid refrigerant heat

transfer, and two-phase boiling heat transfer are minimal. In order to reduce

computational time, VapCyc assumes that the overall heat transfer is equal to the vapor-

side heat transfer [25]. The correction factor is a constant multiplier to this heat transfer

coefficient as shown in Equation (7).

$$U_{SLHX} = C1 * HTC_{vap} \tag{7}$$

Where:

$U_{SLHX}$ = overall heat transfer coefficient of SLHX [W/m$^2$-K]

$C1$ = SLHX heat transfer correction factor

$HTC_{vap}$ = convective heat transfer coefficient of vapor side of SLHX as

calculated using the Gnielinski correlation [W/m$^2$-K]

It was found that a SLHX heat transfer correction factor of 4.0 was adequate. The

results of the corrected model for an ambient temperature of 32.2°C and thermostat

settings of "warmest" are shown in Table 19.

**Table 19: VapCyc R134a baseline modeling results, with SLHX heat transfer correction factor (T$_{amb}$ = 32.2°C, "warmest")**

| Variable | Units | Experimental R134a | VapCyc R134a | Difference |
|---|---|---|---|---|
| Mass Flow Rate | g/s | 1.17 | 1.20 | 2.6% increase |
| Suction Pressure | kPa | 128.3 | 129.5 | 0.9% increase |
| SLHX Capacity | W | 44.8 | 42.5 | 5.1% decrease |
| Compressor Power | W | 118.4 | 112.1 | 5.3% decrease |
| Evaporator Capacity | W | 202.6 | 190.7 | 5.9% decrease |
| COP | - | 1.71 | 1.70 | 0.6% decrease |

The results of the VapCyc model when using a correction factor of 4.0 for the SLHX heat transfer match much better than the first iteration of the model. It is seen that all of the relevant modeling results match within 6% of the experimental values. It is also seen that the thermodynamic cycles match much more closely on a P-h diagram because of the correction of the SLHX heat transfer. The updated P-h diagram is shown in Figure 24, with the experimental cycle shown in red and the VapCyc model shown in green. The slight difference in the discharge temperature at state point 1 between the VapCyc model and the experimental data can be attributed to the slight 5.3% decrease in compressor power. A lower compressor power input results in a decreased discharge temperature when the compressor cooling remains constant.
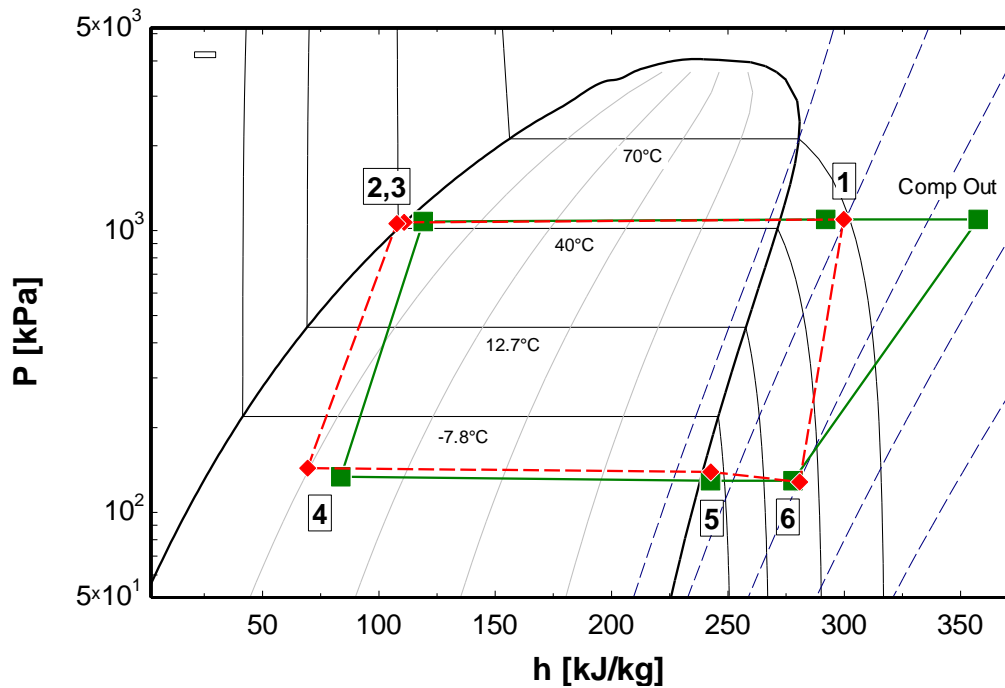


**Figure 24: P-h diagram comparing experimental data and VapCyc model, with SLHX heat transfer correction factor ($T_{amb} = 32.2°C$, "warmest")**

For further validation, the VapCyc model was executed for another quasi-steady-state data point at an ambient temperature of 32.2°C and thermostat settings of "middle."

The convergence criteria for the cycle model was the discharge pressure, which was set to match the experimental discharge pressure of 1,062.4 kPa for the given test conditions. Using the experimental data point, the compressor volumetric efficiency was calculated to be 60.9%, and the compressor cooling load was calculated to be 76.1 W. The results of the R134a baseline model are compared with the experimental R134a baseline data for several important criteria including the mass flow rate, suction pressure, SLHX capacity, compressor power, and evaporator capacity. The tabulated results can be seen in Table 20.

**Table 20: VapCyc R134a baseline modeling results ($T_{amb}$ = 32.2°C, "middle")**

| Variable | Units | Experimental R134a | VapCyc R134a | Difference |
|---|---|---|---|---|
| Mass Flow Rate | g/s | 1.07 | 1.08 | 0.9% increase |
| Suction Pressure | kPa | 123.1 | 121.9 | 1.0% decrease |
| SLHX Capacity | W | 42.4 | 39.1 | 7.8% decrease |
| Compressor Power | W | 114.0 | 102.2 | 10.4% decrease |
| Evaporator Capacity | W | 186.9 | 169.1 | 9.5% decrease |
| COP | - | 1.64 | 1.65 | 0.6% increase |

The results of the R134a baseline model match the given experimental quasi-steady-state point within 11% for several important criteria including the mass flow rate, suction pressure, SLHX capacity, compressor power, and evaporator capacity. It is seen that the compressor power has the largest difference between the model and the experimental data at 10.4%. Once again the thermodynamic cycles match closely on a P-h diagram when implementing a SLHX heat transfer correction factor. The P-h diagram for the "middle" thermostat settings at an ambient temperature of 32.2°C is shown in Figure 25, with the experimental cycle shown in red and the VapCyc model shown in green.
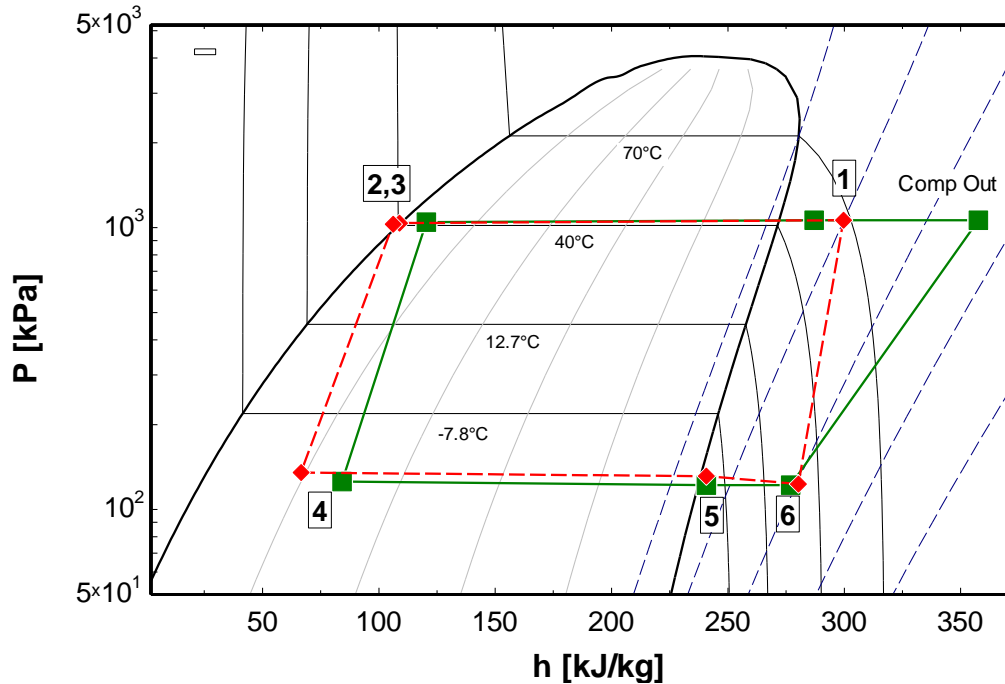
**Figure 25: P-h diagram comparing experimental data and VapCyc model, with SLHX heat transfer correction factor ($T_{amb}$ = 32.2°C, "middle")**

In summary, the experimental results of the DOE test conditions of "warmest" thermostat settings and an ambient temperature of 32.2°C were predicted to within 6% using the VapCyc model, and for the conditions of "middle" thermostat settings and an ambient temperature of 32.2°C, the results were within 11%. This outcome validates that the model can represent the behavior of the system, but that the compressor power and evaporator capacity have only ~10% accuracy. This accuracy is deemed acceptable for utilizing the model to explore general system behavior trends when implementing alternative refrigerants.

### 3.2.2. R1234yf Drop-in Replacement Simulation

The next step in the VapCyc modeling process was to analyze the performance of the system when R1234yf is used as a direct drop-in replacement for R134a without any modification to the system. This means that the R1234yf simulations occur with the same

inputs and under the same conditions as the R134a simulations, including the SLHX heat

transfer correction factor. The results of the R1234yf simulation are compared with the

R134a baseline simulation results for an ambient temperature of 32.2°C and "warmest"

thermostat settings in Table 21.

**Table 21: VapCyc simulation comparison between R134a baseline and R1234yf drop-in ($T_{amb}$ = 32.2°C, "warmest")**

| Variable | Units | VapCyc R134a | VapCyc R1234yf | Difference |
|---|---|---|---|---|
| MFR | g/s | 1.20 | 1.43 | 19.2% increase |
| Suction Pressure | kPa | 129.5 | 138.0 | 6.6% increase |
| SLHX Capacity | W | 42.5 | 52.5 | 23.5% increase |
| Compressor Power | W | 112.1 | 112.3 | 0.2% increase |
| Evaporator Capacity | W | 190.7 | 188.6 | 1.1% decrease |
| COP | - | 1.70 | 1.68 | 1.2% decrease |

The results for the R1234yf drop-in simulation show an increase in the suction

pressure of 6.6%. With the increased suction pressure and the fact that the vapor density

of R1234yf is higher than R134a, the result is a drastic increase in the mass flow rate of

19.2%. This result shows that the capillary tube expansion device needs to be modified to

reduce the evaporation pressure and decrease the mass flow rate in order to more closely

match the R134a system performance. Another factor which possibly affects the capillary

tube expansion device performance is that the liquid viscosity of R1234yf is 17.8% lower

than that of R134a at the inlet to the capillary tube [8], which would indicate less pressure

drop per unit length of capillary tubing. The results also show that the compressor power

increases 0.2% and the evaporator capacity decreases 1.1% when R1234yf is substituted

for R134a. The slight increase in compressor power and slight decrease in evaporator

capacity resulted in a 1.2% decrease in the system efficiency. The fundamental structure

of the thermodynamic cycle is similar for the two refrigerant simulations in terms of

cycle state point locations relative to the two-phase dome. The P-h diagrams can be used to compare the two refrigerant cycles, the R134a cycle was shown previously in Figure 24, and the R1234yf cycle is shown in Figure 26.
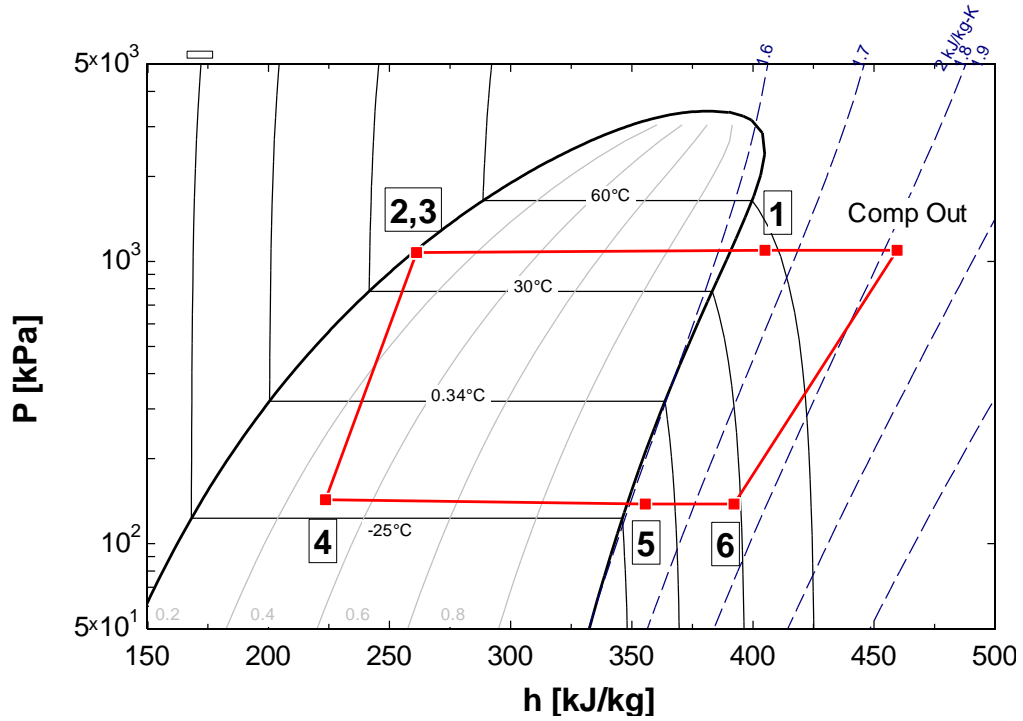


**Figure 26: P-h diagram of R1234yf VapCyc model ($T_{amb}$ = 32.2°C, "middle")**

The VapCyc model was also executed for the R1234yf direct drop-in replacement of R134a at an ambient temperature of 32.2°C and "middle" thermostat settings. The results of the comparison are shown in Table 22.

**Table 22: VapCyc simulation comparison between R134a baseline and R1234yf drop-in ($T_{amb}$ = 32.2°C, "middle")**

| Variable | Units | VapCyc R134a | VapCyc R1234yf | Difference |
|---|---|---|---|---|
| Mass Flow Rate | g/s | 1.08 | 1.28 | 18.5% increase |
| Suction Pressure | kPa | 121.9 | 129.4 | 6.2% increase |
| SLHX Capacity | W | 39.1 | 48.0 | 22.8% increase |
| Compressor Power | W | 102.2 | 102.3 | 0.1% increase |
| Evaporator Capacity | W | 169.1 | 166.8 | 1.4% decrease |
| COP | - | 1.65 | 1.63 | 1.2% decrease |

The R1234yf drop-in simulation at an ambient temperature of 32.2°C and "middle" thermostat settings shows similar results to the previous simulation at the "warmest" thermostat settings. There is an increase in the suction pressure, which increases the refrigerant mass flow rate. Once again the results also show that the compressor power increases slightly and the evaporator capacity decreases slightly, resulting in a decrease in system efficiency of 1.2%.

The decreased efficiency and capacity of the cycle would mean that the on-cycle time during transient operation would slightly increase for fixed thermostat temperatures. Overall the results demonstrate that R1234yf would be an acceptable low GWP direct drop-in replacement for R134a, with only a slight decrease in efficiency.

### 3.2.3.   Alternative Low GWP Refrigerant Simulations

A simulation study was conducted in order to determine the performance of the refrigerator-freezer system when using alternative low GWP drop-in replacements for the original R134a refrigerant. VapCyc was used to investigate the system performance when the alterative refrigerants R1234yf and R1234ze were used to replace R134a. Additionally, a parametric study was performed in order to determine the system performance when using various mixture fractions of R134a/R1234yf as lower GWP and potentially non-flammable replacements for R134a and R1234yf, respectively. In the previous experimental set-up and associated VapCyc model, a capillary tube SLHX was used as the expansion device. When making drop-in replacements for the refrigerants, one of the main issues is that the expansion device will need modification in order to achieve the maximum potential performance. As was shown previously, that would entail

the optimization of the capillary tube specifications in order to maximize the system energy efficiency when using each refrigerant.

In order to simplify the performance analysis of the various refrigerants, the optimization process of the capillary tube dimensions for each refrigerant was avoided. Instead of having a capillary tube SLHX component, the expansion valve component was turned into a "dummy valve" and the VapCyc model solved for a fixed evaporator outlet superheat and condenser outlet subcooling for each case. This change also meant that the VapCyc model no longer required a fixed discharge pressure as an input. This difference is important because different refrigerants and refrigerant mixtures have slightly different saturation temperatures, which affects the condensation and evaporation pressures. The fixed values of superheating and subcooling were chosen as 5 K and 2 K, respectively. The evaporator superheat value was selected to reflect how a vapor compression system could be designed to ensure that a thermostatic expansion valve would sense enough superheat to operate properly and to ensure that the compressor wouldn't receive any potentially damaging liquid droplets. The condenser subcooling value was selected to ensure that the refrigerant at the inlet to the expansion device was fully liquid to prevent vapor bubbles from causing adverse conditions such as vapor block of the expansion valve.

The CoilDesigner models for the condenser and evaporator heat exchangers that were experimentally validated previously were retained for the alternative refrigerant evaluation. The compressor component model attributes were also retained at the same values as those used during the VapCyc model validation, with an increase in the compressor speed to a standard value of 3,600 RPM. As stated before, the capillary tube

SLHX component was replaced with a dummy-valve and instead the VapCyc model

solved for the fixed evaporator superheat and condenser subcooling values.

The first part of the simulation study was to compare the performance of the

simplified model when using the baseline R134a refrigerant to the GAR options of

R1234yf and R1234ze. The simulation results of this refrigerant comparison are shown

for several important parameters in Table 23.

**Table 23: VapCyc simulation result comparison for R134a, R1234yf, and R1234ze**

| Variable | Units | R134a | R1234yf | R1234ze |
|---|---|---|---|---|
| COP | - | 1.604 | 1.461 | 1.731 |
| Compressor Power | W | 121.3 | 124.9 | 88.2 |
| Evaporator Capacity | W | 194.5 | 182.5 | 152.7 |
| Mass Flow Rate | g/s | 1.51 | 1.96 | 1.28 |
| Discharge Pressure | kPa | 1,196.0 | 1,203.6 | 851.0 |
| Suction Pressure | kPa | 132.6 | 153.3 | 102.0 |
| Evaporator Inlet Quality | - | 0.407 | 0.485 | 0.404 |

It is shown in Table 23 that the system performance varies moderately between

the three refrigerants. When taking R134a as the baseline case, it is seen that R1234yf has

a 3.0% increase in compressor power and a 6.2% decrease in evaporator capacity,

resulting in an 8.9% reduction in COP. When comparing R134a with R1234ze, it is seen

that the compressor power decreases by 27.3% and the evaporator capacity decreases by

21.5%, resulting in a 7.9% increase in COP. When comparing these results, it is apparent

that the model predicts that R1234yf will result in a moderate decrease in efficiency when

compared with R134a, whereas R1234ze will result in a moderate increase in COP.

Although R1234ze appears promising from an efficiency stand point, it is important to

note that when compared with R134a the evaporator capacity is significantly lower. Due

to the lower evaporator capacity, the effectiveness of R1234ze as a drop-in replacement

for R134a is limited. In the case of R1234ze, it is likely that the system would need to be redesigned with a compressor capable of a larger volumetric flow rate in order to have a comparable evaporator capacity to R134a. Although the model shows that the system efficiency decreases when using R1234yf as a replacement for R134a, it is seen that the evaporator capacity is within 6.2%. Another item of note is that the R1234yf vapor quality at the evaporator inlet is significantly higher than that of R134a, a 19.2% increase. This shows that a significant portion of the refrigerant at the inlet to the evaporator is vapor, which provides only a minor portion of the cooling capacity. The significance of this finding is that among the three refrigerants, R1234yf may have the largest potential for efficiency improvement if a SLHX is implemented in the cycle. The effect of the SLHX is further proved in the previous direct drop-in analysis where the system efficiency of R1234yf was only about 1.2% lower than R134a.

The second part of the simulation study was to investigate the performance of the system when using a variety of mixture fractions of R134a and R1234yf as drop-in replacements for R134a. The results of a parametric study from pure R134a (fraction of 0) to pure R1234yf (fraction of 1) are shown graphically in Figure 27 through Figure 32 for several important parameters as functions of the fraction of R1234yf in R134a on a mass basis. The plotted values include the system COP, heat exchanger capacities, compressor power, mass flow rate, suction and discharge pressures, evaporator inlet quality, and heat exchanger pressure drops. The performance changes relative to the baseline R134a case are shown on a single graph in Figure 33 for several of the most important parameters including the COP, evaporator capacity, compressor power, suction pressure, discharge pressure, mass flow rate, and evaporator inlet vapor quality.
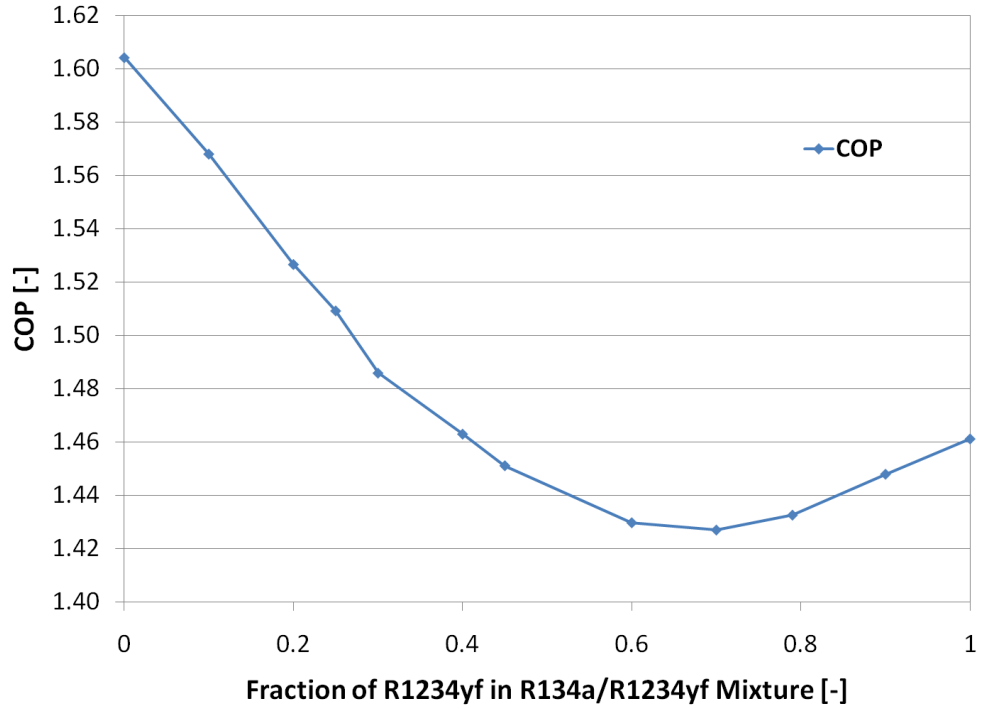
**Figure 27: VapCyc results for COP as a function of the fraction of R1234yf in an R134a/R1234yf mixture**
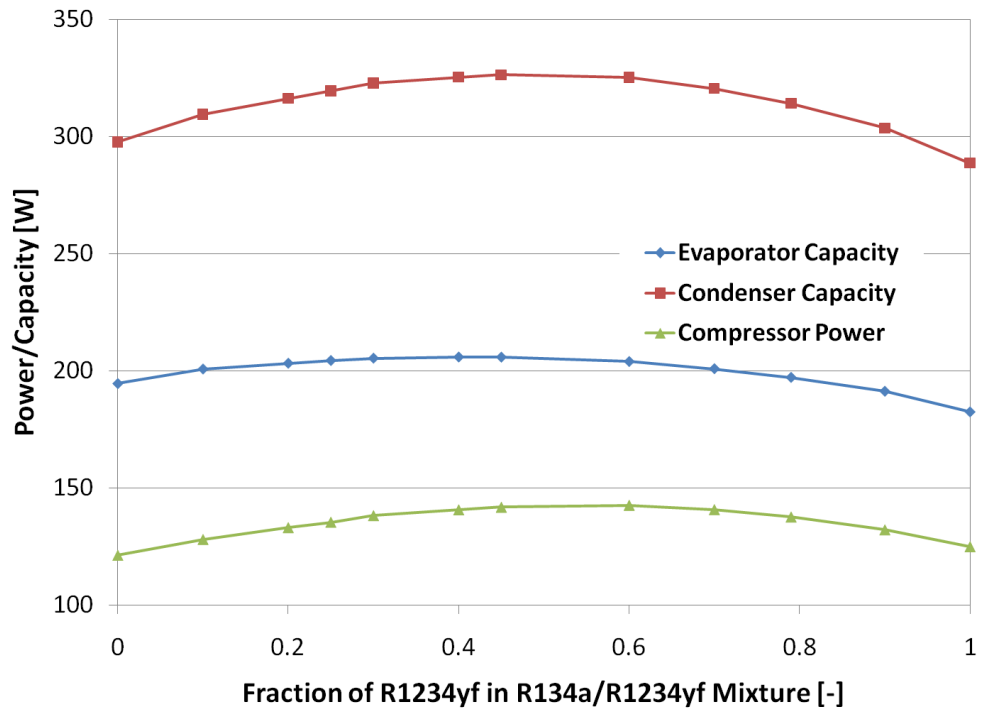


**Figure 28: VapCyc results for power and capacities as functions of the fraction of R1234yf in an R134a/R1234yf mixture**
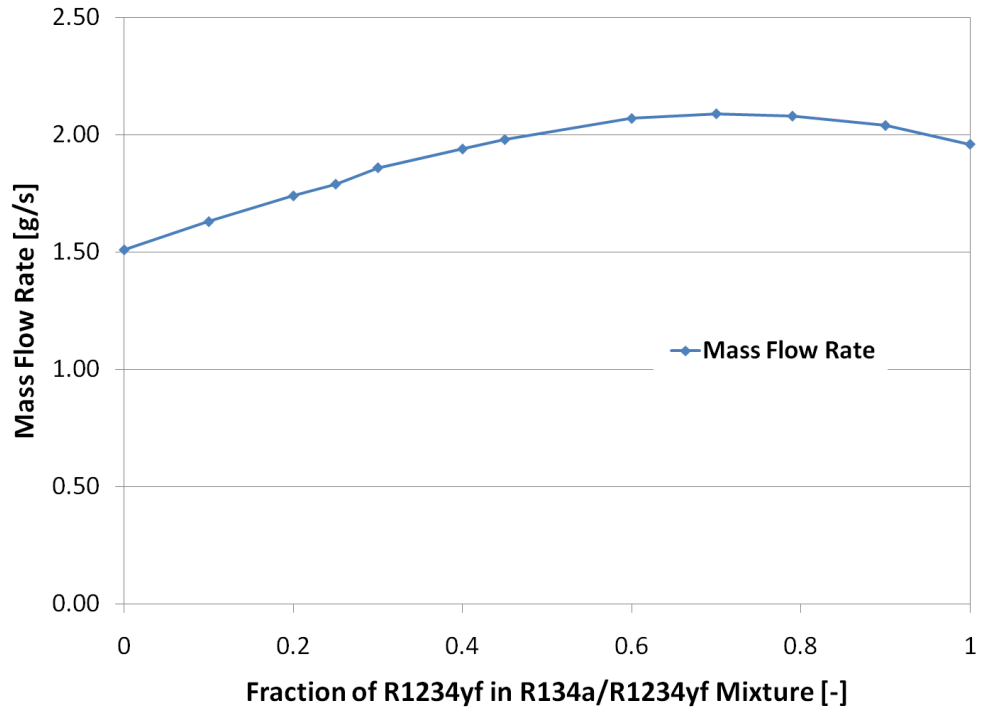
**Figure 29: VapCyc results for refrigerant mass flow rate as a function of the fraction of R1234yf in an R134a/R1234yf mixture**
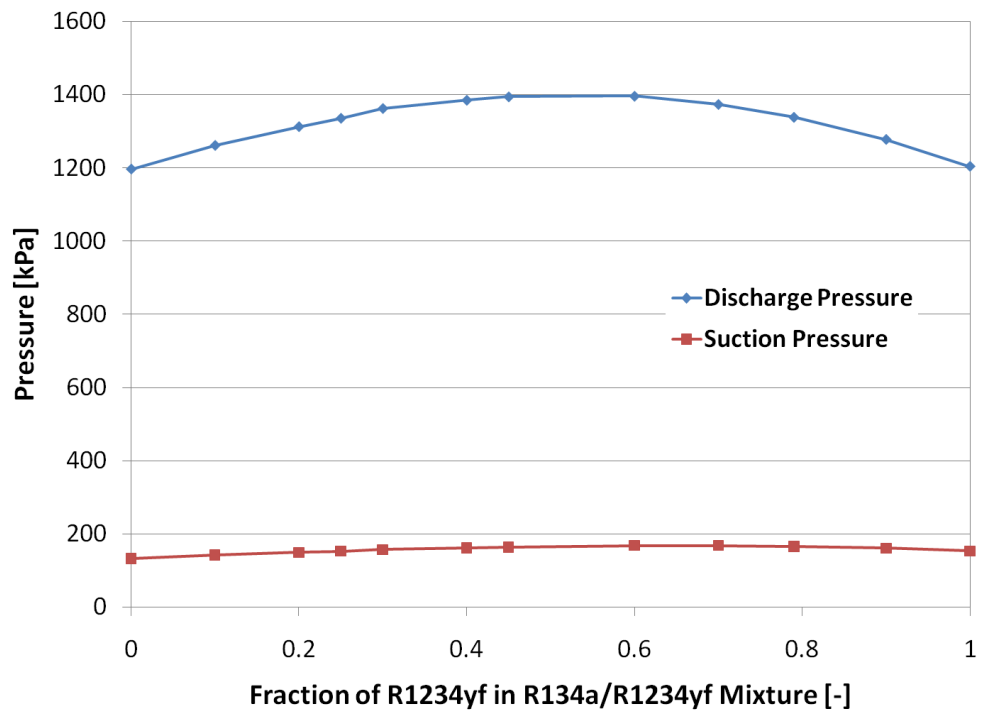


**Figure 30: VapCyc results for pressures as functions of the fraction of R1234yf in an R134a/R1234yf mixture**
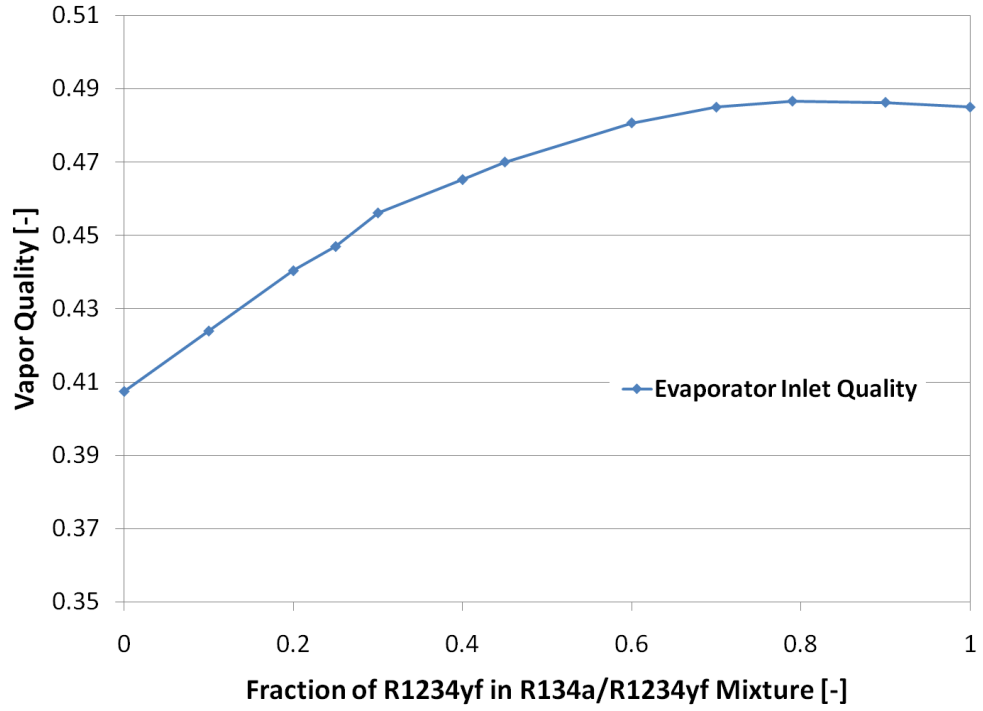
**Figure 31: VapCyc results for evaporator inlet vapor quality as a function of the fraction of R1234yf in an R134a/R1234yf mixture**
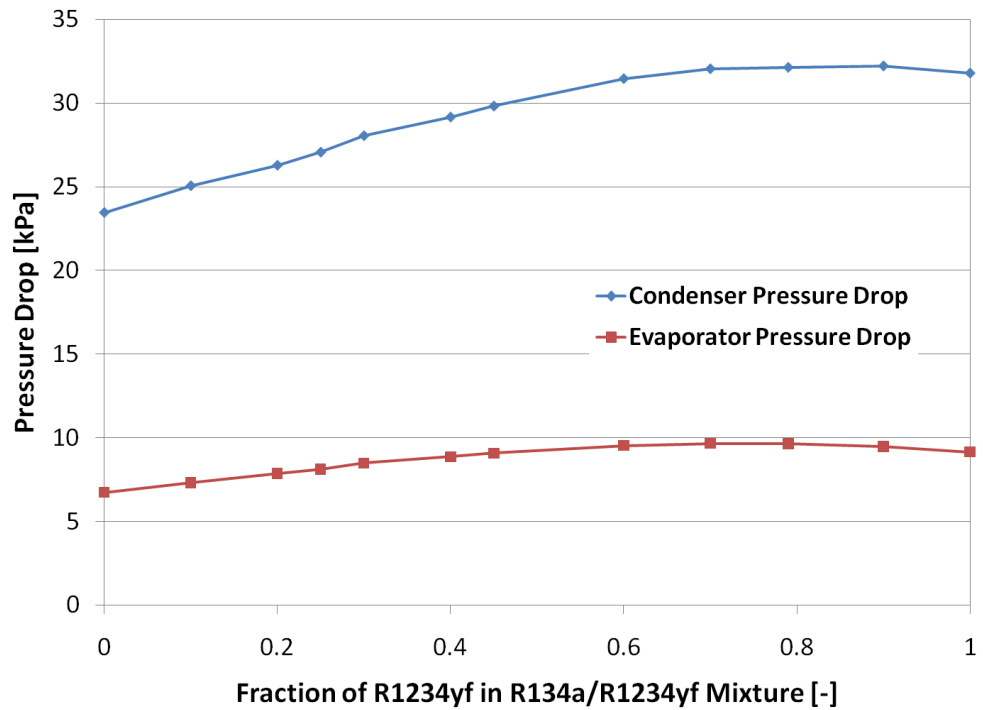


**Figure 32: VapCyc results for heat exchanger pressure drops as functions of the fraction of R1234yf in an R134a/R1234yf mixture**
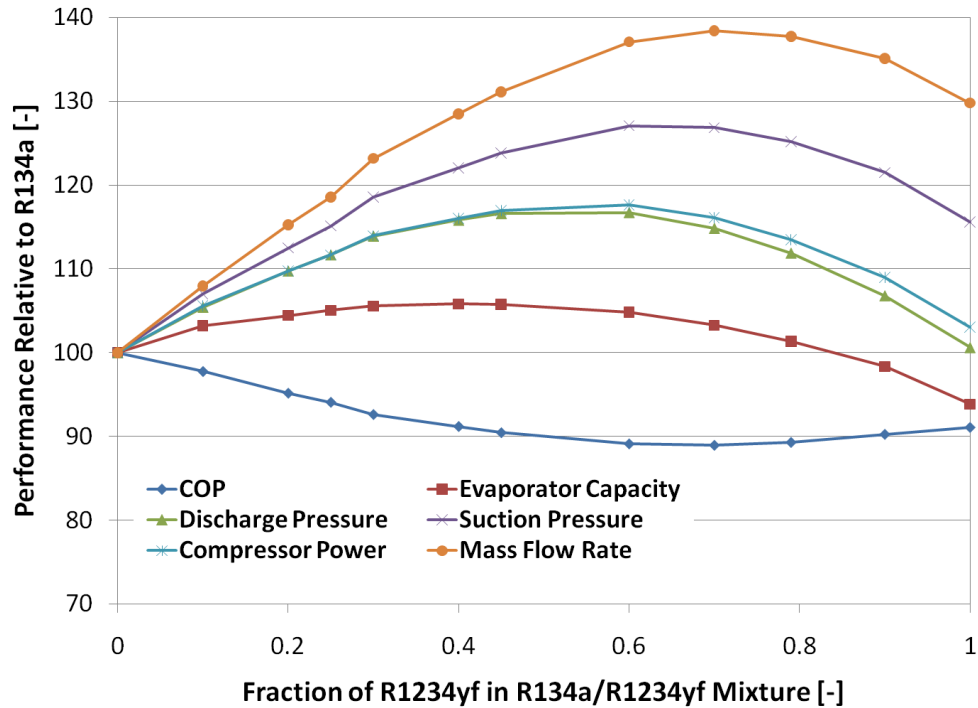
**Figure 33: Selection of VapCyc results relative to R134a baseline as functions of the fraction of R1234yf in an R134a/R1234yf mixture**

In the graphs from Figure 27 through Figure 32 the actual values are shown for each of the key variables as functions of the R134a/R1234yf mixture fraction, but what is more interesting for comparison purposes is Figure 33. In Figure 33, all of the important variables are plotted relative to the R134a baseline, which gives a clear visual indication of the effects that increasing the R1234yf fraction has on system performance. The main reason behind the variable system performance for the different mixture fractions is the changing saturation pressures. The changing suction pressure is closely linked with the mass flow rate, because increasing the suction pressure causes the suction density to increase, which increases the mass flow rate. The mass flow rate is also increased as the R1234yf mass fraction is increased because the density of R1234yf vapor is higher than R134a vapor at the given suction conditions. The increasing mass flow rate is in turn

responsible in part for the increasing compressor power consumption. The main reason that the evaporator capacity initially increases as R1234yf is added to the mixture is because of the increased mass flow rate. After an R1234yf fraction of approximately 0.4, the evaporator capacity begins to decrease because of the increasing evaporator inlet vapor quality. This increasing trend of evaporator inlet vapor quality can be attributed in part to the increasing discharge pressure, which results in a higher enthalpy at the expansion valve inlet. This increasing trend of evaporator inlet vapor quality also indicates that as the fraction of R1234yf is increased, the benefit of adding a SLHX to the system would also likely increase.

When evaluating the system performance, the first parameter that is analyzed is the COP because the energy efficiency of the system is of paramount significance in the decision of which refrigerant mixture ratio to use. The graph shows that as the fraction of R1234yf increases, the COP of the system decreases until a fraction of approximately 0.7, at which point it begins to increase. This trend is important because it shows that although the COP of pure R1234yf is lower than R134a by 8.9%, for R1234yf fractions between 0.4 and 1.0, the COP is lower than either pure R134a or pure R1234yf. The other significance of an R1234yf fraction of 0.4 is that it is approximately the point at which the evaporator capacity is at a maximum. Beyond an R1234yf fraction of 0.4, the evaporator capacity decreases as the fraction of R1234yf increases until it hits a minimum at pure R1234yf, which is 6.2% lower than the R134a baseline. These characteristics make an R1234yf fraction of 0.4 an interesting mixture to consider when balancing the various trade-offs.

Two extremely important characteristics of the different mass fractions of R1234yf in R134a/R1234yf mixtures are the flammability and the GWP rating. In the available scientific literature the flammability and GWP of both pure R134a and pure R1234yf have been tested, but these characteristics haven't been demonstrated for a range of R134a/R1234yf mixtures. The results of these tests would be important for two reasons: they would identify the mixture ratio at which the transition occurs for the refrigerant flammability classification from ASHRAE Class 1 to Class 2L, and they would identify the mixture ratio thresholds for the different legislative GWP barriers, such as the European Union's introduction of a MAC regulation of 150. This information has the potential to be extremely useful if it is found that there exists a mixture fraction which satisfies the Class 1 flammability requirements while also meeting a GWP restriction such as the European Union regulation.

### 3.3. *TransRef*

TransRef is a CEEE software package that simulates the transient performance of a vapor compression cycle. It also has the capability of implementing a cabinet model that takes into account the geometry and properties of the insulated refrigerator and freezer compartments. The compressor and capillary tube SLHX models require the input of all of the basic specifications in order to execute physics-based models. The capillary tube model is actually a correlation based model that was developed by the CEEE during the creation of the software package from data calculated using segmented physics-based simulations [26]. This correlation was developed in order to reduce the calculation time of the simulations. For the heat exchanger models, TransRef utilizes a lumped physics-based modeling approach which requires the basic specifications of the heat exchangers

71

including the average heat transfer coefficients for both the air side and each of the refrigerant phases.

For transient simulation several control algorithms can be selected. In the case of the refrigerator-freezer, two control algorithms were utilized. The first algorithm controlled the compressor state (on/off) based on the average air temperature inside the freezer cabinet, which means that it acted as a thermostat control for the system based on the freezer temperature. The second control algorithm controlled the air-side damper state based on the average air temperature inside of the refrigerator cabinet. The damper state toggled between circulating all of the evaporator air flow through the freezer cabinet or splitting a fixed portion of the volumetric air flow for circulation through the refrigerator compartment. A schematic of the system model created within TransRef is shown in Figure 34.
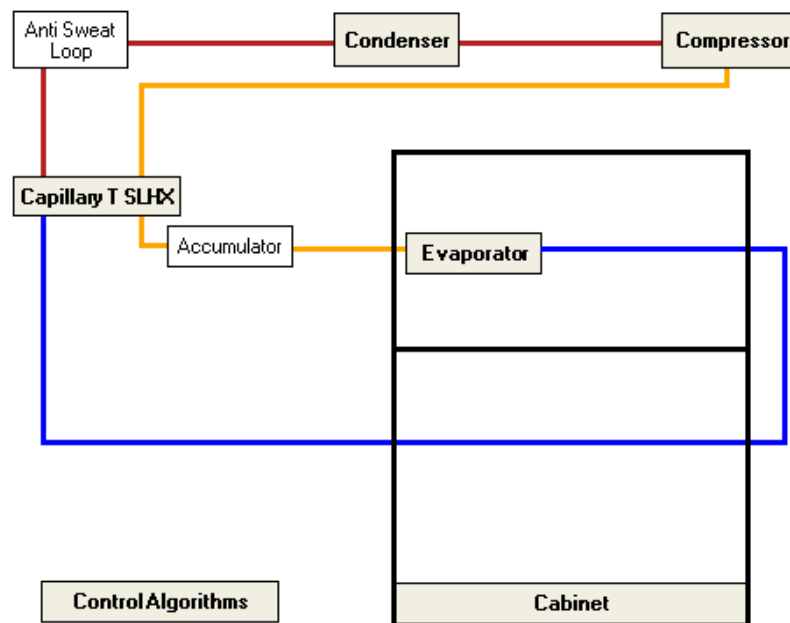


**Figure 34: TransRef model schematic**

### 3.3.1. Experimental Validation of R134a Baseline Model

The basic inputs for the evaporator and condenser were either known, measured

directly, or calculated using CoilDesigner for a quasi-steady-state point at an ambient

temperature of 32.2°C and thermostat settings of "warmest." The inputs for the

evaporator and condenser are shown in Table 24.

**Table 24: TransRef inputs for condenser and evaporator models**

| Parameter | Units | Evaporator | Condenser |
|---|---|---|---|
| Total Internal Volume | $cm^3$ | 440.8 | 125.0 |
| Total Surface Area | $m^2$ | 2.37 | 1.39 |
| Total Internal Surface Area | $m^2$ | 0.269 | 0.147 |
| Heat Exchanger Heat Capacity | J/K | 875.7 | 1361.6 |
| Air-Side Heat Transfer Coefficient | $W/(m^2$-K) | 27.4 | 45.0 |
| Air-Side Heat Transfer Coefficient (Fan Off) | $W/(m^2$-K) | 5 | 12 |
| Refrigerant-Side Heat Transfer Coefficient | $W/(m^2$-K) | 304.9 | 530.0 |
| Volumetric Air Flow Rate | $m^3$/s | 0.0211 | 0.028 |
| Ambient Air Temperature | °C | N/A | 32.2 |
| Damper Fraction (open / closed) | - | 0.213 / 0 | N/A |

The inputs for the capillary tube SLHX model were known. The capillary tube

length was 2.545 m, the capillary tube inner diameter was 0.8 mm, and the SLHX length

was 1.939 m. The compressor inputs were known, and are shown in Table 25.

**Table 25: TransRef inputs for compressor model**

| Parameter | Units | Value |
|---|---|---|
| Swept Volume | $cm^3$ | 6.9 |
| Clearance Volume | $cm^3$ | 0.04 |
| Shell Surface Area | $m^2$ | 0.12 |
| Surface Heat Transfer Coefficient | $W/(m^2$-K) | 18 |
| Heat Capacity | J/K | 2,600 |
| Polytropic Constant | - | 1.05 |
| Rotational Speed | rev/min | 3,000 |
| Isentropic Efficiency | - | 0.69 |
| Mechanical Efficiency | - | 0.85 |
| Ambient Temperature | °C | 32.2 |

The cabinet model was created through a combination of known, measured, and

estimated/calculated quantities. Correction factors for the refrigerator and freezer

compartments were then used so that the overall UA values would match the experimentally measured values. The cabinet model input GUI is shown with all of the specifications, units, and a schematic of their meaning in Figure 35.
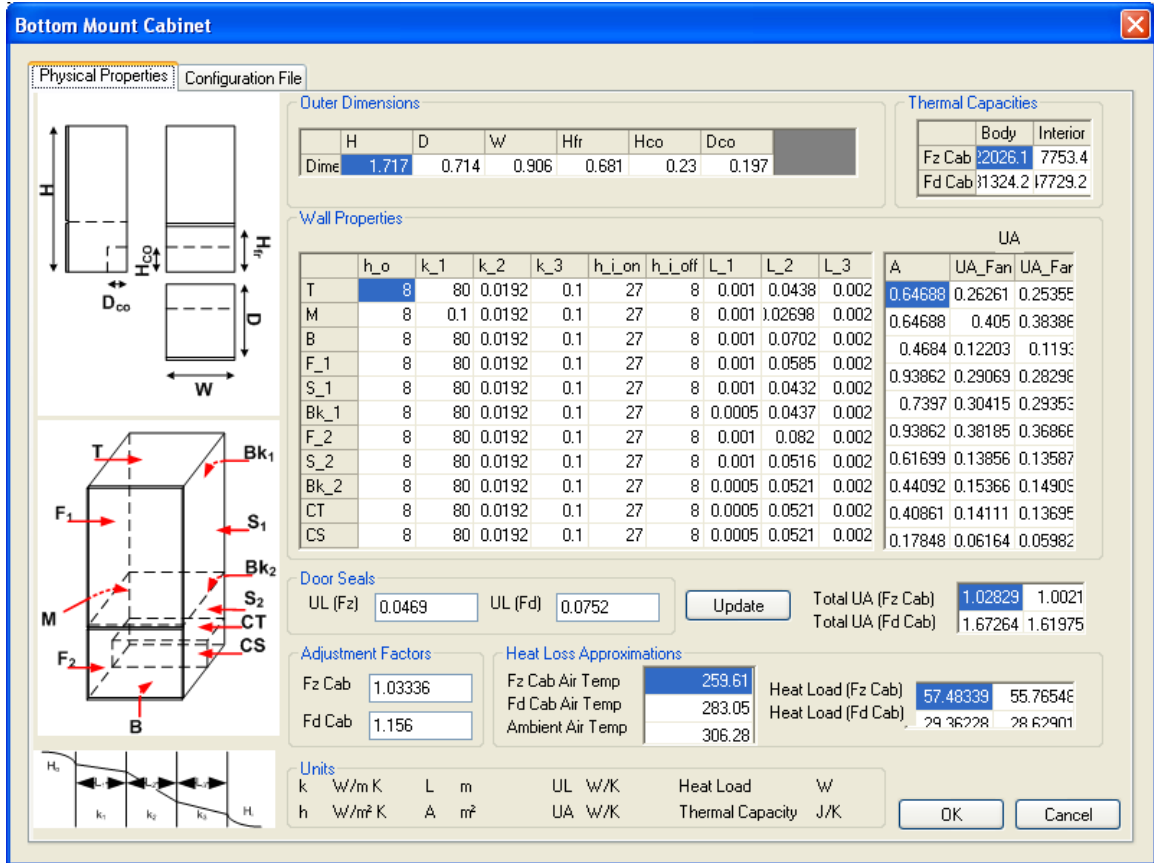
**Figure 35: GUI of TransRef cabinet model with model specifications shown**

For the control algorithm temperatures, the experimentally measured cut-in and cut-out points were used. The cut-in temperature for the freezer cabinet is defined as the warmest air temperature achieved in the freezer cabinet before the compressor is turned on, and the cut-out temperature is the coldest temperature achieved before the compressor is turned off. For the warmest thermostat settings, the freezer cabinet control algorithm temperature bounds were -10.8°C and -16.8°C. For the damper control the cut-in temperature is defined as the warmest air temperature achieved in the refrigerator cabinet

74

before the damper is opened, and the cut-out temperature is the coldest temperature

achieved before the damper is closed. For the warmest thermostat settings, the

refrigerator cabinet control algorithm temperature bounds were 9.8°C and 8.7°C.

The model was executed for the inputs mentioned previously using R134a as the

refrigerant with an ambient temperature of 32.2°C and the thermostat settings at the

"warmest" values. Several of the relevant transient outputs are shown for six "steady"

cycles in the graphs of Figure 36 through Figure 39. The compressor powers, damper

setting, average cabinet temperatures, mass flow rates, and system pressures are

compared between the TransRef model and the experimental R134a baseline data.
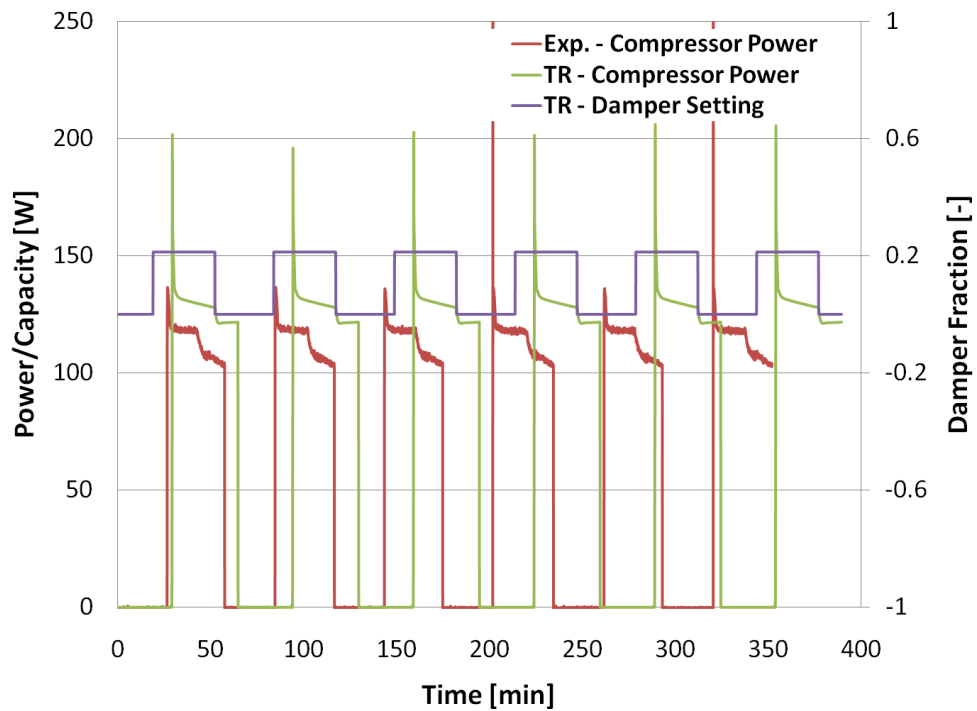


**Figure 36: Compressor power and damper fraction - comparison between experimental and TransRef baseline R134a results**
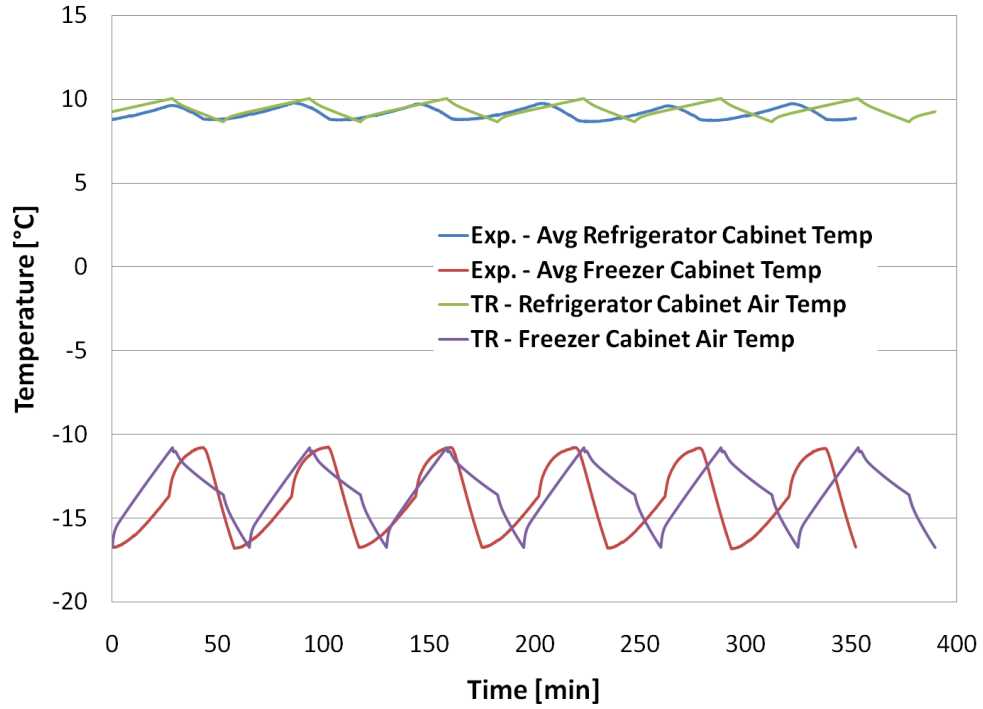
**Figure 37: Average cabinet air temperatures - comparison between experimental and TransRef baseline R134a results**
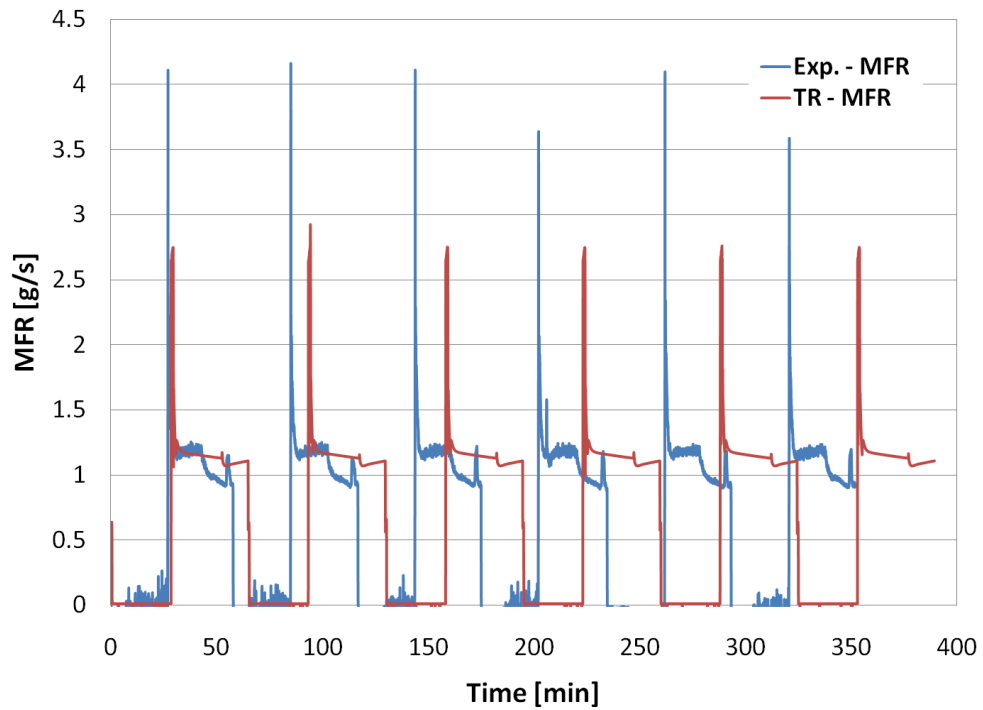


**Figure 38: Refrigerant mass flow rate - comparison between experimental and TransRef baseline R134a results**
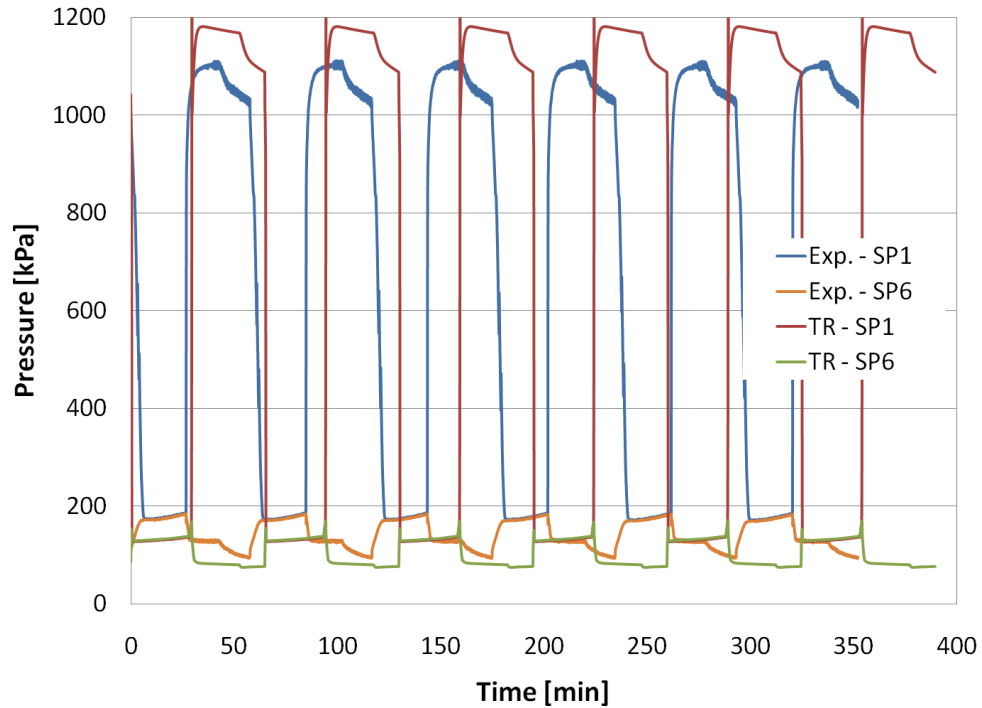
**Figure 39: Pressures - comparison between experimental and TransRef baseline R134a results**

It is apparent from the transient data that the cycle profiles match reasonably well, though there is some discrepancy in the on and off cycle durations as well as the compressor power, as shown in Figure 36. The experimental data and the TransRef model exhibit similar transient responses for all of the variables when the damper is abruptly closed and when the compressor is abruptly turned on and off. The average cabinet air temperatures shown in Figure 37 match well between the experimental data and the TransRef model, which indicates that the modeled thermostat controllers perform reasonably well. The refrigerant mass flow rates match reasonably well between the experimental data and the TransRef model, as shown in Figure 38. Finally, Figure 39 shows that there is some discrepancy between the compressor discharge and suction

pressures, with the on-cycle values being higher and lower, respectively, for the TransRef model.

In order to make quantifiable comparisons between the TransRef model results and the baseline experimental data, some of the key parameters are tabulated in Table 26. Average on-cycle values are given for parameters other than the cycle duration information and yearly energy consumption.

**Table 26: Average on-cycle results – comparison between experimental and TransRef baseline R134a results**

| Variable | Units | Experimental R134a | TransRef R134a | Difference |
|---|---|---|---|---|
| On-Cycle Duration | min | 31.7 | 35.1 | 10.7% increase |
| Off-Cycle Duration | min | 27.0 | 29.8 | 10.4% increase |
| On-Cycle Fraction | % | 54.0 | 54.1 | 0.2% increase |
| Compressor Power | W | 114.0 | 127.7 | 12.0% increase |
| Refrigerant Mass Flow Rate | g/s | 1.12 | 1.15 | 2.7% increase |
| Discharge Pressure | kPa | 1,066.9 | 1,146.3 | 7.4% increase |
| Suction Pressure | kPa | 119.4 | 82.1 | 31.0% decrease |
| Evaporation Temperature | °C | -22.4 | -30.6 | 8.2 K decrease |
| Pressure Ratio | - | 8.9 | 14.0 | 57.3% increase |
| SLHX Capacity | W | 45.0 | 17.7 | 60.7% decrease |
| Yearly Energy Consumption (compressor only, without defrost) | kWh/year | 536.0 | 604.8 | 12.8% increase |

The average on-cycle data shows that the TransRef model under-estimates the evaporator capacity, which is indicated by the 10.7% increase in on-cycle duration. This is likely due to the fact that the pressure ratio increased by 57.3% and the SLHX capacity decreased by 60.7%. This indicates that the capillary tube SLHX model has difficulty predicting both pressure drop and heat transfer. The capillary tube model over-predicts the pressure drop, which leads to a significantly reduced suction pressure and a slightly increased discharge pressure. The reduced suction pressure and increased discharge pressure result in the significantly increased pressure ratio as noted previously. The

increased pressure ratio means that the compressor must do more work to compress the refrigerant, which causes a 12.0% increase in the compressor power. When considering the cycle on a P-h diagram, increased discharge pressure would lead to a higher enthalpy at the capillary tube inlet. The increased capillary tube inlet enthalpy and reduced suction pressure would result in a higher evaporator inlet vapor quality, which contributes to the decreased evaporator capacity. The evaporator inlet vapor quality would also be increased in the simulation because of the 60.7% decrease in SLHX capacity, leading to further reduction in the evaporator capacity. The decrease in SLHX capacity is likely due to an error in the calculation of the SLHX effectiveness.

The average off-cycle duration increase of 10.4% indicates that there is a moderate error in the cabinet model. Since the cabinet model implemented correction factors to reach the overall heat transfer coefficients which were measured experimentally, it is apparent that there is heat gain in the test facility that is unaccounted for in the model. The likely sources of this additional heat gain are threefold. The first and likely most significant source is the capillary tubing which leads from the evaporator compartment to the ambient surroundings in order to measure the evaporation pressure. Although the capillary tube was insulated and had theoretically no refrigerant flow, the high conductivity of the copper tubing and the ~50 K temperature difference between the evaporation and ambient air temperatures meant that there was some heat transfer. A second source of heat gain could potentially be the instrumentation wires that exited the cabinets under the door seals, but the insulation shown in Figure 4 should have minimize it. The last potential source of heat gain could be the drain pain opening from the evaporator compartment. During the reverse heat leak test the temperature of the air in

the freezer cabinet was above the ambient air temperature, so buoyancy effects would minimize air flow through the hole at the bottom of the pan, which means that the air leak contribution of the drain pan opening wouldn't appear in the reverse heat leak testing. During experimentation the air temperature in the evaporator compartment was lower than the ambient air temperature, and therefore the buoyancy effects would tend to leak the colder, denser air from the drain hole at the bottom of the evaporator compartment, leading to additional heat loss.

Although the model has some short comings when predicting the system behavior, the results for the yearly energy consumption are within 12.8% of the experimental case. The difference in the yearly energy consumption is mostly due to the under-prediction of the evaporator capacity. The under-prediction of the evaporation capacity becomes especially apparent when considering that the heat load of the cabinet is also under-predicted. The inaccuracies present in this model indicate that the capillary tube SLHX model needs improvement as highlighted earlier. The moderate overall accuracy of this TransRef model indicates that it can be used to show general transient system performance trends when replacing the refrigerant with a drop-in substitute, but it should be noted that the absolute performance results have limited, though acceptable, accuracy.

### 3.3.2. R1234yf Drop-in Replacement Simulation

After validating the TransRef model for the R134a baseline case using experimental data, simulations using R1234yf as a direct drop-in replacement were performed. For the R1234yf direct drop-in simulation, all of the component models and control algorithms remained the same as the baseline R134a model in order to simulate

the expected response of the system when changing refrigerants. Once again, the DOE test standard conditions were used with an ambient temperature of 32.2°C and the "warmest" thermostat settings. Several of the relevant transient outputs are shown for six "steady" cycles in the graphs of Figure 40 through Figure 44. The compressor powers, damper setting, average cabinet temperatures, mass flow rates, system pressures, and superheat/subcooling values are compared between the TransRef baseline R134a model and the TransRef R1234yf direct drop-in model.
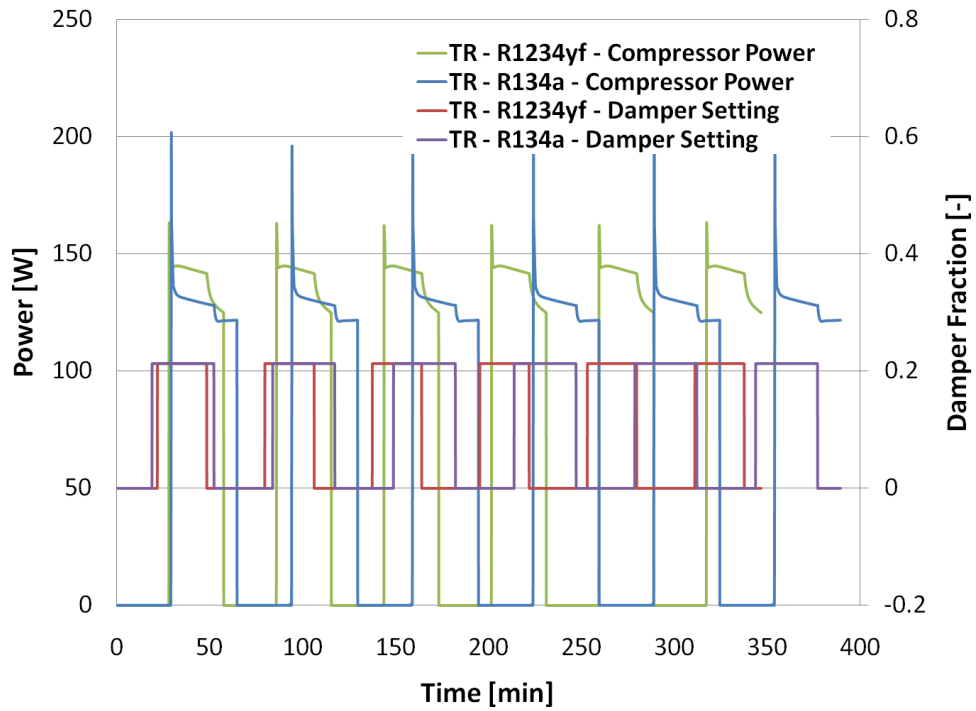


**Figure 40: Compressor power and damper fractions - comparison between TransRef baseline R134a and drop-in R1234yf results**
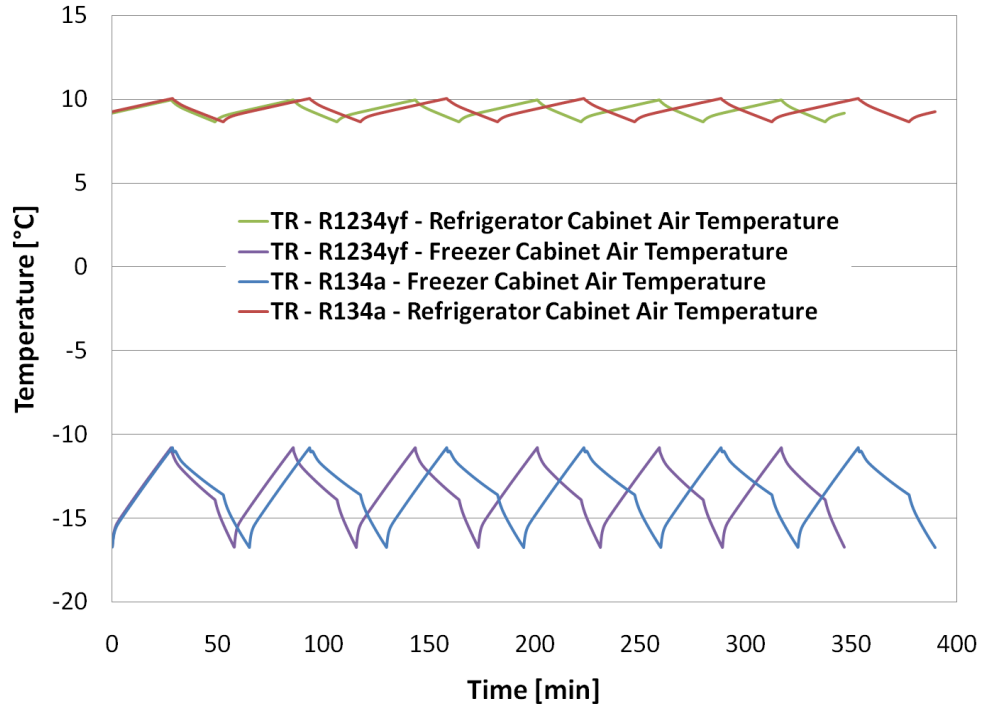
**Figure 41: Average cabinet air temperatures - comparison between TransRef baseline R134a and drop-in R1234yf results**
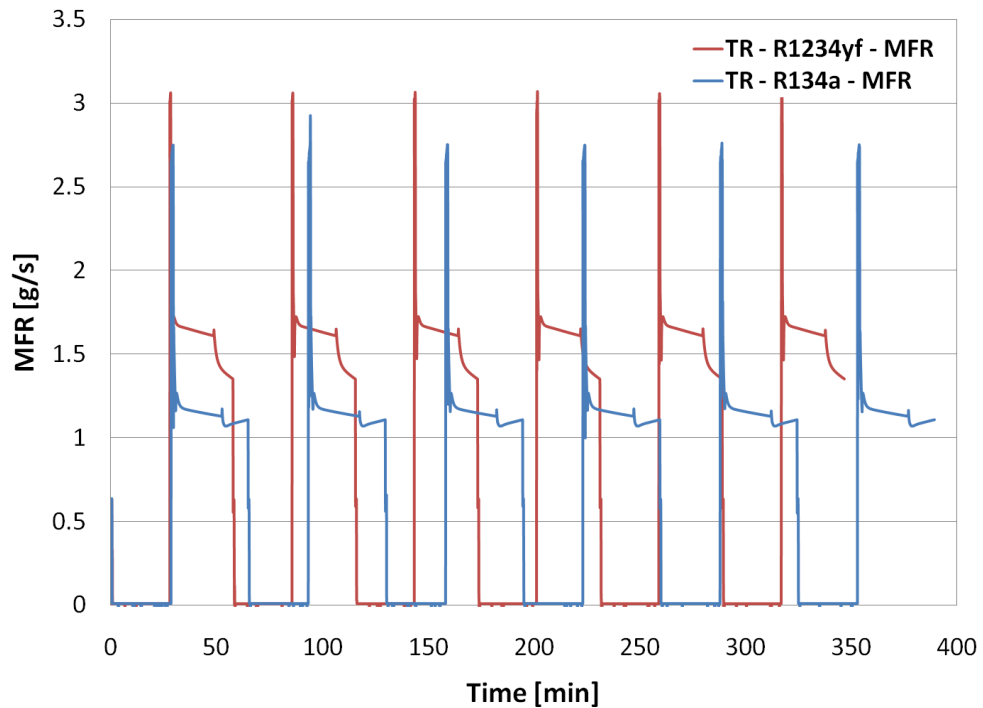


**Figure 42: Refrigerant mass flow rates - comparison between TransRef baseline R134a and drop-in R1234yf results**

82
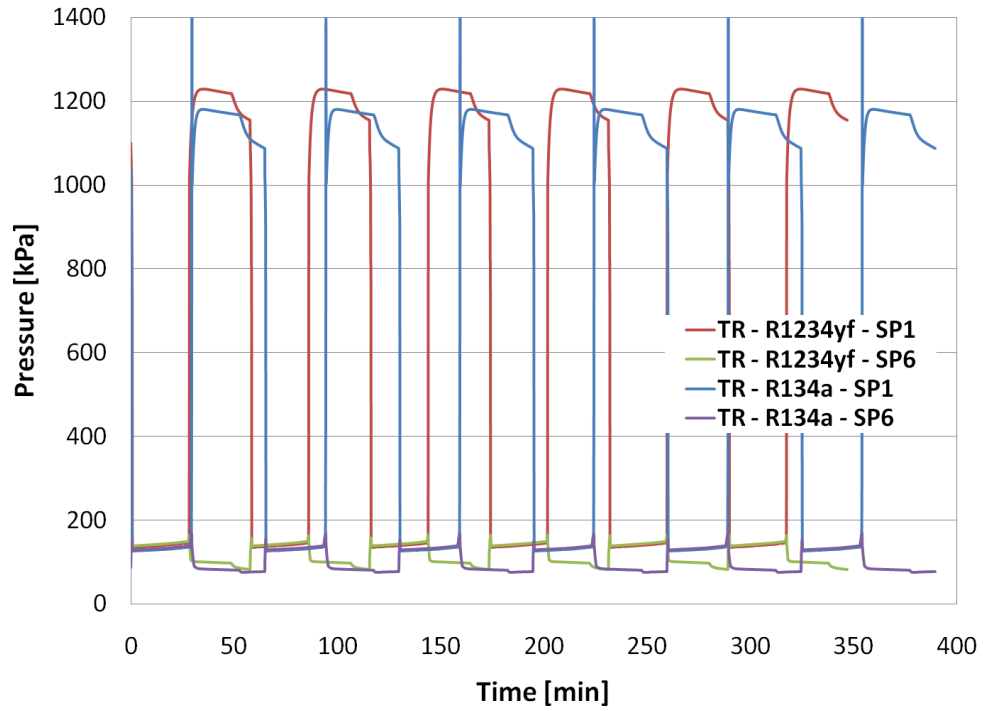
**Figure 43: Pressures - comparison between TransRef baseline R134a and drop-in R1234yf results**
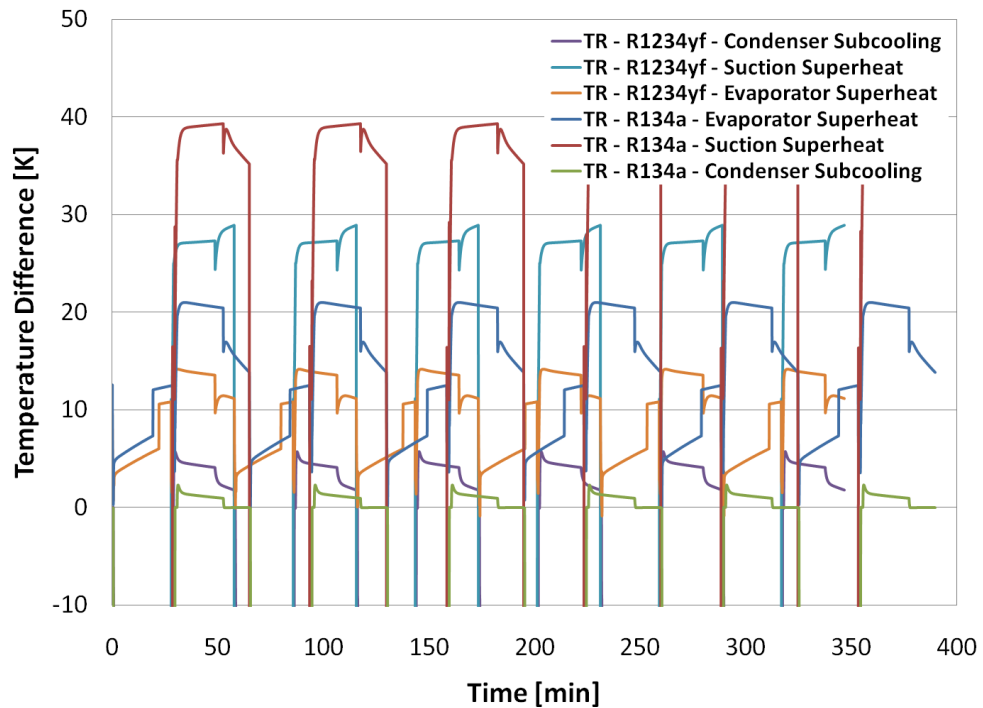


**Figure 44: Subcooling and superheat - comparison between TransRef baseline R134a and drop-in R1234yf results**

83

It is apparent from the transient data shown in Figure 40 that the off-cycle duration is nearly the same between the R134a baseline simulation and the R1234yf drop-in simulation, as would be expected since the cabinet model remains the same. The data also shows that the on-cycle duration is less in the R1234yf case, though the compressor power consumption is greater. This result indicates that the R1234yf cycle has more evaporator capacity than the R134a cycle. The greater evaporator capacity is also supported by the increased refrigerant mass flow rate as shown in Figure 42. The transient response characteristics of the R1234yf drop-in simulation are nearly identical to the R134a baseline when the damper and compressor powers are toggled.

Figure 41 shows that other than the difference in on-cycle duration, the average cabinet air temperature profiles are approximately the same, indicating that the thermostat controls are working as intended. The R1234yf drop-in simulation also predicts that both the discharge and suction pressures will be slightly higher than the R134a baseline case, as shown in Figure 43. Finally, Figure 44 indicates that the condenser outlet subcooling will be higher, and the evaporator and suction superheats will be lower in the R1234yf case as compared with the R134a baseline case.

In order to make quantifiable comparisons between the TransRef R134a model results and the TransRef R1234yf drop-in simulation, some of the key parameters are tabulated in Table 27. Average on-cycle values are given for parameters other than the cycle duration information and yearly energy consumption.

**Table 27: Average on-cycle results – comparison between TransRef baseline R134a and drop-in R1234yf results**

| Variable | Units | TransRef R134a | TransRef R1234yf | Difference |
|---|---|---|---|---|
| On-Cycle Duration | min | 35.1 | 29.2 | 16.8% decrease |
| Off-Cycle Duration | min | 29.8 | 28.6 | 4.0% decrease |
| On-Cycle Fraction | % | 54.1 | 50.5 | 6.7% decrease |
| Compressor Power | W | 127.7 | 139.2 | 9.0% increase |
| Refrigerant Mass Flow Rate | g/s | 1.15 | 1.58 | 37.4% increase |
| Discharge Pressure | kPa | 1,146.3 | 1,199.7 | 4.7% increase |
| Suction Pressure | kPa | 82.1 | 96.6 | 17.7% increase |
| Evaporation Temperature | °C | -30.6 | -30.6 | ~0 K |
| Pressure Ratio | - | 14.0 | 12.4 | 11.4% decrease |
| SLHX Capacity | W | 17.7 | 19.6 | 10.7% increase |
| Yearly Energy Consumption (compressor only, without defrost) | kWh/year | 604.8 | 616.3 | 1.9% increase |

From the TransRef comparison between the R134a baseline simulation and R1234yf drop-in simulation, it is apparent that the performance is similar, though there are some distinct differences. The compressor power is slightly increased by 9.0%, which is due to an increased vapor density at the compressor suction port and subsequently an increased volumetric refrigerant flow rate. The increased vapor density at the suction port is the result of two factors. The first factor is that the vapor density of R1234yf is higher than R134a, and the second is that the suction pressure is predicted to increase by 17.7%. The increased volumetric refrigerant flow rate is the main reason for the significantly increased refrigerant mass flow rate, with the R1234yf simulation being 37.4% higher than the R134a case. The evaporator capacity of the R1234yf drop-in is also strongly increased, which is indicated by the decrease in on-cycle duration of 16.8%. The evaporator capacity increase can mostly be attributed to the increased refrigerant mass flow rate as well as the 10.7% increase in SLHX capacity. The increase in SLHX capacity results in an increase in evaporator capacity because the vapor quality at the evaporator inlet is reduced.

The most important result of the comparison is that the yearly compressor energy

consumption of the transient cycle is increased by only a slight 1.9% when replacing

R134a with R1234yf. This slight difference in yearly energy consumption indicates that

if the capillary tube SLHX is optimized for R1234yf, it may be possible to match or even

exceed the performance of R134a. It is also important to note that if R1234yf is used as a

direct drop-in, the system will perform adequately without modification to any of the

R134a baseline components, and the system pressures will stay within acceptable limits.

# 4. Conclusions

A test facility was constructed in order to evaluate the performance of a household refrigerator-freezer which used the refrigerant HFC-134a as a working fluid. The test facility included instrumentation to measure all of the thermodynamic properties relevant to the system performance. The DOE testing standard to evaluate household refrigerator-freezer energy consumption was used to evaluate the transient performance of the system on a yearly basis. Transient cyclic data was collected and used to determine the yearly energy consumption of the system, which was found to be 607.6±1.9 kWh/year, which was within 8% of the manufacturer's rating of 563 kWh/year. The 8% difference can be attributed to the modifications made to the system for testing purposes.

The R134a baseline experimental data was then used to validate both steady-state and transient models for the system components as well as the entire system. The transient data consisted of six on and off cycles of the system during the DOE tests, and the steady-state data was collected during a short, relatively stable portion of testing referred to as a quasi-steady-state point. The software packages CoilDesigner and VapCyc were used to model steady-state system and component behavior, while the software package TransRef was used to model transient system behavior.

When validated with the experimental R134a data, the computer software models were shown to match the actual system performance within acceptable margins. For all of the tested cases, the CoilDesigner models matched the heat transfer characteristics of the evaporator and condenser heat exchangers to within 2.5%, an excellent result. Considering that the refrigerant two-phase heat transfer correlations have relatively high uncertainties, it was fortunate that the models matched so closely in the tested cases. The

two-phase pressure drop predictions of the CoilDesigner models were in error by as much as 30-70%, though this had little impact on the modeling results for VapCyc and TransRef. Overall the CoilDesigner models and modeling results were validated for use in the VapCyc and TransRef models.

The VapCyc model was shown to match most system properties to within 6% at several different test conditions. There were a few system properties which reached as high as an 11% error. The fundamental structure of the modeled cycle on a P-h diagram was found to match well with the experimental results. Taking into consideration the system uncertainties and the assumptions made, this was considered to be a good result and therefore validated the model accuracy.

The TransRef model was found to match reasonably well with the experimental data. The fundamental behavior of the transient cycles matched well. The main discrepancies in the model were due to an inaccurate capillary tube SLHX model which under-predicted the heat transfer and over-predicted the pressure drop. The model under-predicted the suction pressure by 31.0% and the SLHX capacity by 60.7%. The rest of the relevant system performance characteristics matched within 15%, a reasonable result for transient simulations considering the capillary tube SLHX issues. The yearly energy consumption of the compressor was found to be within 12.8% of the experimentally measured value. The moderate overall accuracy of the TransRef model indicated that it could be used to show general transient system performance trends but that the absolute performance results have limited, though acceptable, accuracy.

Although there were some differences between the experimental and modeling results in the computer models created, the results were useful for determining the

general performance trends of the system when exploring alternative low GWP

refrigerant replacement options for R134a. The first and most relevant replacement

option for R134a for household refrigerator-freezers is HFO-1234yf. R1234yf was shown

to have favorable thermodynamic properties for use in a refrigeration cycle, and the

properties matched closely with R134a. The first step in the evaluation of R1234yf was to

determine if it could be used as a direct drop-in replacement for R134a without any

system modifications. Using VapCyc, it was found that R1234yf exhibited a 1.1%

decrease in evaporator capacity and a 1.2% decrease in system efficiency under steady-

state operating conditions. Using TransRef, it was found that the yearly energy

consumption of R1234yf would be 1.9% larger than R134a, indicating a slight decrease

in system efficiency.

Both the VapCyc and TransRef models indicated that the system had room for

performance improvement through the optimization of the capillary tube expansion

device, though the accuracy of the capillary tube models was questionable, especially in

the case of TransRef. Without system modifications, the two software platforms indicated

that a slight decrease in system efficiency would occur when replacing R134a with

R1234yf, but in both cases the difference was less than 2%. This indicates that R1234yf

is an excellent direct substitute for R134a, and that with minor system modifications it

has the potential to have system performance equal to, or exceeding, R134a.

In order to determine the viability of several potential alternative low GWP

substitutes for R134a without considering the expansion device performance or

optimization, a simplified model was created with VapCyc. This simplified VapCyc

model removed the capillary tube SLHX and replaced it with a dummy valve. The

convergence criteria for the cycle were then set to a condenser subcooling of 2 K and an evaporator superheat of 5 K. The simplified VapCyc model was then utilized to investigate the system performance when replacing R134a with R1234yf and R1234ze, as well as with various mixtures of R134a with R1234yf.

It was found that R1234yf would serve as a suitable drop-in replacement for R134a with a 6.2% lower evaporator capacity and 8.9% lower COP. The difference between this result and the previous R1234yf drop-in case using a capillary tube SLHX indicates that the inclusion of a SLHX has a stronger positive effect on the R1234yf cycle then on the R134a cycle. It was also found that R1234ze would need modification to the system in order to replace R134a, exhibiting a 21.5% lower evaporator capacity, but a promising 7.9% higher COP. To work as a viable replacement for R134a, R1234ze would require a larger compressor, which makes it a more expensive replacement option than R1234yf.

Due to the flammability issues associated with R1234yf and the GWP issues of R134a, a parametric study of mixtures with various mass fractions of R1234yf in R134a was conducted. This study demonstrated that there are trade-offs in system performance for the various mixtures due to changes in the saturation pressures. The most interesting observations were that for R1234yf fractions between 0.4 and 1.0, the system performance was degraded when compared with pure R1234yf, but that a fraction of 0.4 provided the same system COP as pure R1234yf while increasing the evaporator capacity by 5.8% when compared with the R134a baseline. Most importantly, this study shows that if experimentation can be performed to determine the flammability and GWP characteristics of the various R134a/R1234yf mixtures, trade-off decisions could be made

between system performance, flammability hazards, and environmental concerns. The simulation results indicate that any mixture composition of R134a and R1234yf would provide acceptable system performance as a drop-in R134a replacement, with the COP remaining within 11% and the evaporator capacity remaining within 6.2% of the R134a baseline for all mixture compositions.

Overall, the steady-state and transient models which were experimentally verified using R134a indicated that R1234yf would serve as an excellent substitute for R134a as a direct drop-in replacement in a household refrigerator-freezer. This conclusion is similar to the results found in the literature for mobile air conditioners and medium temperature refrigeration. The significantly lower GWP of R123yf when compared with R134a means that using R1234yf as a replacement refrigerant will allow environmental regulations to be met and environmental impact to be reduced. Additionally, it was shown that mixtures of R134a and R1234yf could be used to create a fluid which has performance characteristics similar to the pure fluids, but has the potential to have a lower environmental impact than R134a and a lower flammability than R1234yf.

# 5. Recommendations and Future Work

For future analysis using VapCyc and TransRef, it is recommended that new correlations be implemented for the capillary tube SLHX models for heat transfer and pressure drop in order to improve simulation accuracy. These correlations should be tested and/or developed in conjunction with experimental work.

In order to validate the simulation work performed with R1234yf, experimentation should be performed using R1234yf as a drop-in replacement for R134a. The experimental work could also include capillary tube optimization to ensure that the system is achieving its best possible performance. Additional fluids such as R134a/R1234yf mixtures could also be evaluated as drop-in replacements using the same experimental test facility.

Mixtures of various fractions of R1234yf in R134a should be tested for multiple fluid properties. The properties to test would include some basic thermodynamic and fluid dynamic properties, as well as the stability of the mixtures. It should also be determined if the mixture components have any azeotropic points. Flammability testing could also be performed in order to determine the minimum fraction of R134a required in the mixture to qualify the fluid for non-flammable regulatory categories. Lastly, the GWP of the various mixtures could be tested to determine how the GWP varies as a function of mixture fraction.

# Appendix

DOE test standard "steady-state" cyclic data sets for an ambient temperature of 32.2°C and "middle" thermostat settings, an ambient temperature of 20°C and "warmest" thermostat settings, and an ambient temperature of 20°C and "middle" thermostat settings. The variables plotted include: system powers and average cabinet air temperatures, in-stream temperatures, pressures, mass flow rates, subcooling/superheating, and heat exchanger pressure drops.
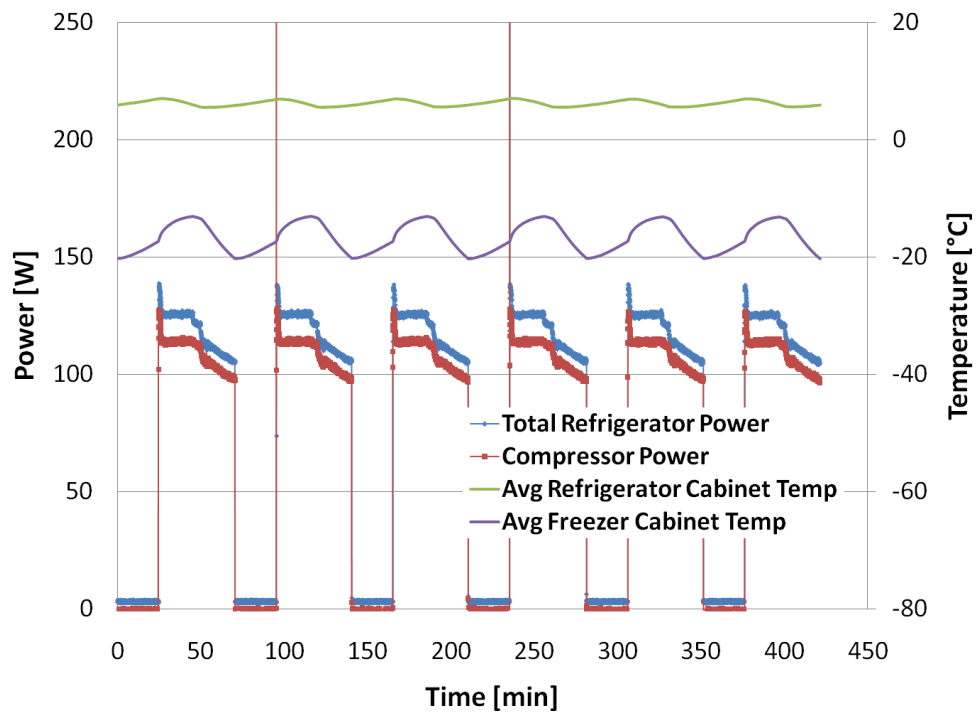


**Figure 45: System powers and average cabinet air temperatures (experimental DOE "steady-state" at $T_{amb}$ = 32.2°C and "middle" thermostat)**
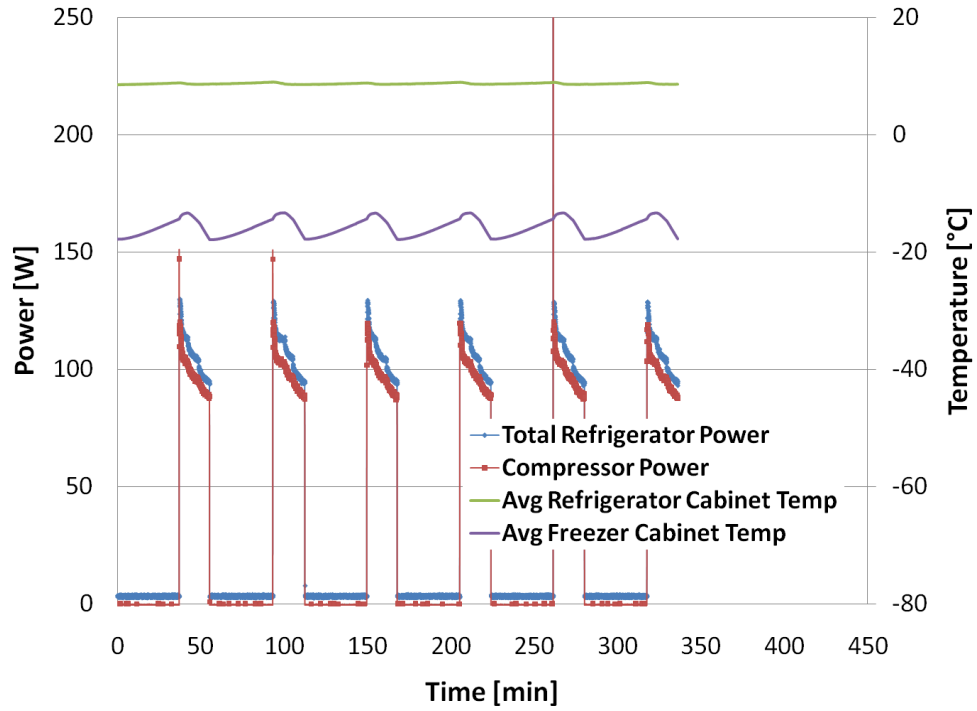
**Figure 46: System powers and average cabinet air temperatures (experimental DOE "steady-state" at $T_{amb} = 20°C$ and "warmest" thermostat)**
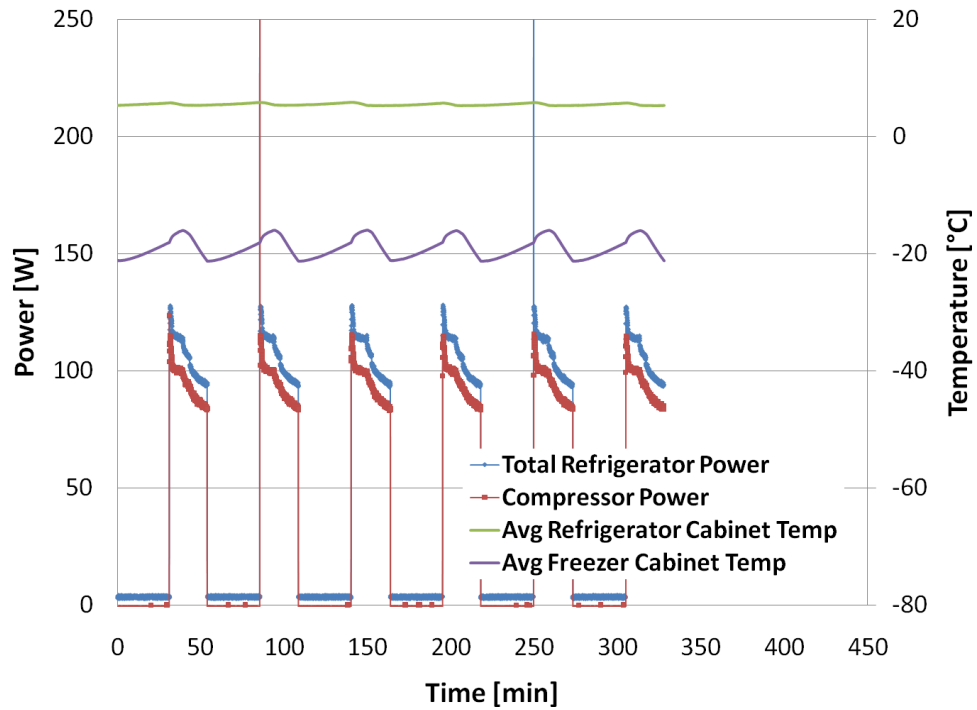


**Figure 47: System powers and average cabinet air temperatures (experimental DOE "steady-state" at $T_{amb} = 20°C$ and "middle" thermostat)**
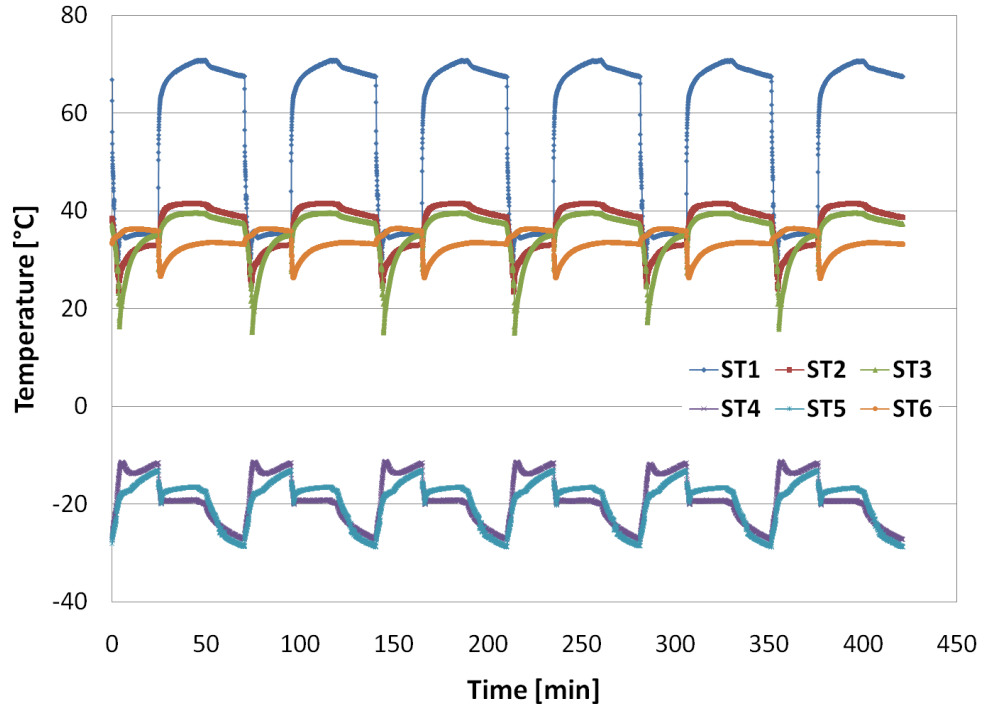
**Figure 48: In-stream temperatures (experimental DOE "steady-state" at T<sub>amb</sub> = 32.2°C and "middle" thermostat)**
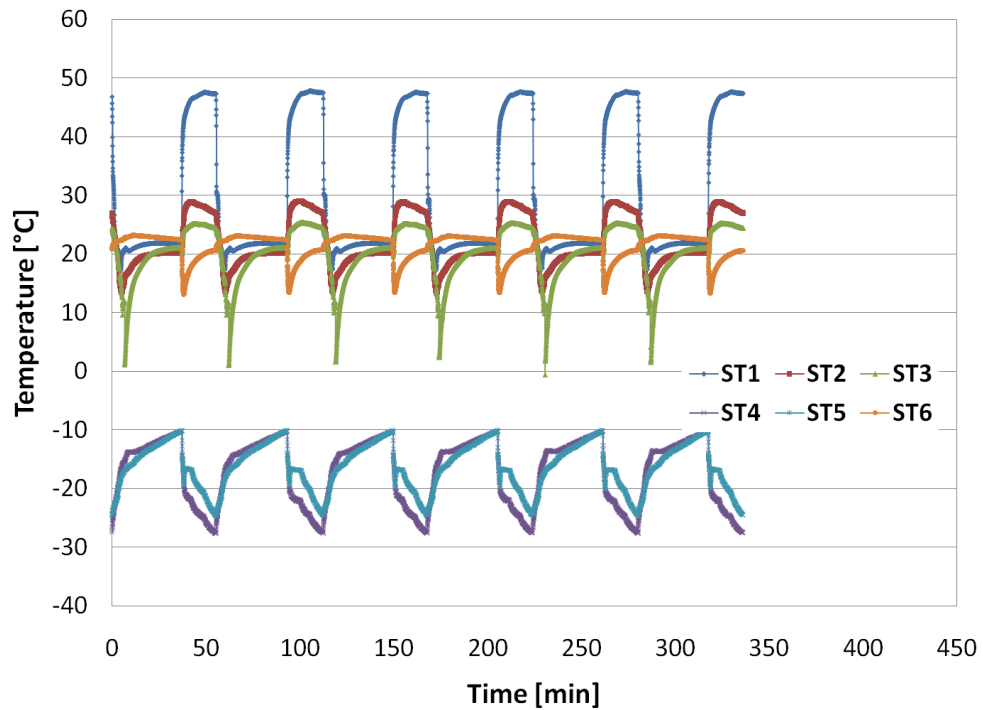


**Figure 49: In-stream temperatures (experimental DOE "steady-state" at T<sub>amb</sub> = 20°C and "warmest" thermostat)**
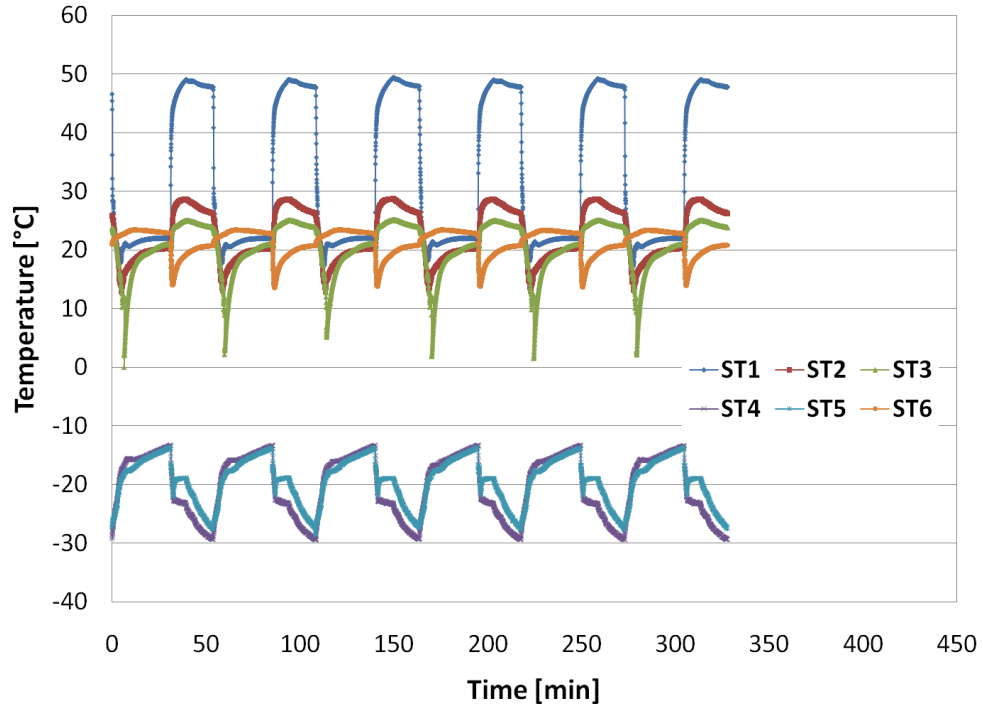
**Figure 50: In-stream temperatures (experimental DOE "steady-state" at $T_{amb}$ = 20°C and "middle" thermostat)**
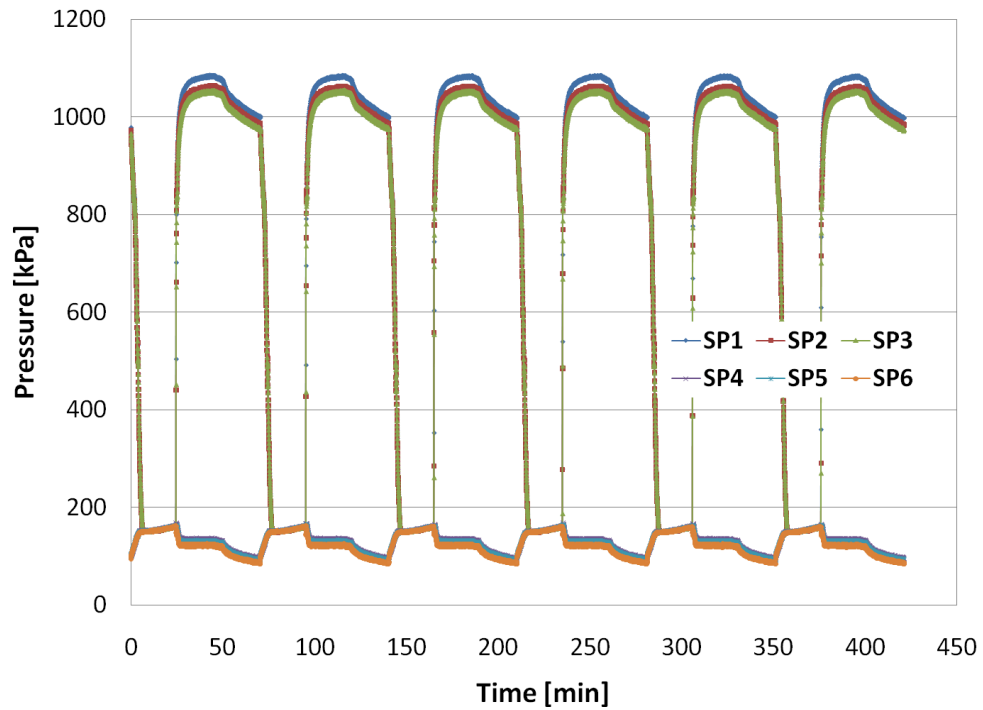


**Figure 51: Pressures (experimental DOE "steady-state" at $T_{amb}$ = 32.2°C and "middle" thermostat)**
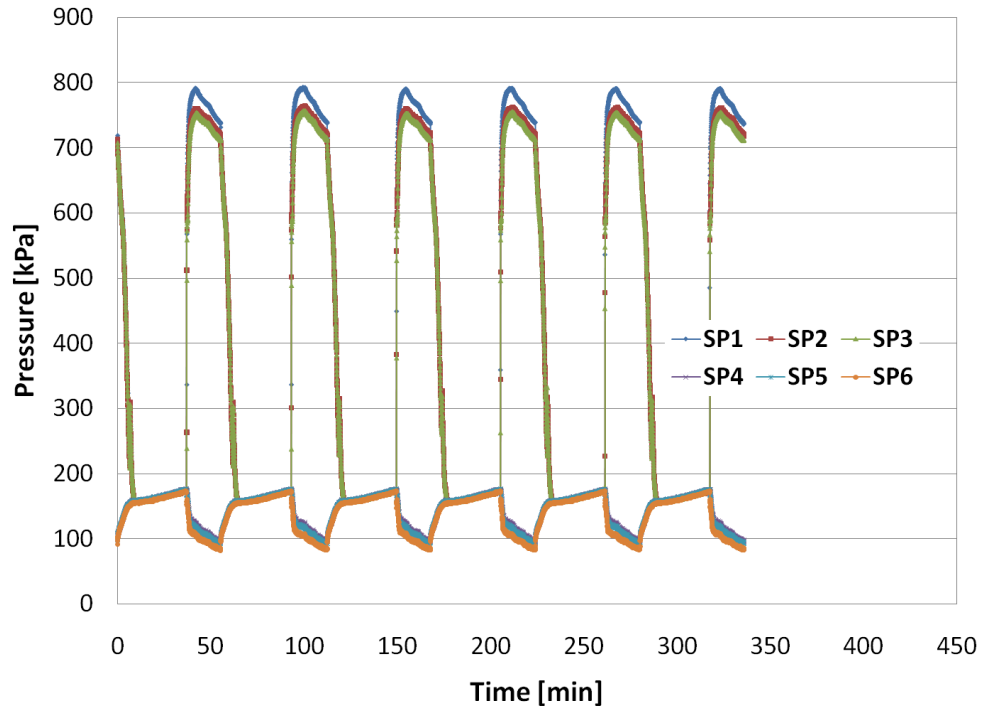
**Figure 52: Pressures (experimental DOE "steady-state" at T$_{amb}$ = 20°C and "warmest" thermostat)**
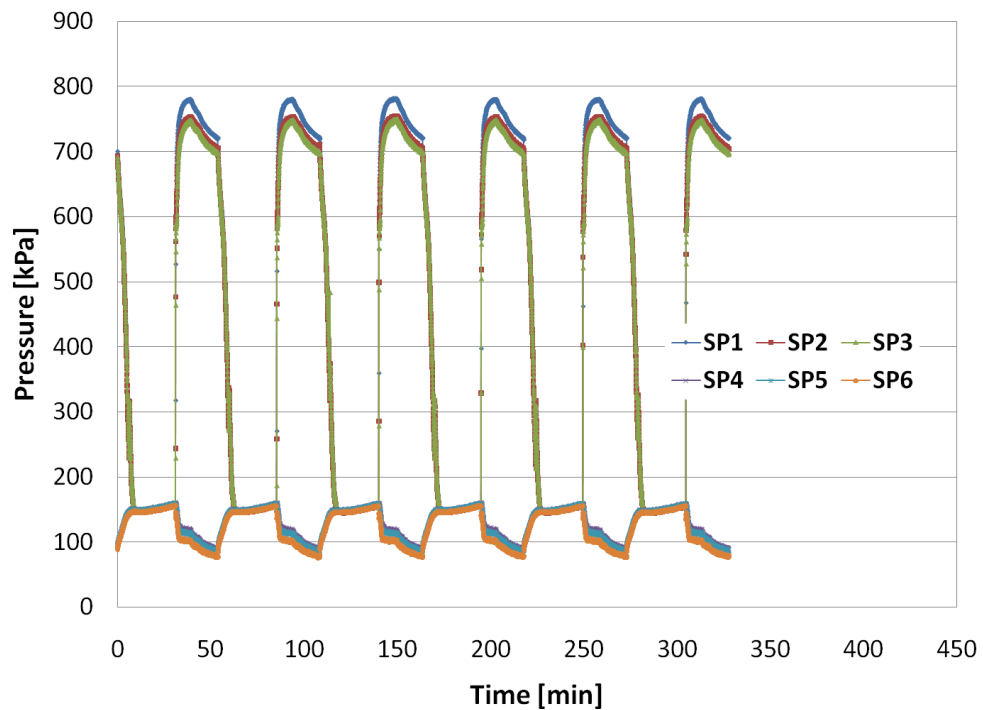


**Figure 53: Pressures (experimental DOE "steady-state" at T$_{amb}$ = 20°C and "middle" thermostat)**
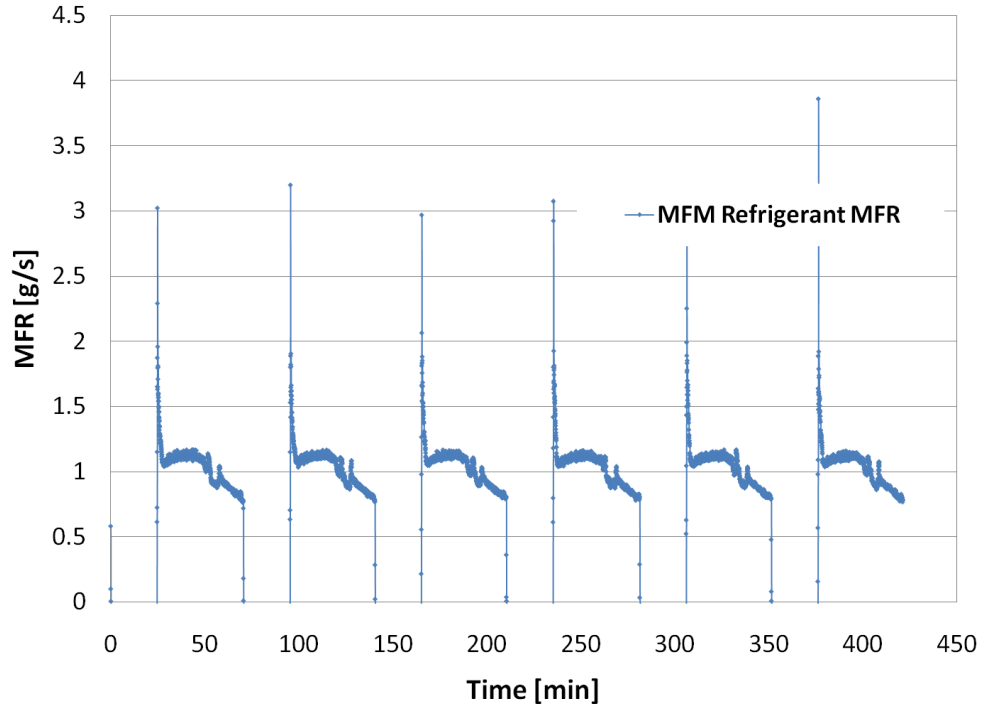
**Figure 54: Refrigerant mass flow rate (experimental DOE "steady-state" at $T_{amb}$ = 32.2°C and "middle" thermostat)**
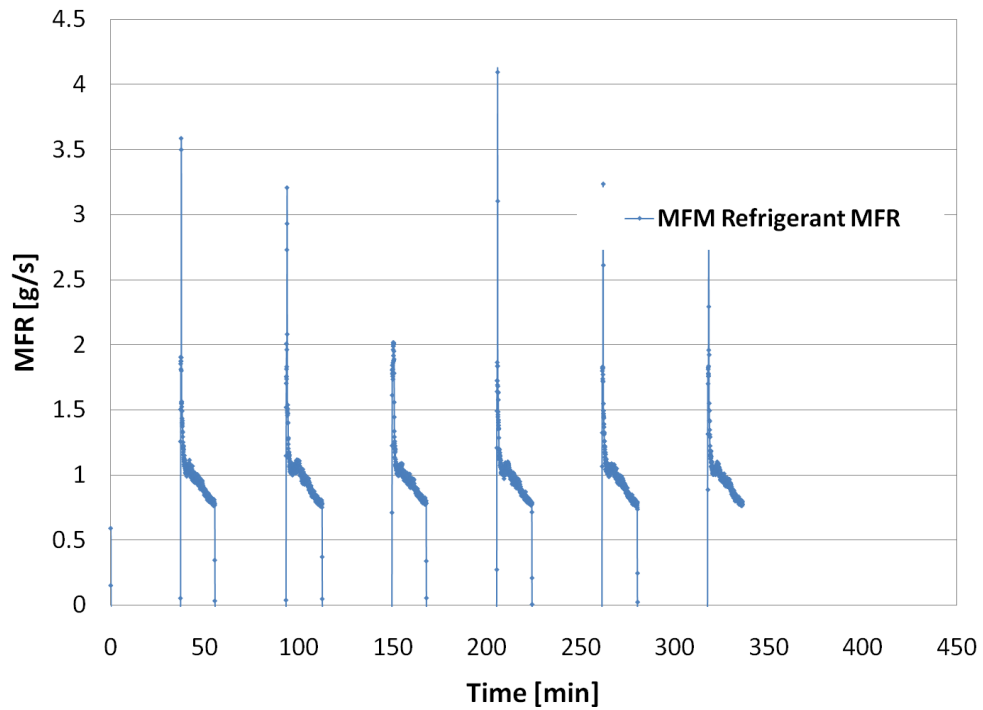


**Figure 55: Refrigerant mass flow rate (experimental DOE "steady-state" at $T_{amb}$ = 20°C and "warmest" thermostat)**
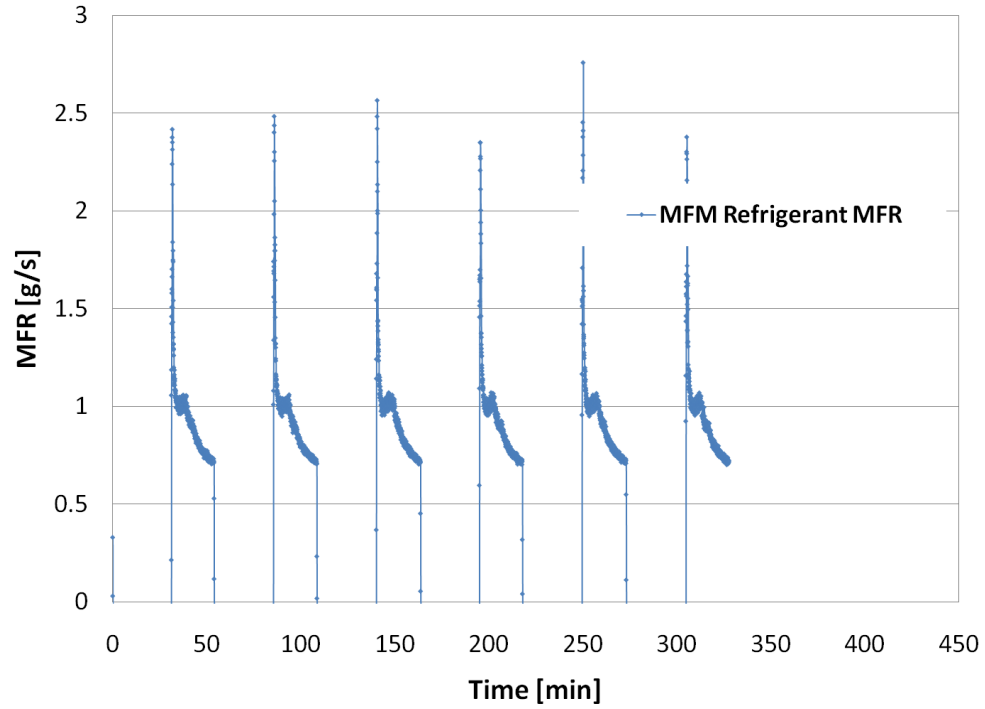
**Figure 56: Refrigerant mass flow rate (experimental DOE "steady-state" at T_amb = 20°C and "middle" thermostat)**
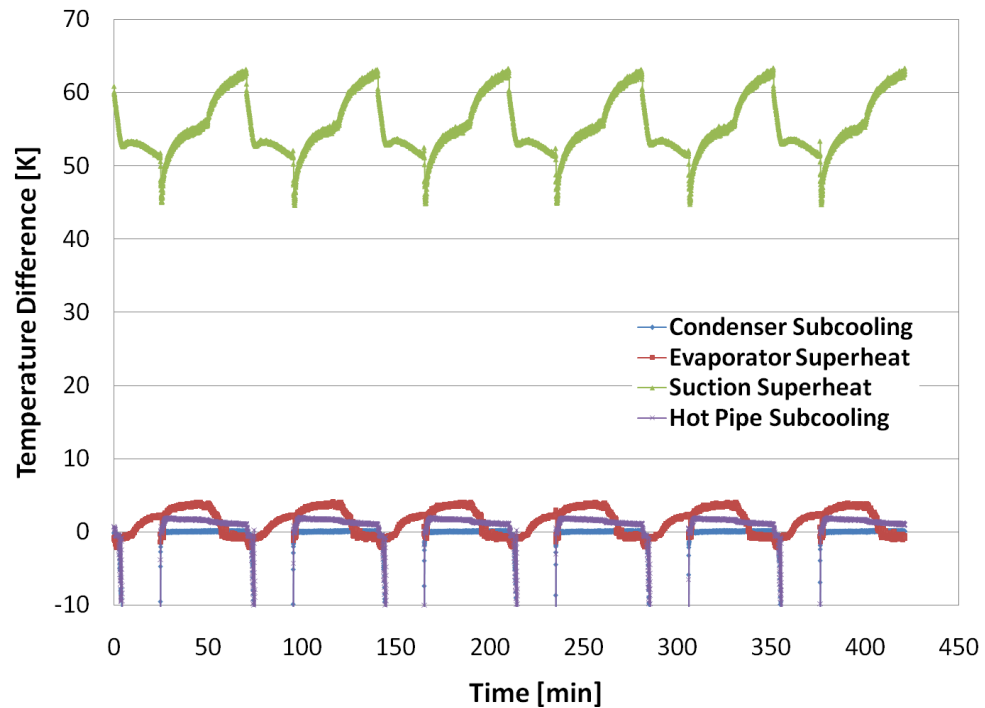


**Figure 57: Subcooling and superheat (experimental DOE "steady-state" at T_amb = 32.2°C and "middle" thermostat)**
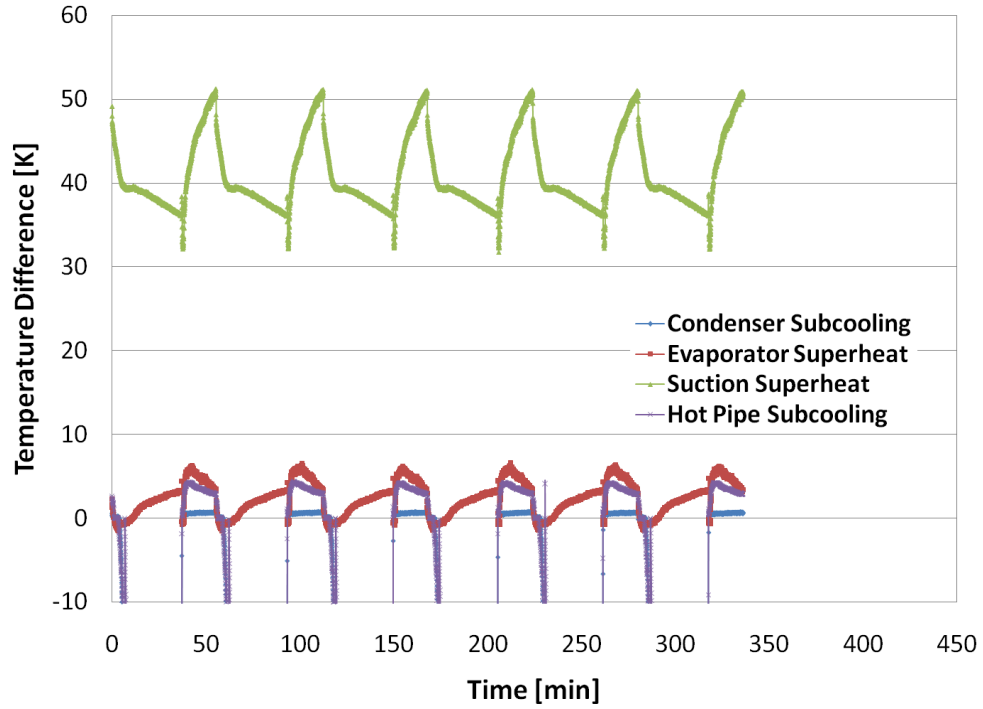
**Figure 58: Subcooling and superheat (experimental DOE "steady-state" at T_amb = 20°C and "warmest" thermostat)**
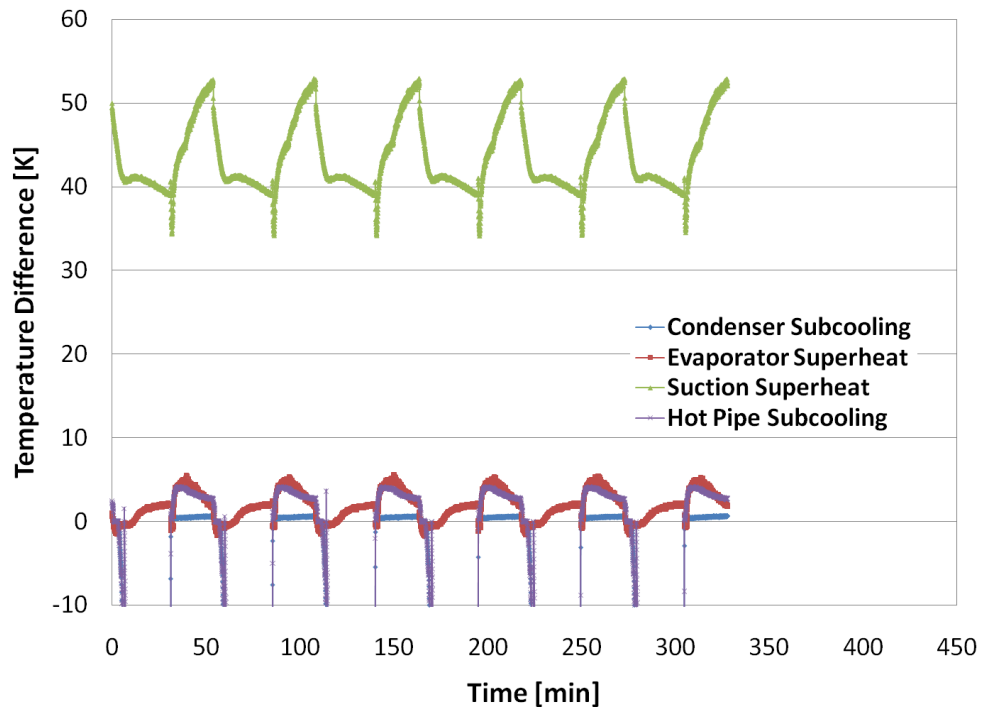


**Figure 59: Subcooling and superheat (experimental DOE "steady-state" at T_amb = 20°C and "middle" thermostat)**
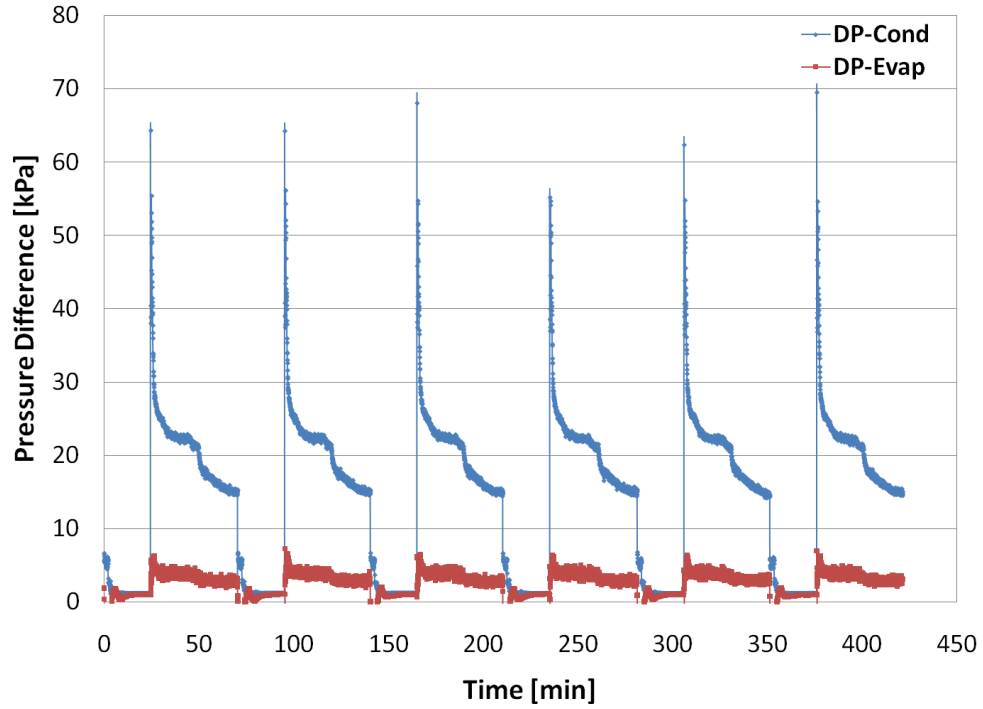
**Figure 60: Heat exchanger pressure drops (experimental DOE "steady-state" at $T_{amb} = 32.2°C$ and "middle" thermostat)**
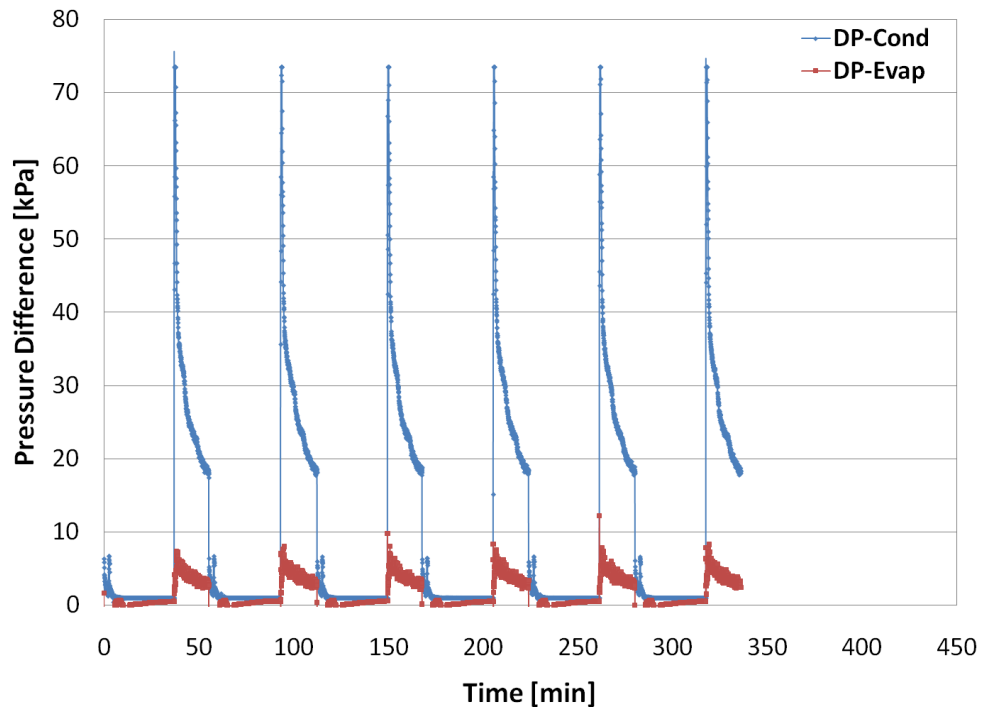


**Figure 61: Heat exchanger pressure drops (experimental DOE "steady-state" at $T_{amb} = 20°C$ and "warmest" thermostat)**
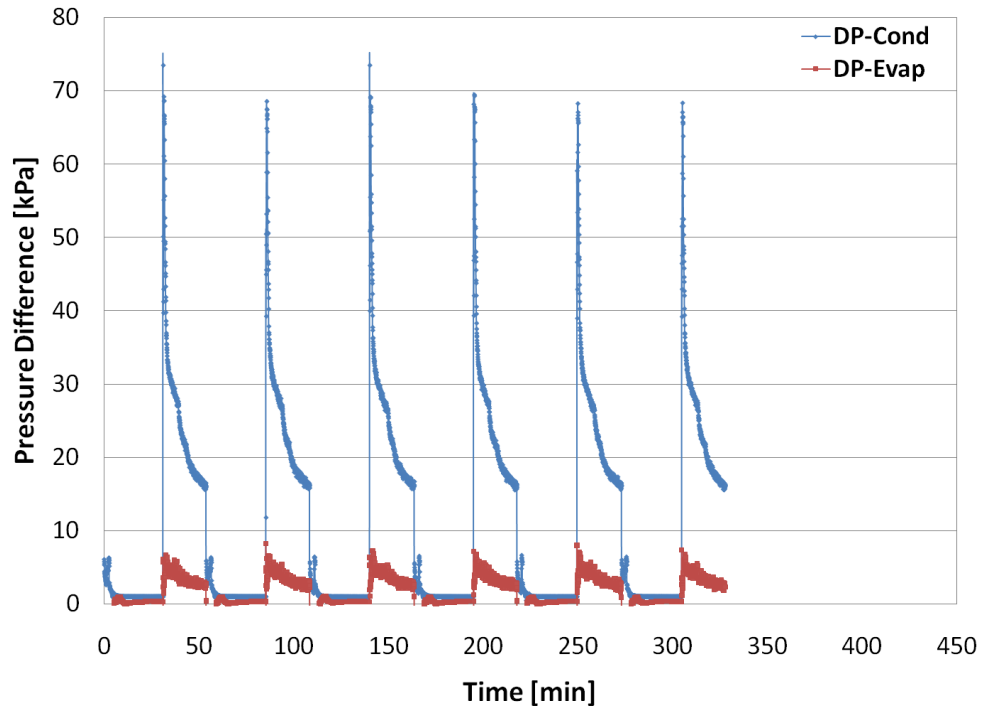
**Figure 62: Heat exchanger pressure drops (experimental DOE "steady-state" at $T_{amb} = 20°C$ and "middle" thermostat)**

# References

[1]  Baker, J., Ghodbane, M., Rugh, J., and Hill, W., 2007, *Alternate Refrigerant Demonstration Vehicles,* SAE Alternate Refrigerant Symposium, Scottsdale, Arizona, USA, July 17-19, 2007.

[2]  United States Environmental Protection Agency (EPA), 2010, *Transitioning to Low-GWP Alternatives in Domestic Refrigeration,* October 2010, <http://www.epa.gov/spdpublc/downloads/EPA_HFC_DomRef.pdf>.

[3]  Intergovernmental Panel on Climate Change (IPCC), 2007, *IPCC Fourth Assessment Report: Climate Change 2007: Working Group 1: The Physical Science Basis: 2.10.2 Direct Global Warming Potentials,* Cambridge University Press, Cambridge, United Kingdom and New York, NY, USA.

[4]  Wilson, D., and Koban, M., 2009, *HFO-1234yf Industry Update,* EPA R1234yf Commercialization Meeting, February 6, 2009.

[5]  Papadimitriou, V., Talukdar, R., Portmann, R., Ravishankara, A., and Burkholder, J., 2008, *$CF_3CF=CH_2$ and $(Z)$-$CF_3CF=CHF$: Temperature Dependent OH Rate Coefficients and Global Warming Potentials,* Physical Chemistry Chemical Physics, Vol. 10, pp. 808 – 820.

[6]  American Society of Heating, Refrigerating and Air-Conditioning Engineers (ASHRAE), *ANSI/ASHRAE Standard 34-200: Designation and Safety Classification of Refrigerants.*

[7]  Underwriters Laboratories (UL), 2011, *White Paper: Revisiting Flammable Refrigerants,* Underwriters Laboratories Inc.

[8]  Klein, S., 2010, *Engineering Equation Solver,* University of Wisconsin, F-Chart Software, LLC., <http://www.fchart.com/>.

[9]  Spatz, M., 2009, *HFO-1234yf Technology Update – Part II,* VDA Alternative Refrigerant Winter Meeting, Saalfelden, Australia, February 11-12, 2009.

[10] Spiegel, C., 2008, *Test Report: GAR Test R1234yf vs. R134a on PQ35 AC Loop,* SANDEN Technical Centre, Bad Nauheim, Germany.

[11] Meyer, J., 2008. *R1234yf System Enhancements and Comparison to R134a,* SAE Alternate Refrigerant Symposium, Scottsdale, Arizona, USA, June 10-12, 2008.

[12] Leck, T., 2009, *Evaluation of HFO-1234yf as a Potential Replacement for R-134a in Refrigeration Applications,* 3rd IIR Conference on Thermophysical Properties and Transfer Processes of Refrigerants, Boulder, CO, USA, June 23-26, 2009.

[13] Leck, T., 2010, *New High Performance, Low GWP Refrigerants for Stationary AC and Refrigeration,* International Refrigeration and Air Conditioning Conference, Purdue, July 12-15, 2010.

[14] Fujitaka, A., Shimizu, T., Sato, S., and Kawabe, Y., 2010, *Application of Low Global Warming Potential Refrigerants for Room Air Conditioner,* 2010 International Symposium on Next-generation Air Conditioning and Refrigeration Technology, Tokyo, Japan, February 17-19, 2010.

[15] Spatz, M., 2009, *Low Global Warming Alternative Refrigerants for Stationary AC&R Applications,* JSRAE Annual Conference, Tokyo, Japan, October 21-23, 2009.

[16] United States Department of Energy (DOE), 2005, *Uniform Test Method for Measuring the Energy Consumption of Electric Refrigerators and Electric Refrigerator-Freezers,* United States Federal Registry: 10 CFR, Part 430, Subpart B, Appendix A1.

[17] Morawetz, D., 2010, *Testing and Cycle Analysis of a HFC-134a Baseline Refrigerator,* Undergraduate Thesis, University of Maryland, College Park, MD, USA.

[18] Vineyard, E., Stovall, T., Wilkes, K., and Childs, K., 1998, *Superinsulation in Refrigerators and Freezers,* "Recent Developments in Refrigerators and Freezers," ASHRAE Seminar, July 1998.

[19] Tao, W., Sun, J., and Chang, C., 2001, *The Development and Improvement of Energy Efficient Refrigerators,* Chemical Engineering Communications, Vol. 186, pp. 161-170.

[20] Center for Environmental Energy Engineering, 2011, *CoilDesigner,* University of Maryland, <http://ceee.umd.edu/isoc/software/index_coildesigner.htm>.

[21] Center for Environmental Energy Engineering, 2011, *VapCyc,* University of Maryland, <http://ceee.umd.edu/isoc/software/index_vapcyc.htm>.

[22] Center for Environmental Energy Engineering, 2011, *TransRef,* University of Maryland, <http://ceee.umd.edu/isoc/software/index_transref.htm>.

[23] Richardson, D. H., Jiang, H., Lindsay, D., and Radermacher, R., 2002, *Optimization of Vapor-Compression Systems Via Simulation,* 2002 International Refrigeration and Air Conditioning Conference, Purdue University, West Lafayette, IN, USA, July 16-19, 2002.

[24] Richardson, D. H., Aute, V., Winkler, J., and Radermacher, R., 2004, *Numerical Challenges in Simulation of a Generalized Vapor Compression Refrigeration System,* 2004 International Refrigeration and Air Conditioning Conference, Purdue University, West Lafayette, IN, USA, July 12-15, 2004.

[25] Qiao, H., 2011, Unpublished personal discussions and computer code, University of Maryland, MD, USA.

[26] Gercek, E., Aute, V., and Radermacher, R., 2005, *Transient Simulation Tool for Refrigeration Systems,* IIR Conference on Commercial Refrigeration, Vicenza, Italy, August 2005.